Università degli Studi di Padova

Dipartimento di Ingegneria Industriale - DII

Ph.D. COURSE: Industrial Engineering CURRICULUM: Materials Engineering SERIES: XXXI

DEVELOPMENT OF STRUCTURED POROUS HETEROGENEOUS CATALYST FOR BIODIESEL PRODUCTION BY TRANSESTERIFICATION OF VEGETABLE OIL

The thesis was developed with the financial contribution of Conselho Nacional de Desenvolvimento Científico e Tecnológico (CNPq) - Brazil

Coordinator and supervisor: Prof. Dr. Paolo Colombo

Co-supervisor: Prof. Dr. Murilo Daniel de Melo Innocentini

Ph.D. student: Renata Fuss Botti

DEVELOPMENT OF STRUCTURED POROUS HETEROGENEOUS CATALYST FOR BIODIESEL PRODUCTION BY TRANSESTERIFICATION OF VEGETABLE OIL

Thesis presented to the Ph.D. program on Industrial Engineering at University of Padova as a partial requirement for the degree of DOCTOR OF INDUSTRIAL ENGINEERING

Supervisor: **Prof. Dr. Paolo Colombo**
Professor of Materials Science and Technology
University of Padova

Cosupervisor: **Prof. Dr. Murilo Daniel di Melo Innocentini**
Professor of Chemical Engineering
University of Ribeirão Preto

PhD Student: **Renata Fuss Botti**

Funding Agency: CNPq (202007/2015-4)

Padova, Italy

2018

SUMARY

ABSTRACT

Many environmental problems are caused when fossil fuels are used in engines. Biodiesel is a promising option to substitute these fuels because it is renewable, biodegradable and not toxic. The most used process to prepare biodiesel is by homogeneous transesterification of vegetable oils, using NaOH or KOH, but it produces a high concentration of impurities in the product. To overcome this, the use of heterogeneous catalysts is being increasingly studied. Geopolymer (GP) is an inorganic material with a chemical composition similar to zeolite and a variable microstructure, obtained by the reaction of aluminosilicates with a highly alkaline medium forming a continuous 3D network. It can be used as a heterogeneous catalyst, due to the high content of metals such as Na and/or K, as well as high basicity and specific surface area. The great advantage of using heterogeneous catalysts is that they can be recovered by filtration and reused in the process, making the biodiesel production more economical and generating fewer effluents to be treated.

This work investigated GP acting as heterogeneous catalysts to produce biodiesel by transesterification reaction of soybean oil with methanol. Three types of GP powder were produced mixing metakaolin with an activating alkaline solution: Na-based, K-based GP and a mixture between them; they were treated at 110, 300, 500 and 700 °C, then lattice-shaped GPs were designed and produced by DIW, adding PEG and filler in the previous formulation and then, they were dried at 110 °C. Porous structures with Ø ~24 mm x 9,6 mm height and unsupported parts were produced. All materials were characterized. The transesterification reaction was carried out using all the samples as a heterogeneous catalyst to evaluate the yield of biodiesel concerning the GP composition, reaction conditions and morphology of samples.

According to the results obtained in this study, it was verified that using GP both in powder and structure as catalyst, it was possible to obtain biodiesel from the transesterification of soybean oil. Comparing the materials with the same molar ratios, Na.K_GP treated at 500°C (powder) achieved the highest conversion (~98%). For the 3D structure tested in the reaction (3D_Na_GP1, 110 °C) a conversion was observed, but lower (~41%) compared to Na.K_GP, even in its powdered version (~53%). To verify the conversion efficiency of the other structures (3D_K_GP1, Na.K_GP) further studies are needed.

ABSTRACT (PORTUGHESE)

Muitos problemas ambientais são causados quando combustíveis fósseis são usados em motores. O biodiesel é uma opção promissora para substituir esses combustíveis por ser renovável, biodegradável e não tóxico. O processo mais utilizado para preparar o biodiesel é por transesterificação homogênea de óleos vegetais, utilizando NaOH ou KOH, porém produz uma alta concentração de impurezas no produto. Para superar isso, o uso de catalisadores heterogêneos está sendo cada vez mais estudado. O geopolímero (GP) é um material inorgânico com composição química semelhante à zeólita e uma microestrutura variável, obtida pela reação de aluminosilicatos com um meio altamente alcalino formando uma rede 3D contínua. Pode ser utilizado como catalisador heterogêneo, devido ao alto teor de metais como Na e/ou K, além de alta basicidade e área superficial específica. A grande vantagem do uso de catalisadores heterogêneos é que eles podem ser recuperados por filtração e podem ser reutilizados no processo, tornando a produção de biodiesel mais econômica e gerando menos efluentes a serem tratados.

Este trabalho investigou o GP atuando como catalisadores heterogêneos para a produção de biodiesel por reação de transesterificação do óleo de soja com metanol. Três tipos de GP em pó foram produzidos misturando metacaulim com uma solução alcalina ativadora: GP à base de Na, a base de K e uma mistura entre eles; eles foram tratados a 110, 300, 500 e 700 °C, em seguida, os GPs em forma de treliça foram projetados e produzidos por DIW, adicionando PEG e preenchimento na formulação anterior e então, eles foram secos a 110 °C. Foram produzidas estruturas porosas com Ø ~24 mm x 9,6 mm de altura e partes não suportadas. Todos os materiais foram caracterizados. A reação de transesterificação foi realizada utilizando todas as amostras como catalisador heterogêneo para avaliar o rendimento do biodiesel em relação à composição do GP, condições de reação e morfologia das amostras.

De acordo com os resultados obtidos neste estudo, verificou-se que, utilizando o GP como catalisador, tanto em pó quanto em estrutura, foi possível obter biodiesel a partir da transesterificação do óleo de soja. Comparando os materiais com as mesmas razões molares, o Na.K_GP tratado a 500 °C (pó) alcançou a maior conversão (~98%). Para a estrutura 3D testada na reação (3D_Na_GP1, 110 °C) foi observada uma conversão, porém menor (~41%) em relação ao Na.K_GP, mesmo em sua versão em pó (~53%). Para constatar a eficiência de conversão das outras estruturas (3D_K_GP1, Na.K_GP), mais estudos são necessários.

INDEX OF FIGURES

INDEX OF TABLE

1. INTRODUCTION

Energy is described as the ability to do work. There are several sources of energy in nature and they can be classified as renewable, for example sun, wind, biofuels, or non-renewable, as fossil fuels (coal, diesel, natural gas), which have a higher concentration of energy, therefore they are easier to use and much of the industrial world, public service and transportation sectors depend on this type of energy [1].

Throughout history and with the Industrial Revolution natural resources began to be continuously exploited by human beings, thus increasing energy consumption and providing the growth of industrial activities and world development. On the other hand, as a consequence of the use of fossil fuels, the planet has been harmed by climate change and environmental problems [2].

The increase in the extraction of these fuels, as well as their burning, connected to the damage of the environmental balance, intensified the concern of the environmentalists and mobilized researchers to make the population aware of the danger of these environmental impacts.

The Earth's atmosphere is made up of only 1% of greenhouse gases, which are released naturally and act as a blanket for the planet, even so with the increase of human activities this blanket has become thicker, increasing the global temperature. The main gas released from the burning of fossil fuels is carbon dioxide, CO_2, which is responsible for approximately 70% of greenhouse gases, in addition to methane, nitrous dioxide, and various industrial gases. In 1997, at the third Conference of the Parties (COP) in the United Nations Framework Convention on Climate Change (UNFCCC) in Kyoto, in which environment related topics were discussed, the participating industrialized countries signed the first international protocol, establishing mandatory targets for reduction of greenhouse gas emission [3,4].

In this context, reconciling economic development with environmental preservation, a cost-benefit balance of the use of natural resources became necessary, thus giving rise to the concept of sustainable development, which proposes: "*development that meets the needs of the present without compromising the ability of future generations to meet their own needs. It contains within it two key concepts:*

· *The concept of 'needs', in particular, the essential needs of the world's poor, to which overriding priority should be given; and*

· *The idea of limitations imposed by the state of technology and social organization on the environment's ability to meet present and future needs*" [5].

Thereby, aspiring to replace diesel with renewable fuels, the search for these sources of energy has been increasing since they are inexhaustible and constantly replenished, besides releasing few greenhouse gases into the atmosphere when burned in engines.

To obtain biodiesel through the transesterification reaction, a source of triglycerides is required, which may be from edible or non-edible oils, animal fat, and algae; an alcohol, the most commonly used are methanol or ethanol; and a catalyst, which may be homogeneous or heterogeneous. Homogeneous catalysts are those that dissolve in the reagents and the reaction has only one phase, different from the heterogeneous catalysts that are in a distinct phase of the reagents and products, but they provide a favorable surface for the reaction.

Triglycerides have been highlighted as a raw material for a renewable energy source with the great potential to replace petroleum diesel. Among these fuels a promising alternative is biodiesel, which can be derived from vegetable sources such as soybean, cottonseed, palm, peanut, rapeseed/canola, sunflower, safflower, coconut, animal fats as well as exhausted oils, and it can be used directly in diesel engines or mixed in various ratios with petroleum diesel.

In industries, the most widely used method to obtain biodiesel is the transesterification reaction using NaOH or KOH as the homogeneous catalyst, which is in the same phase as the triglyceride and methanol. Although there are already satisfactory results in relation to the biodiesel yield using homogeneous catalysts, there are still drawbacks, such as the need for a post-treatment for the purification of biodiesel, besides the sensitivity to water and the content of free fatty acids. On the other hand, heterogeneous catalysts have some advantages, such as non-corrosive, recyclable, easy separation and recovery, therefore the production of biodiesel using heterogeneous catalysts have been extensively studied [6-10].

Among the types of heterogeneous catalysts, alkaline solids are more used than acidic solids due to their higher reaction activity [11]. Many alkaline solids have shown

good activity performance for biodiesel production, as well as metal oxides, metal hydroxides, metal complexes, hydrotalcites and zeolites [12-14].

Geopolymer is a synthetic material with a chemical composition comparable to that of a zeolite, it is obtained by synthesizing an aluminosilicate with a highly concentrated alkali hydroxide or silicate solution providing the formation of a 3D-continuous network and it can consolidate at low and uniform temperature. The microstructure of the geopolymer is temperature dependent: an amorphous structure is present at low temperature and heat treating at temperatures above 500 °C form semi-crystalline structures [15].

This material has been studied as a viable option for Portland cement due to its mechanical, chemical and physical properties [16-17], but in addition, the geopolymer has also been studied as adsorbents, filters, support material and catalyst [18-22].

In this work, it was investigated the biodiesel production by transesterification of soybean oil with methanol, using geopolymers as heterogeneous catalysts.

2. THE AIM OF THE PROJECT

This project proposes the development of a heterogeneous catalyst for biodiesel production by the transesterification reaction of soybean oil based on a cellular porous geopolymer.

This work is divided into two parts, the main aim of the first one is to verify the use of geopolymer as a heterogeneous catalyst to be used in the transesterification reaction to obtain biodiesel and the second one is to develop 3D-printed lattices to be used as a heterogeneous catalyst in the production of biodiesel.

2.1. SPECIFIC AIM OF THE PROJECT

To characterize the geopolymer in relation to its physical properties, mechanical properties, morphology and permeability.

To carry out the alkaline transesterification of soybean oil using the geopolymer as catalyst, quantify the product obtained (biodiesel) and the loss of alkali leached from the catalyst to the product.

3. LITERATURE OVERVIEW

3.1. FUEL

Coal, natural gas and petrochemical products have a key role in the industrial economy of a developing country. For years diesel fuel has been used for transportation of industrial products, agriculture and construction sector [23].

Possibly the diesel engine became popular due to the possibility of using a part of the petroleum-oil that was previously considered waste of gasoline production, later, diesel engines were widely used in the applications that require more engine work due to durability and efficiency of diesel and high torque capacity [24].

Fuels that move the engines are generally made of petroleum-derived materials that can be easily burned with release of large amounts of heat without being subjected to stress [25].

Petroleum-oil is made up of hundreds of chemicals, from methane to asphalt. Its composition is quite varied:

- Hydrocarbons: 83% to 87% carbon and 11% to 15% hydrogen
- Nitrogen: 0% to 0.5%
- Sulfur: 0% to 6%
- Oxygen: 0% to 3.5%

These compounds are usually divided into:

- Paraffins: linear open chain hydrocarbons, C_nH_{2n+2}
- Isoparaffins: open chain branched chain hydrocarbons, C_nH_{2n+2}
- Olefins: unsaturated, open chain hydrocarbons, C_nH_{2n}
- Naphthenes: cyclic and saturated hydrocarbons, C_nH_{2n}
- Aromatic: hydrocarbons with benzene rings, chain C_nH_{2n-6}

The atoms that usually define the quality of the fuel are the carbon, hydrogen and oxygen atoms, whereas the sulfur and nitrogen atoms are undesirable for obtaining fuel because in the combustion reaction of the sulfur they form polluting gases (SO_2, SO_3) and industrial combustion of nitrogen do not present combustion reactions with energy release. The combustion reaction (Equation 1 and 2) can be denominated as the conversion of the potential energy of a fuel into useful thermal energy, reaction that occurs between carbon and hydrogen atoms with oxygen atoms,

releasing energy in various forms, including heat, besides producing compounds like CO_x and H_2O [25,26].

$$C + O_2 \leftrightarrow CO_2 \quad (1)$$

$$H_2 + \tfrac{1}{2} O_2 \leftrightarrow H_2O \quad (2)$$

Cetane number makes it possible to evaluate the flammability characteristic of fuels for diesel engines, so the higher the cetane number of a fuel, the better the combustion in a diesel engine.

Fossil fuels such as coal, natural gas and petroleum-oil are non-renewable energy sources because they come from finite natural resources, due to their long replenishment time in nature.

It is inevitable that the obtention of these resources reaches a peak of maximum extraction, and then begins to decline, this peak can be explained through two essential factors: geological and economic. The geological factor simply shows that once the extraction of the most accessible reserves begins, the rate of production of fuels increases until the moment when it will become increasingly difficult to obtain these natural resources, and its geographical distribution is quite discontinuous in the world. Regarding the economic factor, once the difficulty of extraction increases, product costs will also increase, favoring the transition from non-renewable energy sources to alternative energy sources [27,28].

In addition to these factors, it should be considered the harmful effects that the extraction and use of these fossil fuels cause to the environment, further encouraging the transition to alternative, renewable, efficient, sustainable and economical sources.

Aiming at improving the environment and by encouraging the use of energy from renewable sources, Directive 2009/28/EC of the European Parliament and of the Council has proposed some targets for 2020: reducing greenhouse gas emissions; improve energy efficiency by 20%; 20% of EU energy should be from renewable sources [29].

3.2. BIOFUEL

Biofuels are renewable energy sources that can be constantly replenished for use, either through man or nature, and are inexhaustible as long as the limitations of extraction and use are respected. The energy efficiency of these fuels depends on the raw material, the climate and the production technique.

The advantages of biofuels over petroleum fuels are:

- they can be produced from plants that absorb CO_2 and allow the production of fuels that do not emit greenhouse gases, the main responsible for global warming;
- they enable the closing of the carbon cycle;
- they are sustainable, due to the biodegradable property;
- their handling and storage are safer [30].

There are three types of biomass used as a source of energy: solid (wood charcoal and organic vegetable and animal waste), liquid (ethanol, biodiesel and other liquids obtained through chemical or biological processes) and gaseous (obtained by industrial or organic waste, such as biogas).

Biofuels are classified into three categories: first, second and third generation, based on the chemical nature of biomass and the conversion technology used for their production [30,31].

First-generation biofuels are obtained through food-crop feedstock and are usually made from sugar, starch or vegetable oils. Ethanol and biodiesel are the most common examples of this category. Ethanol can be obtained by the fermentation of carbohydrates using yeasts containing enzymes that promote the conversion of sugars such as glucose ($C_6H_{12}O_6$) into ethyl alcohol. Biodiesel can be obtained through the transesterification reaction of vegetable oils using catalysts (enzymatic, acid or alkaline) and short chain alcohol (methanol or ethanol).

Second-generation biofuels are obtained through non-food raw materials, i.e. lignocellulosic biomass, as well as discarded biomass from food processing and agricultural waste. Syngas, methane and natural gas are examples of this category. Syngas (synthesis gas) can be obtained by gasification and can be converted into fuel by catalytic processes. Methane and natural gas can be obtained by anaerobic digestion.

Third generation biofuels are obtained through marine resources such as macro- and micro-algae. The fuel can be obtained by refining the oil produced by the algae. This biomass can be produced both in photoelectric bioreactors and in lagoons with open channels.

3.2.1. The biodiesel

3.2.1.1. Historic

Rudolf Diesel (1858-1913), the inventor of the motor that takes his name, during the Paris Exhibition in 1900 presented an engine that used peanut oil for its operation. This engine, which was built to run on oil, was operated with vegetable oil without any modification. However, some factors have prevented its long-term use in diesel engines. The kinematic viscosity of these oils is about an order of magnitude greater than that of conventional petroleum-derived diesel. The use of vegetable oil as fuel presents difficulties of injection in the combustion chambers of the engine due to its high viscosity, besides causing operational problems as carbon deposit in the cylinders and the injectors [24].

Walton, J. [32] was the first to propose an explanation for the problem, saying that it would be necessary to separate the triglycerides and control the residual fatty acid to obtain better efficiency of the vegetable oils as fuel. Although he did not mention the esters, his statements suggest what is nowadays called biodiesel.

In this context, a research conducted to the discovery of transesterification, which is a chemical reaction where a triglyceride reacts with an alcohol in the presence of a catalyst, resulting in esters of fatty acids and glycerol.

In 1937, the Belgian scientist Charles G. Chavanne published and patented the first report on biodiesel, patent 422,877 (Appendix A), which reports the obtention of ethyl esters of palm oil through acid-catalyzed transesterification used as fuel. One year after the patent, the fuel obtained from the transesterification of vegetable oil is used, with satisfactory performance, in a bus on the route between Brussels and Leuven [24].

In Brazil, the oil crisis in the 1970s together with the sugar crisis propelled the “Pro-alcohol” program. Its aim in the first phase was to mixture anhydrous alcohol into

the gasoline, whilst in the second phase the aim was the production of hydrated alcohol to be used in engines adapted to that fuel. In the 1990s, the “Pro-oil” program, the national program for vegetable oils for energy production, was implemented and in 2005 the National Program for the use of biodiesel was launched with the initial purpose of introducing biodiesel into the Brazilian energy sector, to achieve social inclusion and regional development [33].

In 2008, the mixing of pure biodiesel with diesel oil became mandatory. Between January and June 2008, the blend was 2%. Between July 2008 and June 2009, it was 3%, between July and December 2009 4%. Between July and October 2014, the content was 6% and between November 2014 and February 2017 it was 7%. This mixture of biodiesel and diesel oil, besides strengthening the Brazilian industry and reducing the use of fossil fuels, aimed to increase the Brazilian biodiesel commercialization. From March 2017, the mix became 8% in volume, according to Law 13.263/2016 [33]. Figure 1 shows the evolution of biofuel in Brazil.

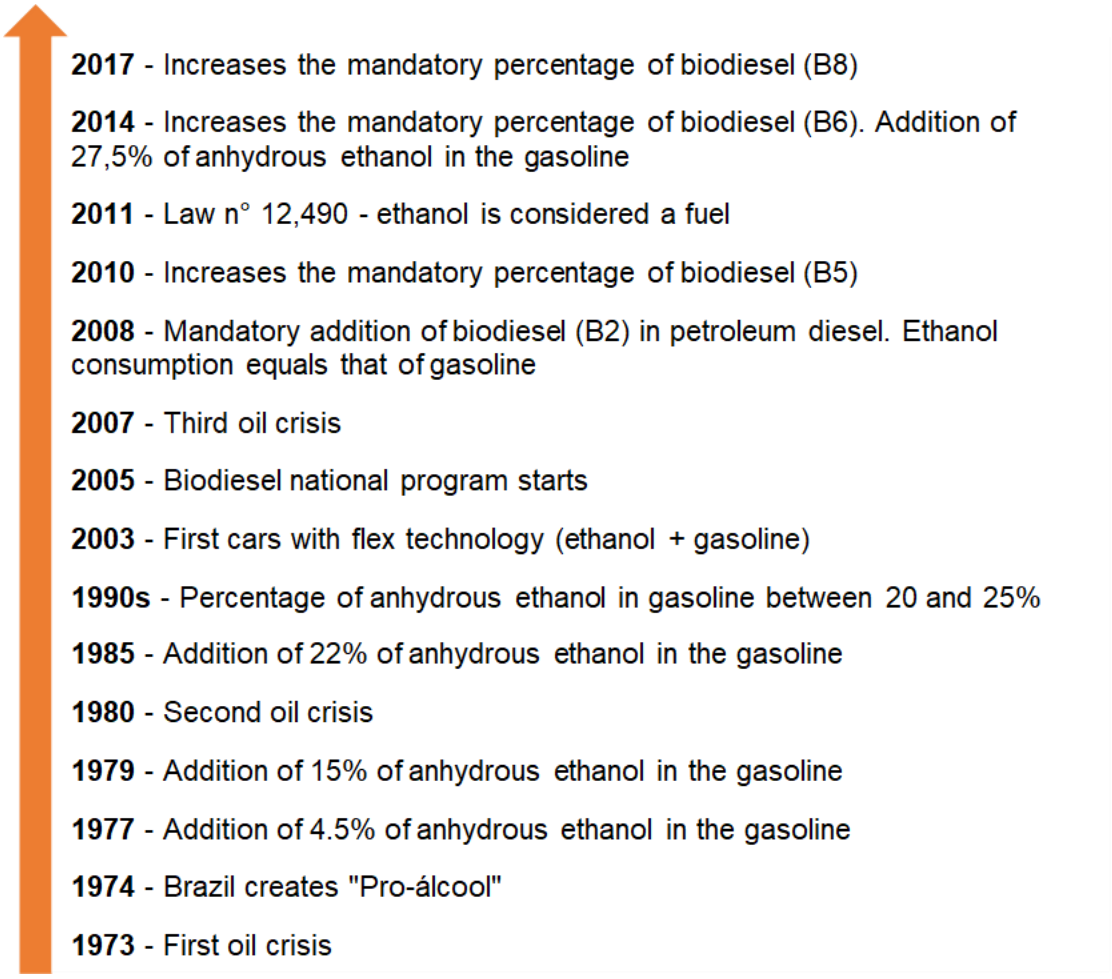

Figure 1. Evolution of biofuel in Brazil. (Adapted from [33])

In Brazil, the specification and determination of biodiesel characteristics commercialized by authorized economic agents are governed by ANP Resolution n°45 (2014), and by the standards of the Brazilian Association of Technical Standards (ABNT). In the United States the standards for biodiesel are determined and set by the American Society for Testing and Materials (ASTM D-6751) and in Europe by the European Committee for Standardization (EN 14214).

According to ANP data, Brazil is among the largest producers and consumers of biodiesel in the world, with an annual production in 2017 of approximately 4.3 billion of liters. In addition to Brazil, the United States, Germany and France are among the largest biodiesel producers in the world.

3.2.1.2. Definitions and characteristics

Biodiesel is a biodegradable and renewable source of energy, it is defined as alkyl esters fatty acids of long carbon chain derived from vegetable oils or animal fats, obeying the requirements of the specification standards. Biodiesel blend (Figure 2) is defined as a mixture of diesel fuel with biodiesel, it is denominated as BXX, where XX represents the volumetric percentage of biodiesel in the mixture (e.g. B20 is 20% biodiesel and 80% diesel oil [34].

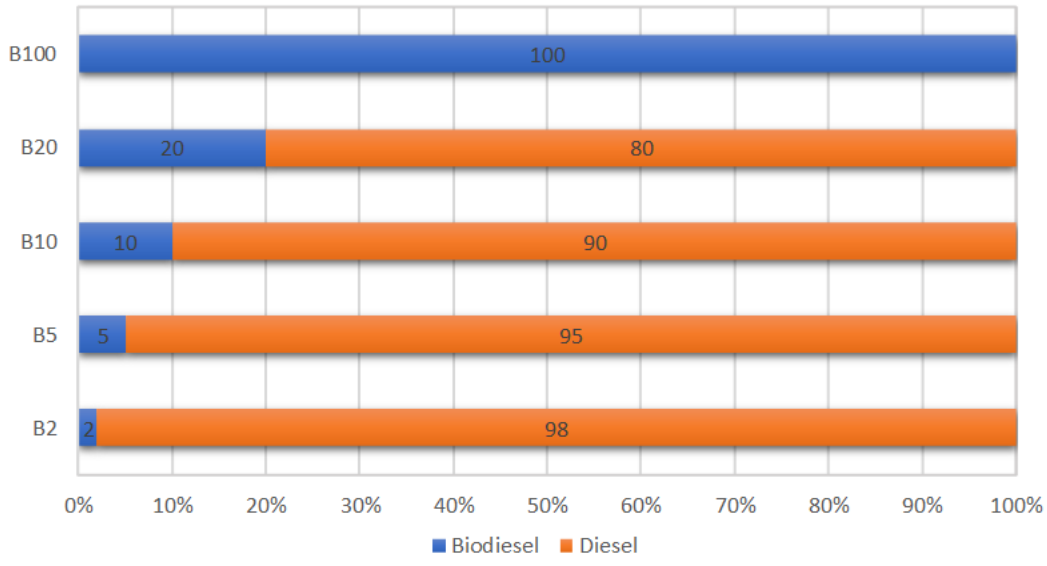

Figure 2. Compositions of biodiesel blends.

The raw material for the production of biodiesel can be divided in four groups: edible vegetable oils (e.g. soybean, sunflower, rape, palm oil) and non-edible oils (e.g. jatropha), animal fats, and oils produced by algae. For all raw materials there are pros and cons. In the case of edible vegetable oil, the big problem is to supply the demand for oil as a food along with its usage for biofuel production. Animal fat has a lower price, however there is great limitation of availability, besides its high melting point. The waste oils have much lower value than edible oils, but due to contamination by impurities of the cooking process, it is difficult to control the biodiesel conversion. Algae oils still require advances in their extraction technology, so they can be used as raw materials [35-38].

Fatty acid methyl esters (FAME) are accepted as biodiesel in the American, Brazilian and European standards, different from fatty acid ethyl esters (FAEE), which are not accepted in the European standard [35].

Quality standards comprise the production, marketing and storage of biofuel to maintain a standard of the product sold.

The parameters can be divided into two groups: general parameters, which can also be used by other fuels, and specific parameters of methyl esters of fatty acids, such as chemical composition and purity. Most of the parameters, such as the flash point, viscosity, cloud point, cetane number, sulfur content, ash content, water content and glycerol content, have similar values in the different standards (US, EU, Brazil) and they can be considered key biodiesel properties.

Table 1 shows the values of the parameters in three patterns: European American and Brazilian.

Table 1. Comparison of biodiesel standards: American, European and Brazilian.

Parameters	USA	EU	Brasil
Flash point (°C)	min. 130	min. 120	min. 100
Viscosity at 40°C (cSt)	1.9 - 6	3.5 - 5	-
Sulphated ash (%mass)	max. 0.02	max. 0.02	max. 0.02
Sulphur (%mass)	min. 0.001	min. 0.001	
Cloud point (°C)	-	-	-
Cetane number (-)	min. 47	min. 51	-
Water content (vol.%)	max. 0.05	-	max. 0.05
Free glycerine (%mass)	max. 0.02	max. 0.02	max. 0.02
Total glycerine (%mass)	max. 0.24	max. 0.25	max. 0.38
Destilation temperature (°C)	<360	-	<360

The flash point is an important parameter for the transport and storage of the fuel because it measures its flammability and corresponds strictly to the methanol content. The flash point of biodiesel is higher than the set limits but can be decreased by increasing residual alcohol [36].

Viscosity is a characteristic that must be considered, because it may affect engine performance and it is related to the unreacted triglyceride content. The kinematic viscosity of biodiesel is higher than that of diesel and low temperatures can compromise engine integrity [37].

The cloud point corresponds to the initial crystallization temperature of the fuel, it negatively influences the engine power system as well as the fuel filter, especially in low temperature conditions. The melting point of biodiesel depends on the length of the carbon chain and the degree of saturation [37].

The ash content is defined as the amount of impurities of inorganic matter, as catalyst residue. These impurities are oxidized during combustion to form ashes that settle on the engine and obstruct the filter [36].

As the density, cetane number and sulfur content are mainly linked to the type of vegetable oil and are not influenced by the production methods or purification steps.

Sulfur content is the indicator of the sulfur concentration in the fuel. It is undesirable, due to its corrosive action and the formation of toxic gases such as SO_2 and SO_3, which occurs during the combustion of the product. The biodiesel has a low amount of sulfur and excellent lubricity and it can play a role of additive, correcting the diesel lubricity.

Cetane number is a primordial indicator of fuel quality and it is related to the ability of a fuel to combust under certain temperature and pressure conditions. The longer the carbon chains of fatty acids and the more saturated the molecules, the higher the cetane number of the fuel is. Biodiesel has a higher cetane number than diesel [35,37].

Water content is the amount of water that biodiesel possesses after the washing and evaporation step, when produced using homogeneous catalysts. Due its high hygroscopy, biodiesel can absorb water during storage and, once the solubility limit is exceeded, the water separates from the fuel forming a layer at the bottom of the storage tanks. In addition, large amounts of water are related to the hydrolysis reaction, which converts esters (biodiesel) to free fatty acids [35,36].

The total glycerol content is the sum of free and bound glycerol, determining the amount of mono-, di- and triglycerides present in biodiesel. This parameter depends mainly on the transesterification process of the vegetable oil, the use of specific catalysts and the reaction conditions [36].

From the environmental point of view, biodiesel is an environment friendly fuel, non-toxic and biodegradable. It has a clean combustion with low emission of gases. Figure 3 shows that with the increase of biodiesel added to diesel the emissions of carbon monoxide (CO), hydrocarbons (HC) and particulate matter (PM) decrease proportionally.

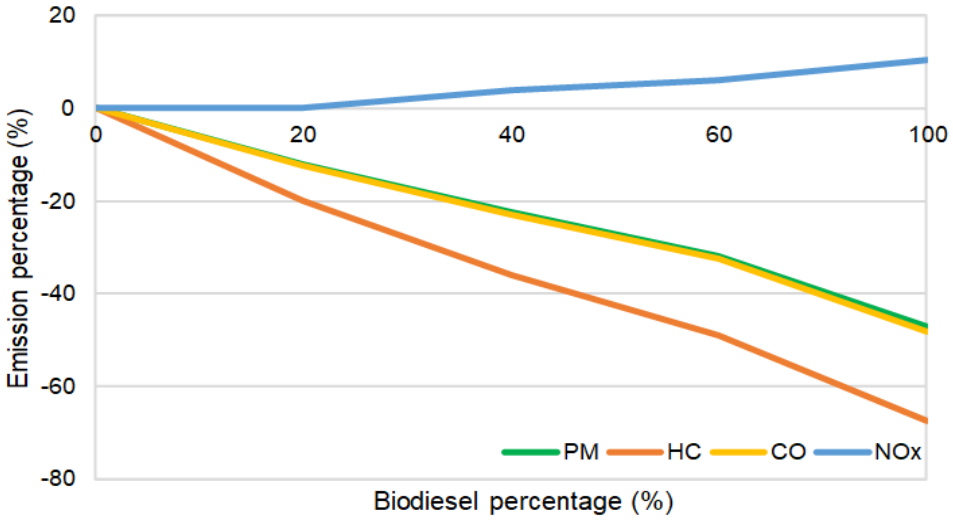

Figure 3. Decrease in the percentage of gases emitted in relation to biodiesel blends. (Adapted from [34])

3.2.1.3. Production of biodiesel

Most vegetable oils contain 90-98% of triglycerides and a small fraction of mono- and diglycerides, and generally they contain free fatty acids, phospholipids, water and impurities. For the production of biodiesel, crude vegetable oil should initially be considered for better quality and conversion efficiency [11]. Table 2 shows the chemical composition of some oils used for the production of biodiesel.

Table 2. Composition of fatty acids of vegetable oils. (Adapted from [11])

Acid name	Chemical formula	Oil				
		Soybean	Sunflower	Rapeseed	Palm	Jatropha
Lauric	12:0	-	-	-	0.1	-
Myristic	14:0	-	-	-	1	0 - 0.1
Palmitic	16:0	11	6.08	3.49	42.8	14.1 - 15.3
Palmitoleic	16:1	-	-	-	-	0 - 1.3
Stearic	18:0	4	3.26	0.85	4.5	3.7 - 9.8
Oleic	18:1	23	16.93	64.4	40.5	34.3 - 45.8
Linoleic	18:2	54	73.73	22.3	10.1	29.0 - 44.2
Linolenic	18:3	8	-	8.23	0.2	0 - 0.3
Arachidic	20:0	-	-	-	-	0 - 0.3
Behenic	20:1	-	-	-	-	0 - 0.2

The triglycerides have in their structural formula three groups of the organic function ester (R-COO-R). The carbon chains of each radical can have different carbon numbers and degree of unsaturation, so the chemical activities of triglycerides depend on these groups.

Transesterification of vegetable oils is the most commercially used method to obtain biodiesel. In this chemical reaction the triglyceride reacts with an alcohol, in the presence of a catalyst, producing esters and glycerol. Alcohols are generally primary and secondary monohydric aliphatic ones, having 1 to 8 carbon atoms, such as methanol, ethanol, propanol and butanol, but the most commonly used are methanol or ethanol, since they are more polar and have short chains and it is directly related to the low viscosity, besides the methanol have low price and great availability [39-41].

To complete, stoichiometrically, the transesterification reaction requires 3:1 molar ratio of alcohol:triglyceride. In practice, the ratio needs to be higher to shift the equilibrium to the maximum yield of esters (e.g. 6:1) [40].

Figure 4 shows the reversible reactions that occur in the transesterification reaction of vegetable oil to obtain methyl esters.

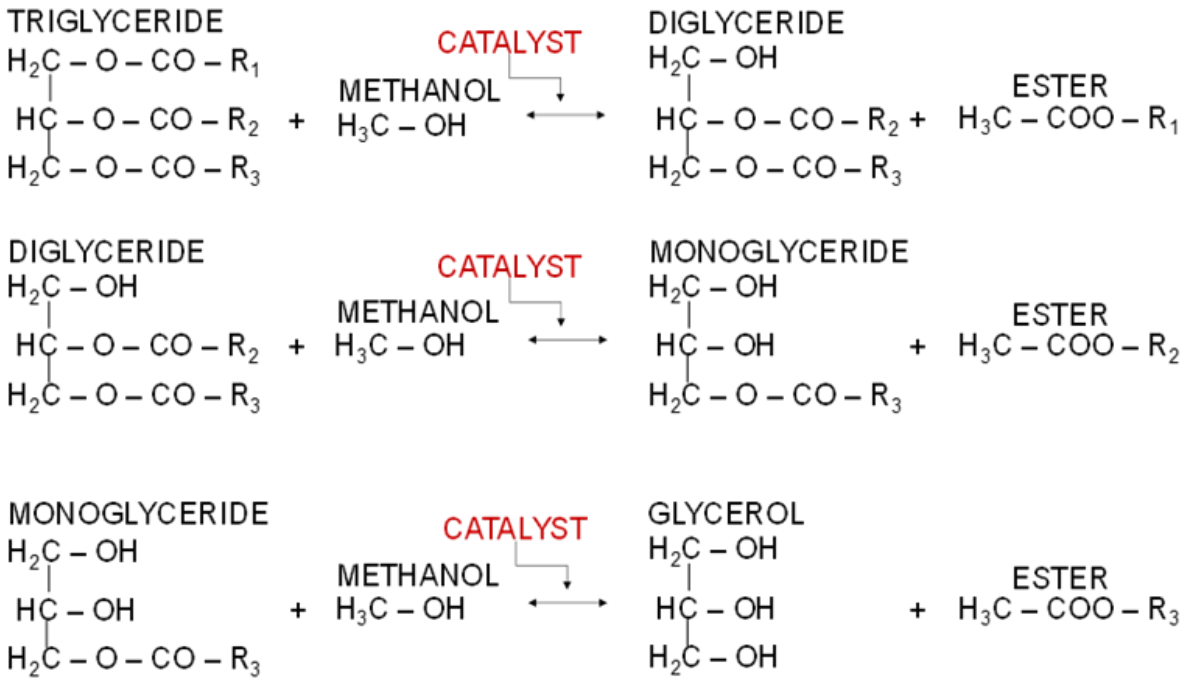

Figure 4. Reversible and consecutive step-by-step reactions to obtain biodiesel.

3.2.1.4. Catalysts

A catalyst is usually used to increase the speed and yield of the reaction, and, since the reaction is reversible, excess alcohol is used to shift the balance towards the products.

The transesterification reaction can be done using homogeneous or heterogeneous catalysts, which can be divided into three groups: acid, alkaline or enzymatic. The homogeneous catalysts act in the same phase as the reaction mixture, whereas the heterogeneous catalysts act at a different phase of the mixture. Most of the published work shows advantages for the alkaline catalysis process, where higher yield and selectivity are observed, besides presenting smaller problems related to the corrosion of the equipment [40,41].

3.2.1.4.1. Homogeneous catalysts

In general, the transesterification reaction of vegetable oils is carried out in presence of basic or acidic homogeneous catalysts. The basic catalysts are generally used with crude vegetable oils because they have a lower content of free fatty acids, since the high free fatty acids content can cause saponification, making it difficult to separate the products. NaOH, KOH, CH_3ONa and CH_3OK are the most common catalysts of this category, they can be used in low temperature (40 - 60 °C), low reaction time (30 - 90 min) and atmospheric pressure processes. Acid catalysts are usually used with food waste oil. This category includes H_2SO_4, H_3PO_4, HCl, however, they are not as popular as the basic catalysts because the reaction using them is 4000 times slower [6,42,43].

The commercial biodiesel production is dominated by the application of homogeneous catalysts due to their easy use and shorter conversion time. However, biodiesel needs washing and neutralization, resulting in a large excess of residual water. These limitations can be avoided by using heterogeneous catalysts; several industrial processes have already obtained promising results using these catalysts in the biodiesel production.

3.2.1.4.2. Heterogeneous catalysts

Many industrial processes use heterogeneous catalysts, reducing energy consumption and facilitating the separation of the catalyst from the reaction mixture, also reducing the cost of the process, as well as reducing problems related to equipment corrosion.

The use of these catalysts in the production of biodiesel does not cause the formation of soaps, and can be used in batch reactors, continuous stirred tank reactors and fixed bed reactors.

Solid acids are most frequently used in the petrochemical industry especially for organic reactions. They favor both esterification and transesterification, besides the advantage of being tolerant to water and free fatty acids, however, the transesterification reaction has a slow reaction rate. Options for acid catalysts are transition metal oxides such as zirconia, titanium oxide and zinc oxide [6].

Basic solids are used in the synthesis of biodiesel because of their higher activity compared to acids. These can be subdivided into other groups: single metal oxides, doped and mixed metal oxides, zeolites, salts supported on alumina, supported alkali, alkaline earth metal oxides and hydrotalcite [6].

Zeolite is a material with a microporous structure and has been considered a heterogeneous catalyst due to its defined pore system, high surface area and high stability. However, this material presents limitations when it acts in reactions with large molecules, triglycerides, in the case of biodiesel production, especially in liquid phase systems. The diffusion of the reactants at the catalytic sites has been improved by increasing the pore size of the zeolites, decreasing the size of the zeolite crystal or forming mesopores within the microporous crystals [44,45].

3.3. GEOPOLYMERS

Geopolymer is part of the group of ceramic materials that are chemically obtained, the reaction occurs between an aluminosilicate powder (e.g. metakaolin, flay ash) and an alkaline activator, which may contain hydroxides, silicates, aluminates, carbonates or sulfates, or combination of them. The reaction of these reagents produces a material known as geopolymer, which has a continuous three-dimensional network, a variable microstructure, from amorphous to semi crystalline, and a chemical composition similar to zeolites [46].

The term "geopolymer" is adopted in the 70s by scientist and engineer prof. Joseph Davidovits, this material has a bi- or tri-dimensional polymeric structure and is classified into: sialate; sialate-siloxo; sialate-disiloxo; sialate link; according to the atomic ratio Si:Al, with chains or networks of molecules connected through covalent bonds. The term “sialate” corresponds to a silicon-oxygen-aluminum bond (Si-O-Al-O) and “siloxo” corresponds to a silicon-oxygen-silicon bond (Si-O-Al-O-Si-O) [15]. The lower the Si: Al ratio, the more rigid is the 3D network of the material and the lower its polymeric character. Figure 5 shows examples of molecular structures regarding Si:Al ratio.

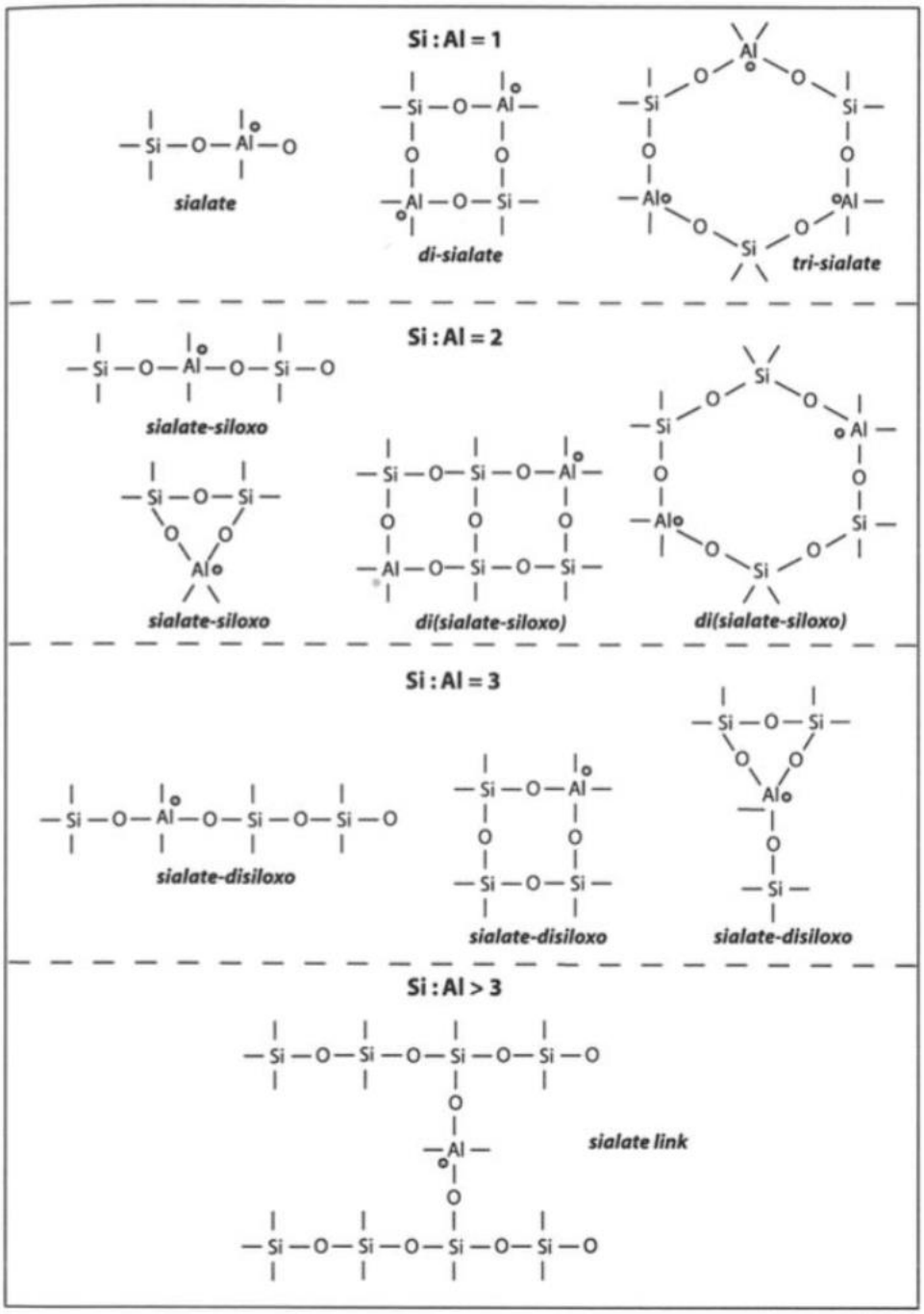

Figure 5. Classification of the aluminosilicate material in relation to the atomic ratio Si:Al [15].

Phosphate-based geopolymer is another variety of geopolymer, it is produced through an acid-base reaction between an inorganic oxide and phosphoric acid. Synthesis procedure is what best distinguishes silicate-based geopolymers, which require a basic environment, and phosphate-based geopolymers.

Geopolymerization occurs initially with the dissolution of a solid aluminosilicate oxide in an alkali metal silicate solution, forming ortho-sialate molecules, then gel formation occurs (polycondensation in oligomers), and finally the structure reorganizes until complete solidification. The mechanism of the reaction is shown in Figure 6. The kinetics of Na-poly (sialate-siloxo) geopolymerization are different from K-poly (sialate-siloxo) ones in relation to the different sizes of Na^+ and K^+ cations (K^+ is bigger than Na^+): generally, Na^+ favors alkaline hydrolysis, while K^+ favors polycondensation [46,47].

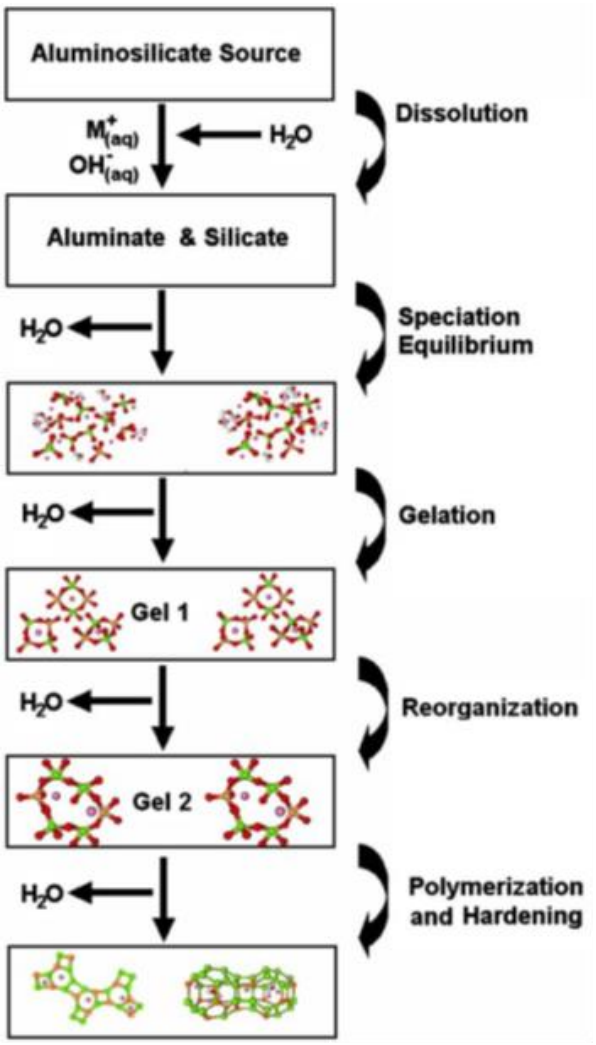

Figure 6. Mechanism of the geopolymerization reaction [48].

According to Davidovits [15], there are parameters that must be controlled to ensure that the geopolymerization occurs, which influence durability and mechanical strength of the material. The curing temperature should be in the range of 30 to 90 °C

and the cure time between 6 and 96 hours, furthermore, the molar ratios of the present species should respect the following ranges:

$(Na_2O; K_2O) / SiO_2$	=	0.25 a 0.48
SiO_2 / Al_2O_3	=	3.3 a 4.5
H_2O / Al_2O_3	=	10.0 a 25.0
$(Na_2O; K_2O) / Al_2O_3$	=	0.8 a 1.6

Geopolymers are mainly studied as an alternative to Portland cement due to their more ecological nature. In addition, they can be used as low-cost ceramic, ceramic matrix for composite, structures for fire protection, host matrix in waste encapsulation. Applications such as inorganic support material, adsorbent, filter and catalyst, where the material needs more complex forms and can take advantage of its zeolitic characteristic (intrinsic mesoporosity) are less exploited.

The possibility of using direct 3D printing method for geopolymer structures production makes the material very interesting as catalysts, since it is possible to accurately design the desired shape, besides controlling the drop pressure and the fluids dynamics within the structure.

3.4. ADDITIVE MANUFATURING - DIRECT INK WRITIING

At the beginning of the “Rapid prototype” development, the flexibility in the design was the main aim, while over the years the physical properties of the produced parts began to be more prominent in the studies and this terminology changed to additive manufacture. AM is defined by the ASTM (American Society for Testing and Materials) as “process of joining materials to make objects from 3D model data, usually layer upon layer, as opposed to subtractive manufacturing methodologies, such as traditional machining” [49].

Although the media uses the term "3D printing" for all AM processes, there is a classification that varies with the manufacturing method of the layers and the individual processes are different depending on the material and the technology used. According to ASMT, AM is divided in seven groups: material extrusion (e.g. direct ink writing (DIW) or robocasting, fused deposition modeling (FDM)); material jetting: (e.g. direct inkjet

printing, DIP); binder jetting (e.g. powder based 3D printing); sheet lamination: (e.g. laminated object manufacturing, LOM); vat photopolymerization: (e.g. stereolithography (SL)); powder-bed fusion: (e.g. selective laser sintering/melting (SLS/SLM); selective electron beam melting) and direct energy deposition.

AM can also be divided in relation to the type of printing: direct and indirect. Direct means that the material is deposited only in the shape of the desired object, indirect means that, it is initially deposited a layer of material, in which the cross section of the object will be inscribed, after the end of the impression of all layers, the excess material surrounding the object is removed. The advantages of direct printing are the following: there is no excess material, there is not much geometric limitation, it is possible to print using multimaterials. For indirect printing the advantages are the following: the excess deposited material serves as support for the next layers, printing is faster [50].

These techniques can process ceramic, polymeric and metallic materials, and can be used in the form of powder, liquid, paste, filament or sheet.

DIW, initially called “Robocasting”, is a layer-by-layer printing technique, in which the material is continuously extruded into filament form through a nozzle and undergoes rapid solidification while maintaining the desired shape.

The DIW requires a Bingham pseudo plastic fluid which has a rising shear rate decreasing the viscosity and has an initial yield stress, therefore, there is no need for high pressure to extrude the ink and maintain the shape of the filament deposited even supporting back layers. A reversible gel has this behavior and it may be obtained by flocculating a ceramic slurry or by adding polymeric binder and plasticizer in the ceramic ink, or by adding gelling additives [51].

In order to print geopolymeric inks, it must be considered their continuous geopolymerization reaction, which modifies their rheology until the extrusion is no longer possible. The 4D printing considers time as fourth dimension and geopolymeric inks may be an option as their reaction can be controlled over time [52].

4. MATERIALS AND METHODS

This work was divided in two main parts: in the first part the geopolymer powder was used and in the second part was used a 3D-printed geopolymer structure, both as catalysts in the transesterification reaction to produce biodiesel.

4.1. GEOPOLYMER POWDER

For the geopolymer powders, three investigations were performed. Initially, the sodium-based geopolymers (Na_GP1 and Na_GP2) were used with constant molar ratio of alkali, changing the molar ratio of water, as shown in Table 3.

Table 3. Molar ratios of the samples for the first investigation.

Ratio	Na_GP1	Na_GP2
SiO_2 / Al_2O_3	4.0	4.0
Na_2O / Al_2O_3	1.3	1.3
H_2O / Al_2O_3	18.5	14.0

The second investigation was done comparing the sodium-based (Na_GP1), potassium-based (K_GP1) and sodium.potassium-based (Na.K_GP) geopolymers, keeping the alkali and water ratios constant, as shown in Table 4.

Table 4. Molar ratios of the samples for the second investigation.

Ratio	Na_GP1	K_GP1	Na.K_GP
SiO_2 / Al_2O_3	4.0	4.0	4.0
Na_2O / Al_2O_3	1.3	-	0.65
K_2O / Al_2O_3	-	1.3	0.65
H_2O / Al_2O_3	18.5	18.5	18.5

In parallel, using potassium-based geopolymers (K_GP1, K_GP2 and K_GP3), the influence of the alkali molar ratio was investigated keeping the water molar ratio constant, as shown in Table 5.

Table 5. Molar ratios of the samples for the third investigation.

Ratio	K_GP1	K_GP2	K_GP3
SiO_2 / Al_2O_3	4.0	4.0	4.0
K_2O / Al_2O_3	1.3	1.35	1.0
H_2O / Al_2O_3	18.5	18.5	18.5

All the geopolymers were prepared using metakaolin (Argical 1200S, Imerys S.A., Paris, France) as aluminosilicate source mixed with an activating alkaline solution.

4.1.1. Production of geopolymer

For the sodium-based geopolymers, an activating solution was prepared using sodium silicate solution (SS2942, Ingessil S.r.l., Montorio, Italy), sodium hydroxide pellets (NaOH, Sigma–Aldrich, Steinheim, Germany) and distilled water.

For the potassium-based geopolymers, an activating solution, composed by potassium silicate (205K, Tillmanns, Milan, Italy), potassium hydroxide pellets (KOH, Sigma–Aldrich, Steinheim, Germany) and distilled water, was prepared.

For the sodium.potassium-based geopolymer, an activating solution was prepared mixing potassium silicate (205K, Tillmanns, Milan, Italy), potassium hydroxide pellets (KOH, Sigma–Aldrich, Steinheim, Germany), sodium hydroxide pellets (NaOH, Sigma–Aldrich, Steinheim, Germany) and distilled water.

The activating alkaline solutions were prepared at least 24 h in advance and were stored at 4 °C. The composition of the metakaolin and of the sodium and potassium silicates is summarized in Table 6.

Table 6. Compositions of reagents.

Reagent	SiO_2 (wt.%)	Al_2O_3 (wt.%)	Na_2O (wt.%)	K_2O (wt.%)	H_2O (wt.%)
Metakaolin	55	39	<1	-	-
Na silicate	28.35	-	9.77	-	61.88
K silicate	57.26	-	-	27.24	15.5

All the types of geopolymers were prepared using a mixer (Qualtech Products Industry, Manchester, UK), with a 50 mm stainless steel 316 paddle, alkaline resistant.

The metakaolin powder was added to the activating alkaline solution under mechanical stirring for 10 min and 1000 rpm at room temperature, then the slurry was poured in a covered plastic mold and placed in an oven at 75 °C for 2 days to complete the geopolimerization reaction, afterward the geopolymer blocks were ground and sieved to a particle size between 45 to 125 µm.

Finally, the geopolymer powders were dried at 110 °C overnight, to release the remaining water and then they were heat treated for 1 h in static air (heating rate = 10 °C/min) at three different temperatures (300 °C, 500 °C and 700 °C).

The process flowchart used to produce geopolymer is shown in Figure 7.

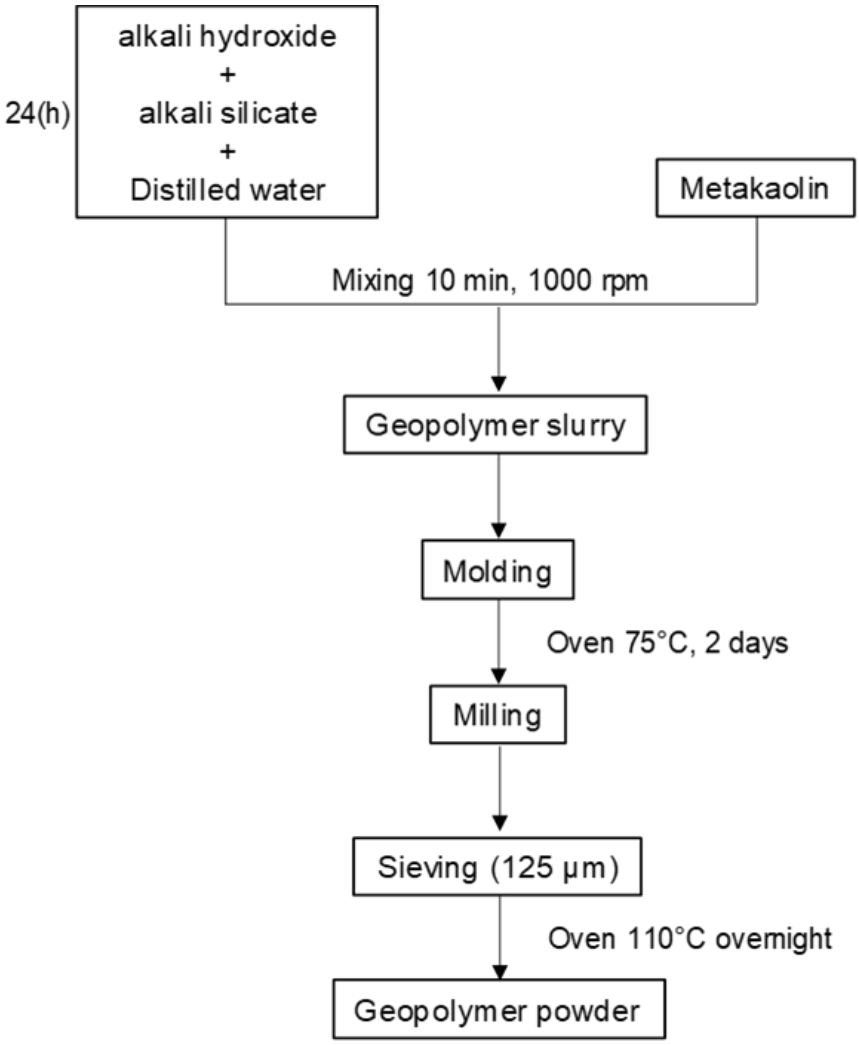

Figure 7. Schematic diagram of the process to produce geopolymer.

4.1.2. Characterization of geopolymer powder

All the types of geopolymer powders were characterized by X-ray diffraction, thermogravimetry and differential scanning calorimeter analysis, Brunauere, Emmette, Teller (BET) and Barrett, Joyner, Halenda (BJH) methods and density analysis.

4.1.2.1. X-ray diffraction (XRD)

X-ray diffraction (XRD) pattern of the pure metakaolin and the heat-treated geopolymers was investigated using an X-ray diffractometer (D8 Advance, Bruker Corporation, Karlsruhe, Germany) with Cu Kα radiation, operated at 40 kV and 40 mA with 0.05 ° step width, a scanning range of 10 - 70° and a scanning speed of 3 s/step.

4.1.2.2. Thermal analysis (TGA/DSC)

Thermogravimetry and differential scanning calorimeter analysis (TGA/DSC 3+, Mettler Toledo, USA) were carried out in static air from room temperature to 1400 °C with a heating rate of 10 °C/min. The analysis was conducted on the geopolymers previously ground and dried in the oven at 110 °C overnight.

4.1.2.3. Pore characterization

The specific surface area (SSA) of the samples was measured by the N_2 adsorption at liquid nitrogen temperature using the multi-point Brunauere, Emmette, Teller (BET) method in the Quantachrome Autosorb iQ (Quantachrome Instruments, Boynton Beach, Florida).

Prior to the analysis, the samples were degassed at 250 °C for approximately 17 h under reduced pressure.

After the BET data was obtained, the total pore volume, the average pore diameter, and the pore size distribution were calculated using the Barrett, Joyner, Halenda (BJH) method.

4.1.2.4. Physical properties

The true density of the geopolymers was measured by a pycnometer (Micromeritics AccuPyc 1330, Norcross, GA, USA), operating with helium gas.

All samples analyzed had a particle diameter of up to 125 μm and they were dried at 110 °C overnight.

4.2. RHEOLOGY OF GEOPOLYMERIC INKS

The study of ink rheology before the 3D printing process is crucial for fabricating structures that, when printed, have to bear their own weight with the least deformation, which gives the possibility of making lattices with unsupported filaments.

Rheological tests were carried out to evaluate the suitability of the inks for DIW printing, using a rotational rheometer (MCR 92, Anton Paar, Graz, Austria) (Figure 8) equipped with a 25 mm diameter parallel plate with a set temperature of 20 °C and a gap of 1 mm.

Figure 8. Rotational rheometer MCR 92, Anton Paar.

For fixed printing parameters, in order to evaluate the rheological behavior of the inks, the deflection value of spanning elements can be used.

Smay et al. [53] found that the stiffness of the suspended filaments increases with increasing span length, and for deflection below 5% of the filament diameter they also demonstrated that the relation in Equation 3 must be satisfied.

$$G' \geq 0.35\,\gamma \left(\frac{L}{D}\right)^4 D \tag{3}$$

Where G' is the shear storage modulus of the ink, γ is the ink specific weight (ρ_{ink} x g; with g ~9.81m/s^2), L is the distance between two points supporting the filament and D is the filament diameter, as shown in Figure 9.

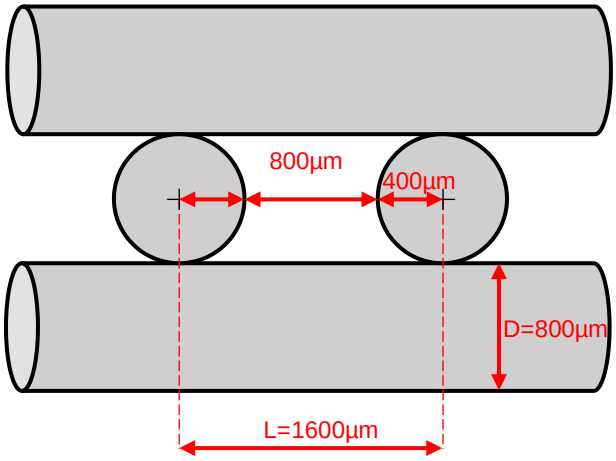

Figure 9. Filaments dimensions.

Schlort et al. [54] focused on the deformation of the filaments (Figure 10) and proposed a model for the midspan deflection (Equation 4).

$$z(t) \sim \frac{1}{2}\sqrt{\left(L(t)^2 - {L_o}^2\right)} \tag{4}$$

Where z(t) is the time-dependent midspan deflection, L_o is the beam initial length and L(t) is the time-dependent beam length due to elongation, expressed by Equation 5.

$$L(t) = L_o \left(1 + \int_0^t \frac{\rho\, g\, L_o}{6\, \eta(t)}\, dt\right) \quad (5)$$

Where ρ is the density of the filament, g is the gravitational constant and $\eta(t)$ is the time-dependent viscosity. Viscosity is the most important parameter and the only time-dependent, as a Bingham pseudoplastic system is expected: the ink is extruded at low viscosity and high shear rate, but after printing a layer, the filaments viscosity should rapidly recover to minimize the deflection.

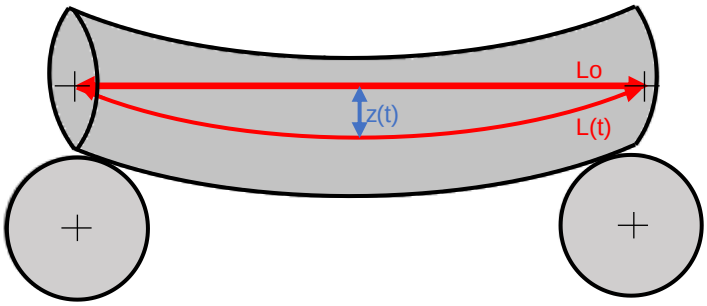

Figure 10. Filament deflection.

To characterize the inks several experiments were conducted. Specifically:

- Steady rate sweep: shear rate increasing from 0.01 to 10 $^{s-1}$.
- Dynamic strain sweep: deformation varying from 0.001 to 10 mm/mm.
- Viscosity recovery in two steps: first, it was applied to shear rate of 0.5 $^{s-1}$ for 60 s, then it was applied to controlled shear rate of 0.0001 $^{s-1}$ for more 175 s in order to measure the viscosity recovery. In the first stage, a shear rate corresponding to a high stress was needed to overcome the initial yield stress of the ink; in the second stage, to allow the ink to recover, the shear stress was lower than the yield stress. Values were chosen according to the results of the first two tests.
- Working time: constant deformation of 0.01% with a frequency of 0.1 Hz over 6 h.

The sequence of the analysis was always the same for all the inks tested, so it was possible to analyze their behavior at a comparable stage of the geopolymerization reaction.

Working time tests were conducted on freshly prepared inks.

4.3. GEOPOLYMERIC 3D-PRINTED STRUCTURES

Three types of 3D-printed geopolymers, 3D_Na_GP1, 3D_K_GP1, and 3D_Na.K_GP were produced with the molar ratio used in the second investigation (SiO_2 / Al_2O_3 = 4.0; (Na_2O; K_2O) / Al_2O_3 = 1.3; H_2O / Al_2O_3 = 18.5).

The initial procedure to prepare the lattices was the same used to prepare the powders, it was mixed metakaolin (Argical 1200S, Imerys S.A., Paris, France) as the aluminosilicate source with the activating alkaline solution, adding polyethylene glycol 1000 (PEG, Merck KGaA, Germany), used to provide pseudoplasticity to the slurry, and adding the geopolymer powders (Na_GP1, K_GP1 and Na.K_GP) with particle diameter up to 300 µm. Each type of geopolymer powder previously prepared was used as filler in its correspondent 3D-printed structure.

Since the initial blend (without PEG and filler) was very fluid, the filaments did not support the weight of the successive layers, for this reason it was necessary to use a rheological agent and a filler so that the filaments had the least possible deformity and the lattice maintained the designed shape. It is possible to use several types of materials as filler, such as sand or different fibers, but the inert geopolymer powder was chosen as a filler to avoid the use of other elements that could interfere or modify the conversion of the transesterification reaction. This system can be seen as a geopolymer-geopolymer composite.

4.3.1. Production of 3D-printed structures

To prepare the three types of ink to obtain geopolymer structures, PEG was added to the alkaline solution and it was mixed by mechanical stirring, 1000 rpm, until complete dissolution. Then the filler was added, and it was mixed until homogenization of the combined solution, finally the metakaolin was added to the combined solution, increasing the stirring to 1700 rpm for 10 min in order to obtain a homogeneous ink. The percentages of PEG[I] and filler[II] for each sample are shown in Table 7.

[I] It was calculated on the metakaolin and activating solution weights.
[II] It was calculated on the metakaolin, activating solution and PEG weights.

Table 7. Percentage of additives added to the fabrication of 3D-printed geopolymer structures.

Sample	PEG (wt.%)	Filler (wt.%)
3D_Na_GP1	4.5	25
3D_K_GP1	4.0	30
3D_Na.K_GP	4.0	40

The next step was to fill two 30mL-syringes with the geopolymer ink and place them in the fridge for 30 min before starting the printing process, keeping there the second syringe until its use. The fridge step was done to homogenize the ink and to decrease the number of bubbles formed by mixing the slurry and filling the syringes.

The 3D-printer (Delta Wasp 2040 Turbo, Wasproject, Massa Lombarda, IT) was equipped with a pressure inlet and an infinite screw to facilitate the extrusion (Figure 11). The machine was configured with print speed in a range of 7 to 10 mm/s and extrusion flow as needed to obtain constant writing.

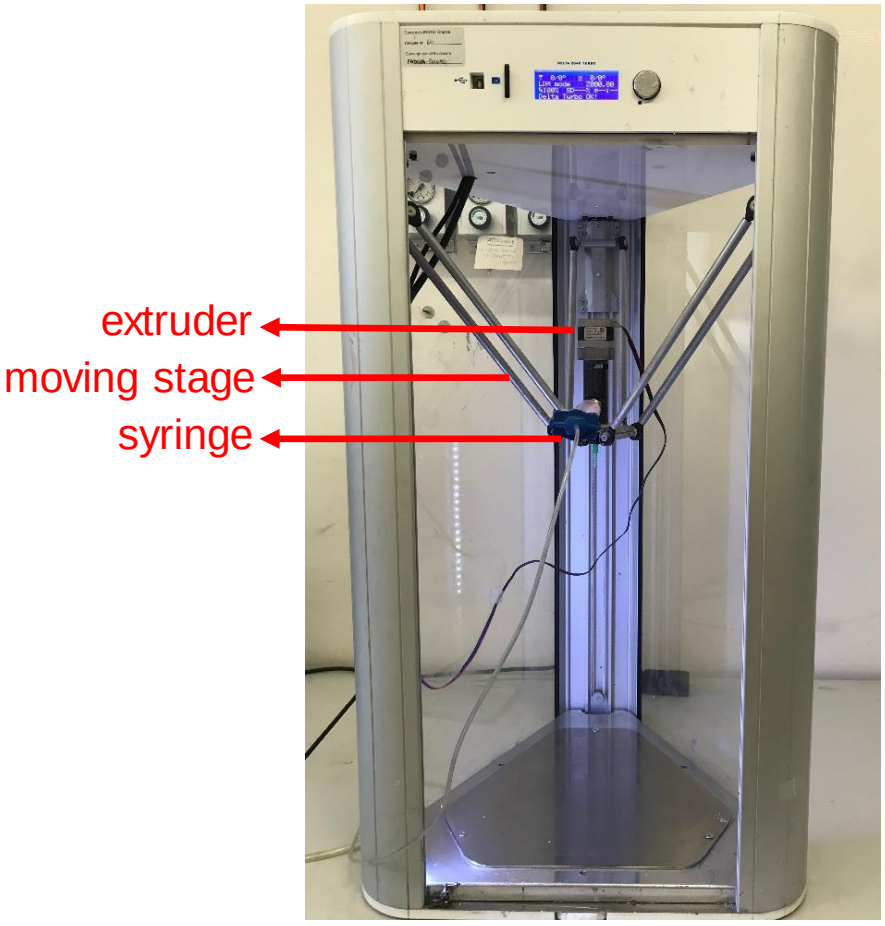

Figure 11. 3D printer - Delta Wasp 2040 Turbo.

The printing was done at room temperature and in the air, extruding the ink through the tip of a conical nozzle with a diameter of 840 µm (Nordson Italia S.p.a., Segrate, IT).

After drawing the first layer, the nozzle was raised of 600 µm in the Z-direction to print the next layer, the overlapping of the layers gave bigger contact between them. The first layer was composed of parallel filaments, the second layer was also composed of parallel filaments but with a rotation of 90° from the previous layer, the third and fourth layers follow the same arrangement but are slightly shifted, providing a denser network to the structure and with a larger contact surface.

As soon as printing was completed the covered plastic mold with the samples was placed in the oven at 75 °C for 2 days for complete geopolymerization, and before characterization and use in the reaction the structures were dried at 110 °C overnight.

The flowchart of the process used to produce the 3D-printed geopolymer structure is shown in Figure 12.

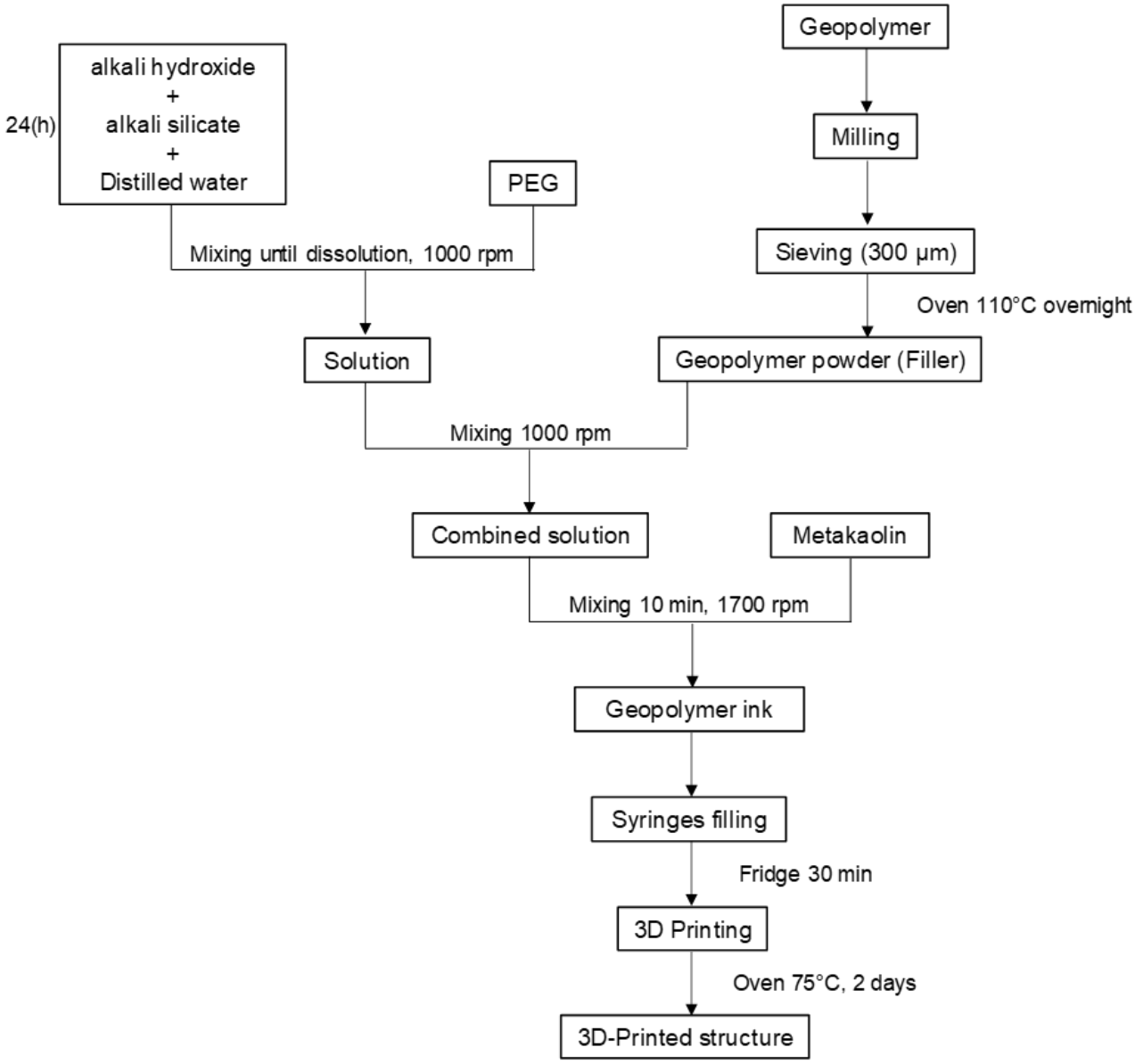

Figure 12. Schematic diagram of the process to fabricate 3D-printed geopolymer structures.

The printing process was repeated for 16 layers to obtain a structure with the designed measures of 25 mm and 9.6 mm for diameter and height, respectively. The structure was designed with Solidworks software and the file was transformed in "*gcode"* file to be used in the printer, as shown in Figure 13.

Figure 13. Top and layer view of the design structure.

4.3.2. Characterization of 3D-printed structures

All the 3D-printed structures were characterized by Brunauere, Emmette, Teller (BET) and Barrett, Joyner, Halenda (BJH) methods, porosity analysis, optical and scanning electron microscopes, mechanical strength analysis and permeability analysis.

4.3.2.1. Pore Characterization

The specific surface area was investigated using BET method, the same procedure explained in the topic “geopolymer powder”. The total pore volume, the average pore diameter, and the pore size distribution were calculated using the BJH method.

4.3.2.2. Physical properties

The bulk density (ρ_g) of the structures was determined by the weight and volume ratio, using a digital caliper and a digital balance. The apparent (ρ_a) and true density (ρ_t) of the samples were measured using a helium gas pycnometer (Micromeritics AccuPyc 1330, Norcross, GA, USA) on structures fragments and finely milled structures, respectively. With the three values of density, it can be calculated the open porosity (OP), close porosity (CL) and total porosity (TP) using the Equations 6-8.

$$OP = \frac{\rho a - \rho g}{\rho a} \times 100 \quad (6)$$

$$TP = \frac{\rho t - \rho g}{\rho t} \times 100 \quad (7)$$

$$CP = TP - OP \quad (8)$$

4.3.2.3. Morphological analysis

The morphology of the 3D-printed structures was investigated using an optical microscope (STEMI 2000-C, Carl Zeiss AG, Oberkochen, DE) and scanning electron microscope (ESEM, Quanta 200, FEI, Hillsboro, OR), with a magnification of 25x, 100x and 5000x.

4.3.2.4. Mechanical strength

The compressive strength of the 3D-printed structures was determined at room temperature using a universal material testing machine, Instron 1121 UTM (Instron Danvers, MA) with a load cell of 10 KN, with a constant crosshead speed of 0.5 mm/min and it was calculated by the Equation 9.

$$\sigma_c = \frac{F}{S} \quad (9)$$

Where F is the maximum stress during the test; S is the value of the surface area in contact with the compressor plates considering it is a circle and r is the radius (Equation 10).

$$S = \pi\, r^2 \quad (10)$$

To assure a homogeneous load distribution a layer of parafilm (Parafilm M, Pechiney Plastic Packaging, Neenah, WI) was used between the plates and the sample. The compressive strength value was obtained by the average ± standard deviation of 20 green samples and 20 samples heat treated at 110 °C.

4.3.2.5. Permeability analysis

The permeability of the lattices was investigated using a laboratory air permeameter (Figure 14) at the University of Ribeirão Preto, SP, Brazil (UNAERP). The test was done in triplicate and it was carried out at room temperature and atmospheric pressure. The sample dimensions, diameter and thickness were measured with a caliper and the sides of the sample were sealed so that the airflow didn't escape.

The air flow passing through the sample was measured by a rotameter and the pressure drop (ΔP) was measured by digital manometers, with these values the sample constants k_1 and k_2 were calculated by Forchheimer's equation (Equation 11).

$$\frac{\Delta P}{L} = \frac{\mu}{k_1} v_s + \frac{\rho}{k_2} {v_s}^2 \quad (11)$$

Where L is the thickness of the sample; μ is the viscosity of the fluid; vs is the flow velocity of the fluid; ρ is the density of the fluid. Considering a compressible fluid, the pressure drop is given by Equation 12.

$$\Delta P = \frac{{P_i}^2 - {P_o}^2}{2\, P_o} \quad (12)$$

Where P_i is the inlet pressure; P_o is the outlet pressure.

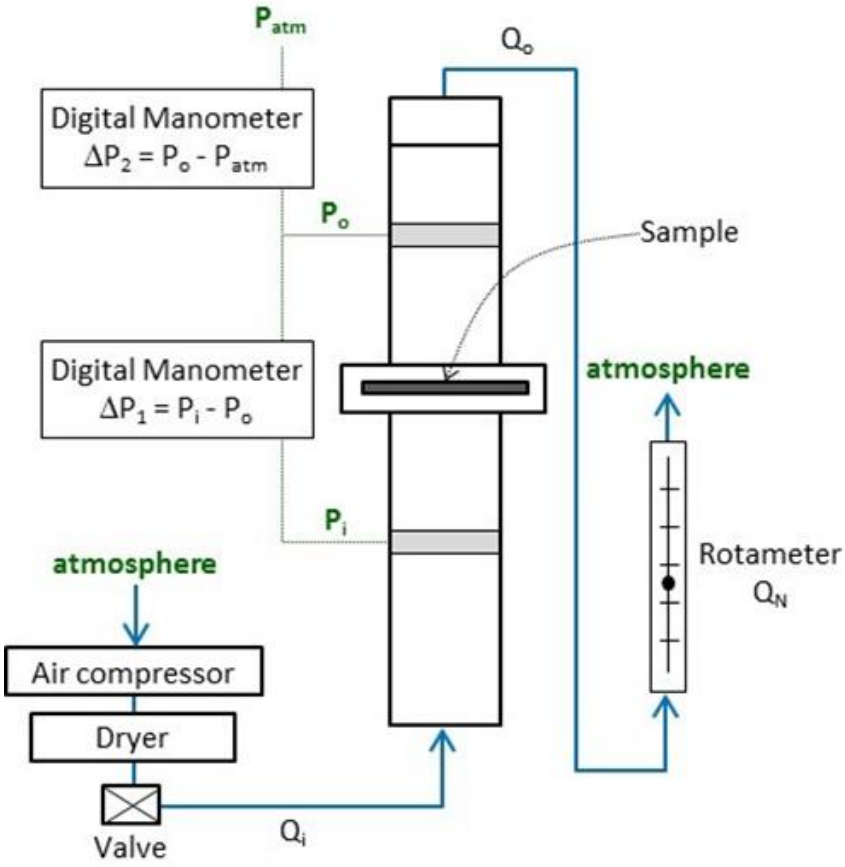

Figure 14. Laboratory air permeator layout.

4.4. BIODIESEL

4.4.1. Production of biodiesel

The transesterification reaction between oil and alcohol was conducted using soybean oil (San Marco, Italy) and methanol (Scharlau, Spain). The reaction was carried out in a 250 mL-flask linked to a condenser with cold water to reflux the methanol in the reaction, under a vigorous agitation with a glycerin bath (Figure 15a). The biodiesel was obtained with a molar ratio methanol:oil of 7.5:1, and 3% of catalyst (w/w oil).

Firstly, the soybean oil was heated, then the mixture of methanol and geopolymer powder as a catalyst was added. In the reaction using the 3D-printed structure, they were tied with a nylon thread remaining completely immersed in the heated oil (Figure 15b) and methanol was added through the condenser. After the reaction time, the mixture was centrifuged to separate the phases, the ester was

evaporated under vacuum for 24 h at room temperature to eliminate the residual methanol and finally the biodiesel was obtained. Two reaction conditions were tested, 60 °C for 1 h and 70 °C for 2 h. All the reactions were done in triplicate.

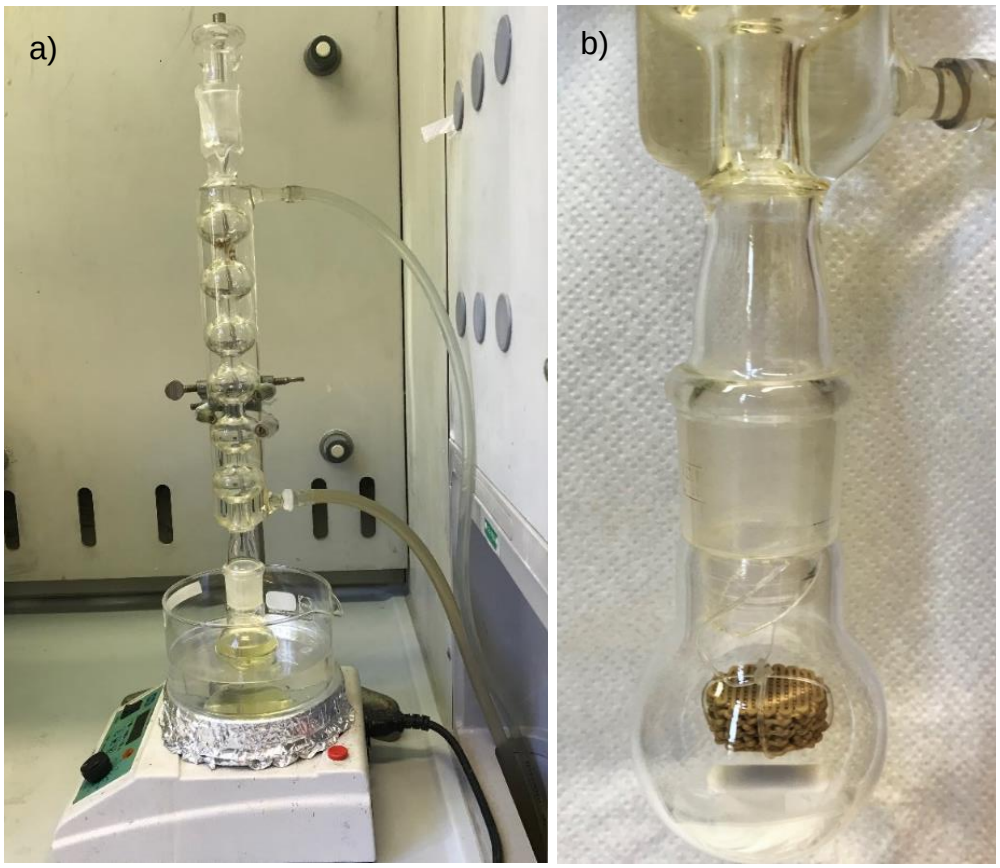

Figure 15. a) Laboratory-scale reactor for the biodiesel production; b) Setup for the reaction using 3D-printed lattice.

The flowchart of the process to produce biodiesel by transesterification reaction is shown in Figure 16.

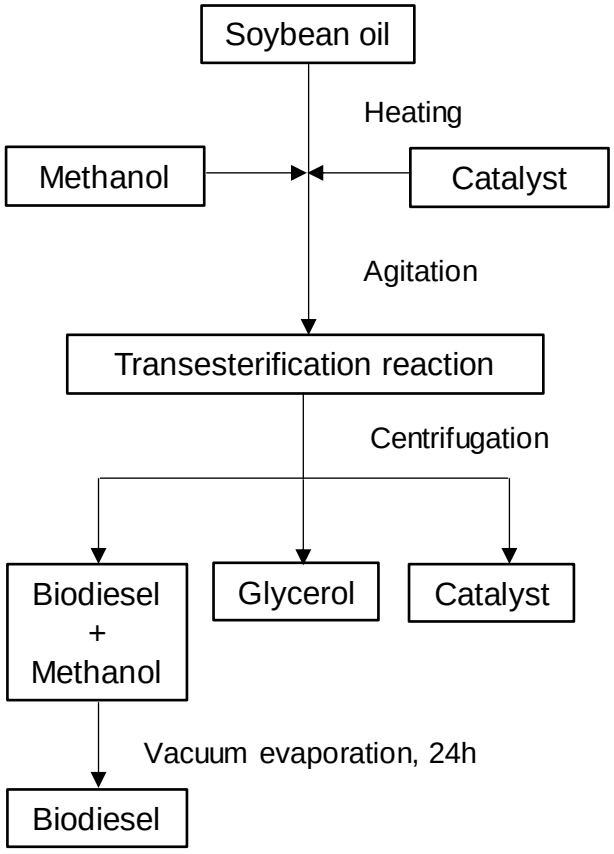

Figure 16. Schematic diagram of the biodiesel production.

4.4.2. Conversion of the transesterification reaction

The biodiesel yield was calculated by means of gas chromatography measurements. The Thermo-Trace DSQ GC-MS was used for the chromatographic analysis, which was equipped with a Supelco SLB®-5ms Capillary GC Column (L × I.D. 30 m × 0.25 mm, df 0.25 µm). Icosane ($C_{20}H_{42}$) was used as an internal standard to normalize the peak areas of the chromatograms

Firstly, the soybean oil was completely esterified, adding 5 mL methanol and 1 mL acetyl chloride at 0 °C into 100 mg of soybean oil, subsequently the mixture was heated at 80 °C for 1 h. After cooling, 1 mL water and 10 mL hexane were added in the mixture. After stirring, the methanol phase was discarded, and the organic phase was washed twice with water. Then, the hexane solution (0.1 mL) and 0.5 mL of internal standard solution (1000 mg/L) were added and diluted to 10 mL before the injection in the equipment.

To analyze the biodiesel samples, 0.1 g of biodiesel were diluted with hexane until obtaining 10 mL of solution, then 0.5 mL of internal standard solution (1000 mg/L)

were added to 0.1 mL of this first solution to obtain a final volume of 10 mL before the injection in the equipment. All samples were prepared in triplicate.

By means of the equipment used to measure the samples, the sum of the peak areas of all the esters found in the samples and the area of the internal standard were obtained.

The sum of the areas of the ester peaks obtained by the complete esterification of the soybean oil was considered as 100% of conversion, reference value for the other samples. The biodiesel yield for the studied samples was obtained by a ratio between the sum of the sample peak areas and the reference value.

The esters were identified by comparison between the peaks of analytical standards and those obtained in the analyzes, for certain retention times.

4.4.3. Leaching of catalyst

The leaching test was done in the ratio of 1 g of geopolymer to 21 g of distilled water under vigorous mechanical agitation at 60 °C for 1 h. The sample was centrifuged to separate the phases and the upper liquid phase was filtered under vacuum using a 0.45 μm membrane filter to remove geopolymer residues that were not sedimented with centrifugation. The liquid was analyzed by atomic absorption.

4.4.4. Atomic absorption analysis

The analysis was done using an Atomic Absorption Spectrometer (Analyst 700, PerkinElmer, Waltham, Massachusetts, USA) to quantify the amount of alkali leached from the geopolymer into the water.

The machine was calibrated to quantify the amount of sodium in the samples, with a calibration curve up to 10 mg/L. The dilution of the samples is shown in Table 8.

Table 8. Dilution of the samples to analyze the leaching of Na by atomic absorption analysis.

Dilution	**x 0**	**x 10**	**x 50**	**x 100**	**x 1000**
Sample	K1.35 (700°C)	K 1.35 (500°C; 300°C; 110°C)	Na 1.3 (700°C; 500°C; 300°C; 110°C)	Na+K 1 (700°C; 500°C)	Na+K 1 (300°C; 110°C)
	K 1.0 (700°C; 500°C)	K 1.0 (300°C; 110°C)		Na+K 2 (700°C; 500°C;	Na+K 2 (110°C)
	K1.3 (700°C)	K 1.3 (500°C; 300°C; 110°C)			

Afterward the equipment was calibrated to quantify the amount of potassium in the samples, with a calibration curve up to 4 mg/L. Dilution of the samples is shown in Table 9.

Table 9. Dilution of the samples to analyze the leaching of K by atomic absorption analysis.

Dilution	x 100	x 1000	x 10000
Sample	Na+K 1 (700°C; 500°C)	Na+K 1 (300°C; 110°C)	K 1.35 (110°C)
	Na+K 2 (700°C; 500°C)	Na+K 2 (300°C; 110°C)	
		K 1.35 (700°C; 500°C; 300°C)	
		K 1.0 (700°C; 500°C; 300°C; 110°C)	
		K 1.3 (700°C; 500°C; 300°C; 110°C)	

5. RESULTS AND DISCUSSION

5.1. GEOPOLYMER POWDER

5.1.1. X-Ray diffraction

The metakaolin and the produced geopolymers were analyzed by X-ray diffraction analysis. Initially the software "*Match*!" supported by the "*PDF-2 Powder Diffraction File*" of ICDD (International Center for Diffraction Data, Newtown Square, PA, USA) was used to identify the crystalline phases of the metakaolin raw material. The XRD pattern for metakaolin (Figure 17) showed the typical amorphous hump between 15° and 30° 2theta and the most evident peaks, between 20° and 25° 2theta correspond to crystalline forms of silicon oxide (quartz), titanium oxide (anatase) and muscovite.

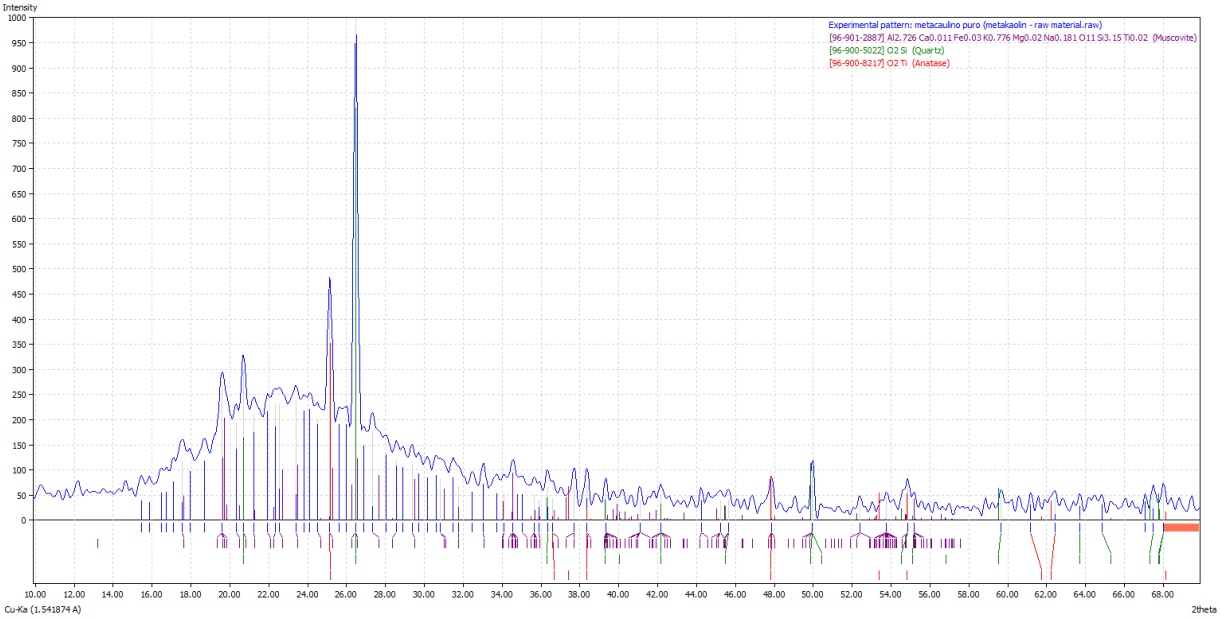

Figure 17. XRD pattern for metakaolin ARGICAL M 1200S.

From the diffractograms of Figures 18 and 19 it is possible to observe that both the sodium-based geopolymer (Na_GP1) and the potassium-based geopolymer (K_GP1) treated at the four temperatures (110 °C, 300 °C, 500 °C and 700 °C) present completely amorphous structures and have no characteristic peak of crystalline phases.

In both graphs, the highest apparent peaks representing the crystalline phases of quartz (20.70° and 26.50° 2theta), anatase (25.14° 2theta) and muscovite (19.60° 2theta) are derived from the impurities contained in metakaolin and do not participate in the geopolymerization reaction, so, they can be identified in the final geopolymer [55].

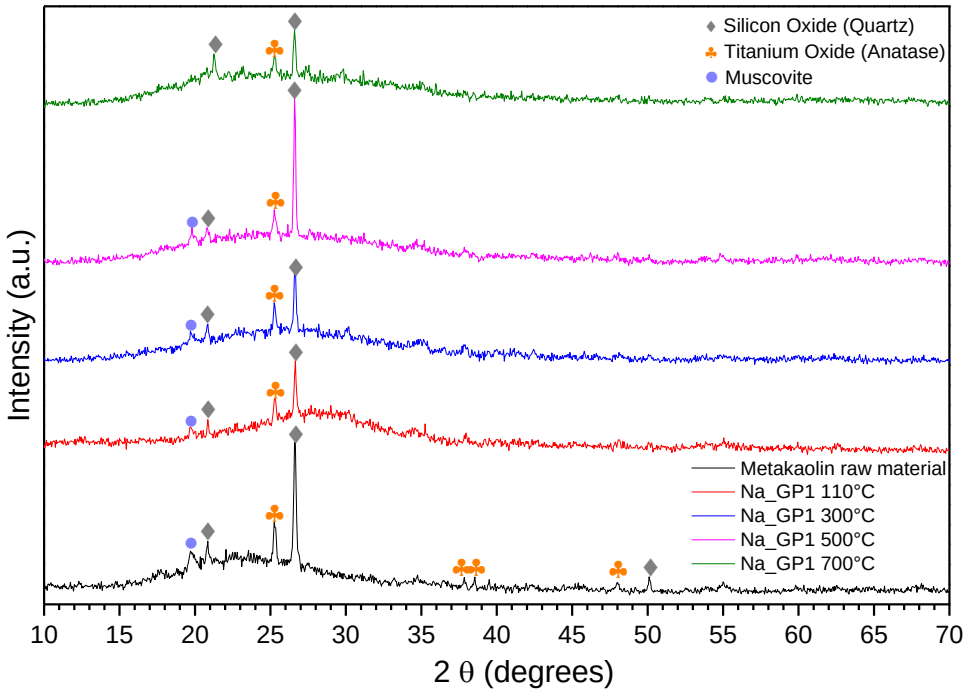

Figure 18. Diffractogram for the Na_GP1.

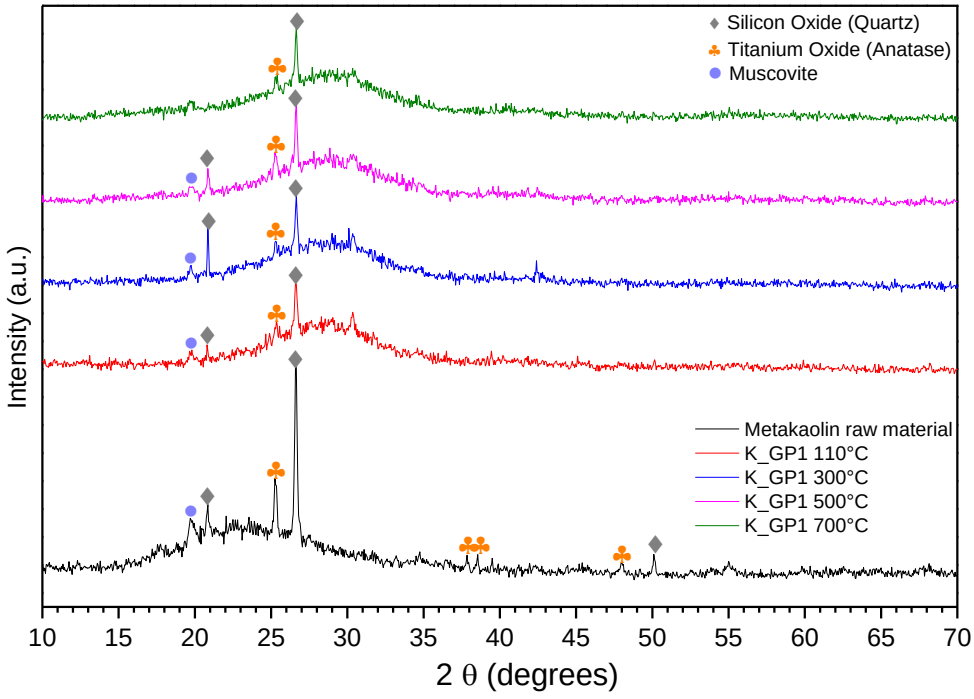

Figure 19. Diffractogram for the K_GP1.

The structures of the Na.K_GP materials heat treated at the first three temperatures are also completely amorphous and contain metakaolin impurities, but the analysis of the material treated at 700 °C (Figure 20) shows the presence of the crystalline phases of potassium aluminum silicate (kalsilite), sodium potassium aluminum silicate (nepheline) and also traces of quartz, originating from the metakaolin.

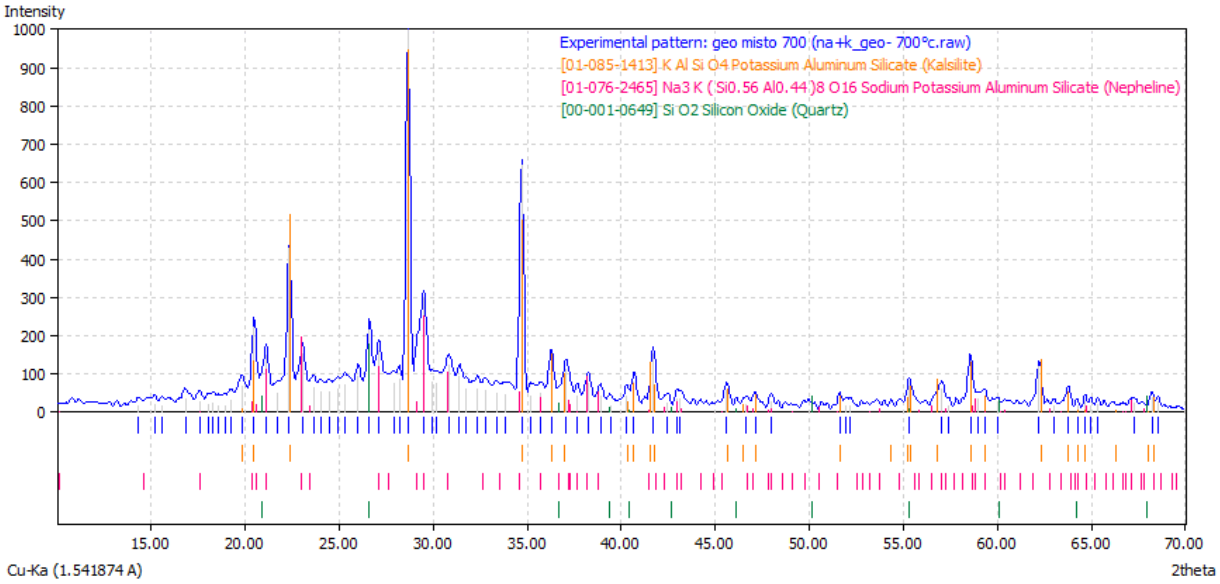

Figure 20. XRD pattern for the material Na.K_GP heat treated at 700 °C.

Figure 21 compares the diffractograms of Na.K-based geopolymers treated at the four temperatures with the metakaolin raw material. At 700 °C the material was largely crystallized in kalsilite, with its most intense typical peaks at 20.5°, 22.4°, 28.6°, 34.8° 2theta, less intense peaks of nepheline between 20° and 30° 2theta and a minor amount of unreacted quartz was also detected at 26.5° 2theta.

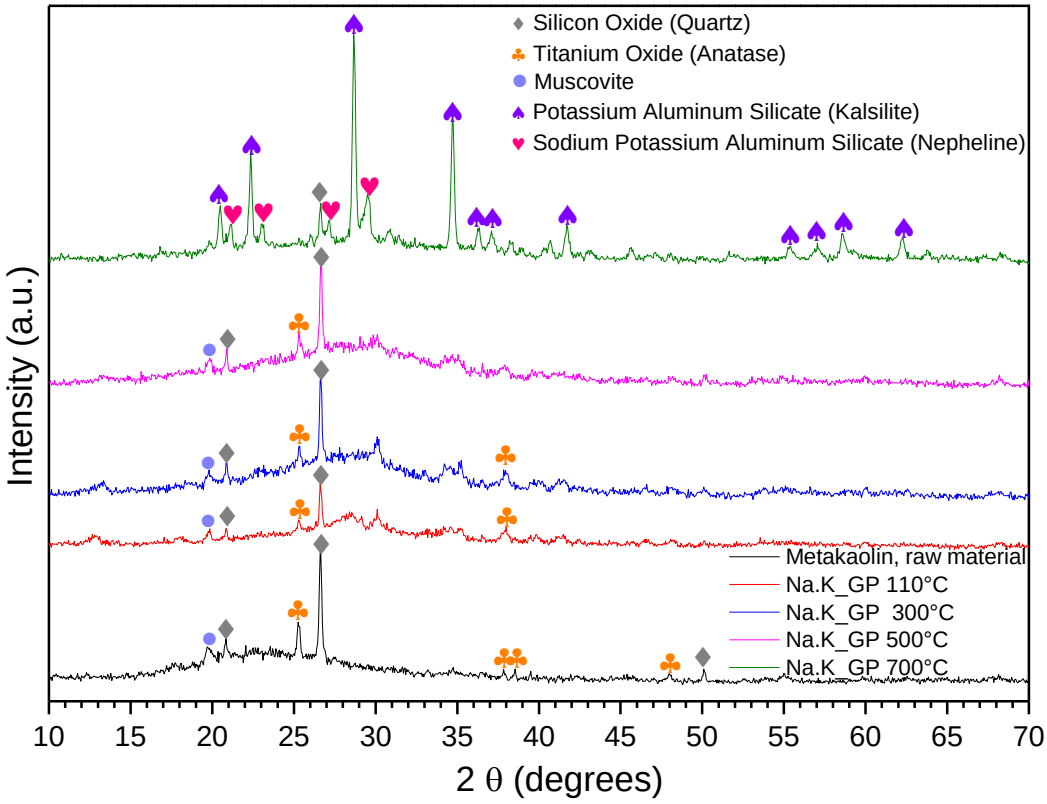

Figure 21. Diffractogram of the Na.K_GP.

5.1.2. Thermal analysis

The results of the thermal analysis for the sodium-based geopolymer (Na_GP1) are reported in Figure 22; in the analysis of differential scanning calorimetry (DSC) with heat flow, the endothermic events (ΔH>0) are characterized by decreasing peaks, where the signal originates from the temperature difference between the sample and the reference.

At approximately 110 °C there is an endothermic peak corresponding to the removal of physical water, and an exothermic peak at around 350 °C corresponding to dehydroxylation of the OH groups and polycondensation into siloxo bond for the unreacted phase in the geopolymeric powder.

At about 800 °C it is possible to observe another exothermic peak corresponding to the crystallization of the geopolymer, in this interval the crystals of nepheline begin to form and this confirms the absence of crystalline phases in the XRD graph, in which the highest treatment temperature was 700°C; at 1200 °C a small exothermic peak was obtained probably due to the melting of the material.

Thermogravimetric analysis (TGA) analyzes the weight loss of the sample. It is possible to relate the first peaks of the DSC curve with the largest weight loss corresponding to approximately 11.1% at 520 °C, due to the trapped water within the tridimensional geopolimeric network. At the end of the analysis there was a total weight loss of 11.5% which remained constant with increasing temperature.

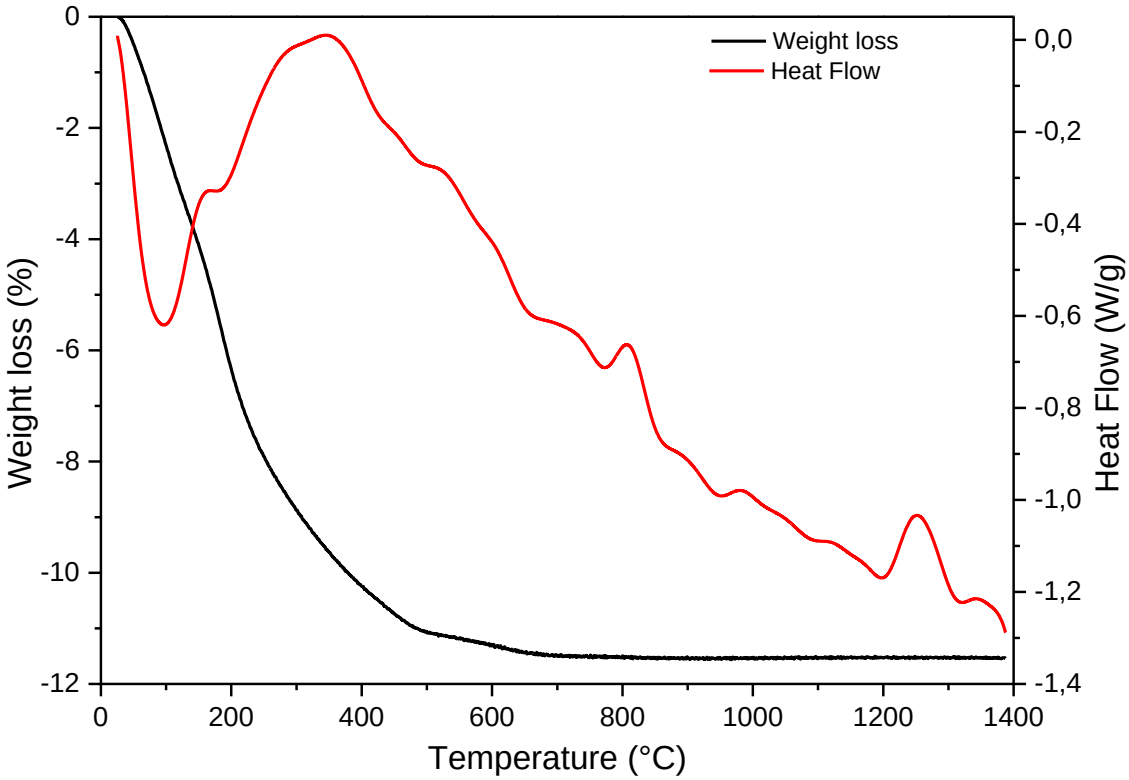

Figure 22. TGA-DSC curves for the Na_GP1.

The results of the thermal analysis for the potassium-based geopolymer (K_GP1) are reported in Figure 23, showing an endothermic peak at approximately 110 °C and an exothermic peak between 260 and 370 °C corresponding to the largest weight loss reaching about 11,6% at 430 °C; these results can also be correlated to the loss of physically and chemically adsorbed water.

Between 800 and 1100 °C the curve has an exothermic behavior and this range corresponds to the formation of crystals of leucite and kalsilite. In this case, the absence of crystalline phases in the XRD graph was confirmed as well.

At the end of the analysis there was a total weight loss of 14.6% and, like the Na_GP1, it did not change with higher temperatures, similar to that reported in literature [19].

This geopolymer had higher water loss because, even though the molar ratio H_2O/Al_2SiO_3 was constant, the molecular weights were different, so a greater amount of water was required for its formulation.

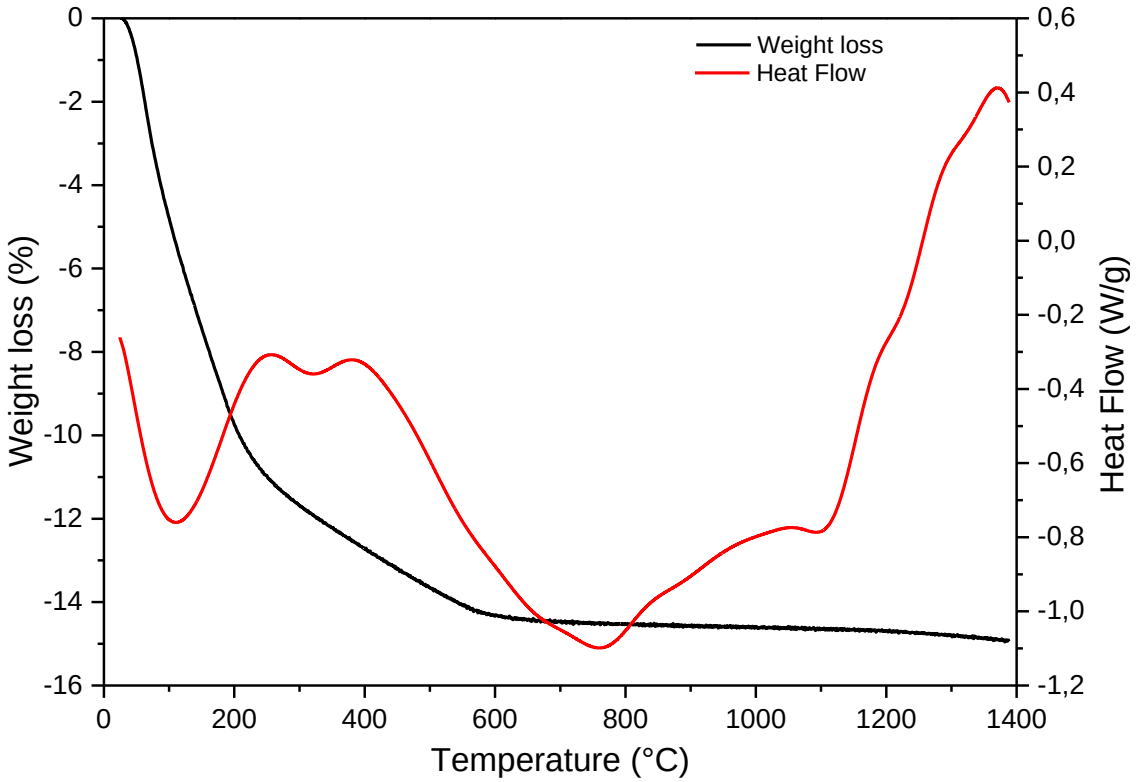

Figure 23. TGA-DSC curves for the K_GP1.

The results of the thermal analysis for the sodiumpotassium based geopolymer (Na.K_GP) are reported in Figure 24, showing an endothermic peak at 120 °C and an exothermic peak at approximately 360 °C corresponding to greater weight loss reaching about 10.6% at 600 °C.

Between 720 and 880 °C it is possible to observe small exothermic peaks due to the onset of the material crystallization, this result agrees with the presence of crystalline phases in the XRD graph for the sample treated at 700 °C.

At the end of the analysis it was possible to identify the melting of the material with an endothermic peak followed by its decomposition, and there was a total weight loss of 11.1% and, as the preceding materials, it remained constant.

The endothermic behavior at the end of the three analyzes is caused by the aimless of the machine.

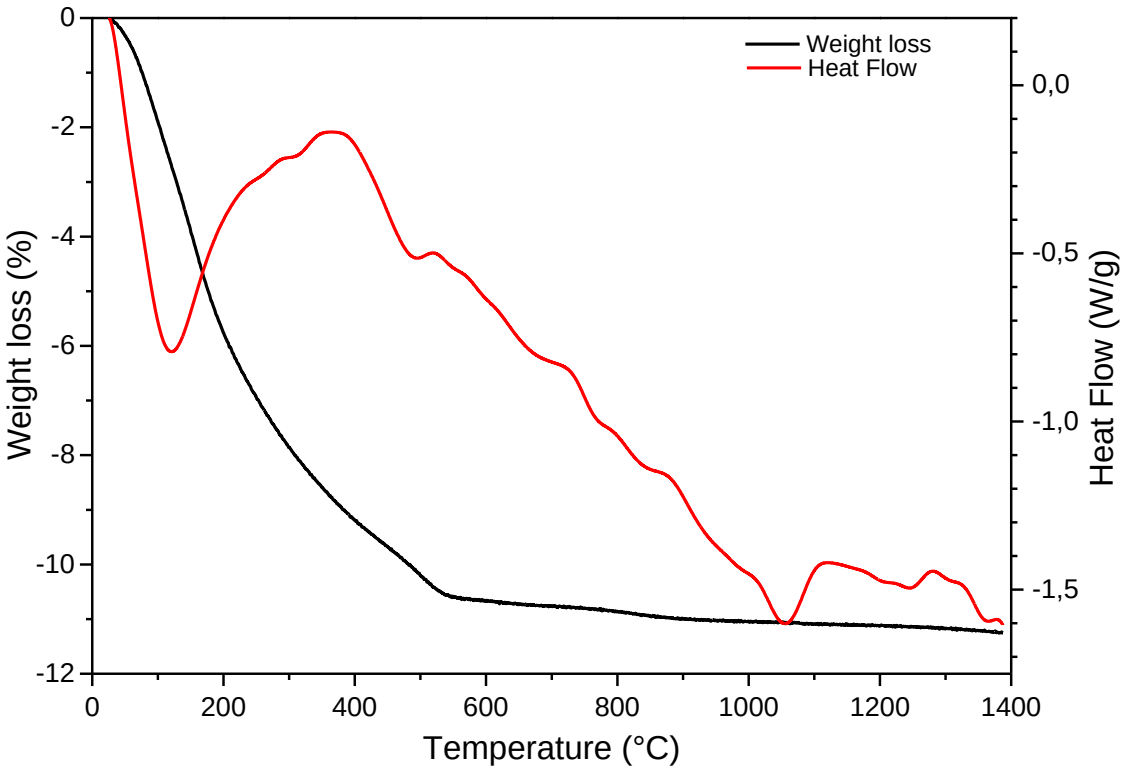

Figure 24. TGA-DSC curves for the Na.K_GP.

5.1.3. Physical properties

The densities of the geopolymers studied were measured by pycnometer operated with Helium. Five samples were analyzed and the densities average ± standard deviations are reported in Table 10. The three materials had a similar behavior, in a range of 2.26 to 2.75 g/cm^3. In the literature there are values of approximately 2.4 - 2.6 g/cm^3 for geopolymers and they can be compared to concrete (ρ = 2.4 g/cm^3).

Table 10. Physical properties of the material Na_GP1, K_GP1 and Na.K_GP.

Sample	Calcination temperature (°C)	Density (g/cm^3)
Na_GP1	110	2.26 ± 0.01
	300	2.31 ± 0.02
	500	2.31 ± 0.03
	700	2.41 ± 0.01
K_GP1	110	2.28 ± 0.03
	300	2.75 ± 0.02
	500	2.33 ± 0.02
	700	2.63 ± 0.01
Na.K_GP	110	2.35 ± 0.02
	300	2.43 ± 0.02
	500	2.42 ± 0.01
	700	2.56 ± 0.01

5.2. RHEOLOGY OF GEOPOLYMERIC INK

The rheology studies the relationship between stress and deformation of the materials, this allows to predict the behavior of this material under certain conditions of use.

The geopolymerization occurs within the mixture of aluminates and silicates by polycondensation, in the initial phase a gel is formed and it tends to harden with time and loss of water.

The rheological behavior of metakaolin-based geopolymers was already studied [56] and it was shown that the pseudoplastic character of the fluid decreases with increasing amount of solid, consequently increasing fluid viscosity and initial yield stress. Another study [52] showed the rheology of various inks using rheological modifiers to enhance such pseudoplastic behavior.

At rest, a pseudoplastic has randomly oriented particles and a network of weak interactions; when forced to move in one direction, all these moieties tend to organize preferentially in the direction of flow, flowing more easily and opposing less resistance to the movement. In these fluids the apparent viscosity decreases with increasing shear rate, in practice they become more fluid increasing the stress applied.

Initially, the applied stress is still too low to break the gel that is forming, so a high viscosity is observed. The stress increases until the gel breaks, consequently the

material has less difficulty to flow and the viscosity curve changes its inclination. It is possible to see this behavior reflected in the shear stress: initially it increases, as it requires more effort to break the gel; however, as soon as it is ruptured, there is no need for high efforts to deform the material, the shear stress curve changes orientation and tends to be constant.

In the case of geopolymer in particular, this behavior can be seen in Figure 25a-b; in addition, it was possible to observe the influence of sample aging on viscosity and shear stress. The first curve obtained after the time of ink homogenization in the fridge (30 min) was the shear stress 1, after around 10 min the test was repeated and the shear stress 2 was obtained, and after around 10 more minutes was obtained the shear stress 3. It has been observed that with the aging of the ink the effort applied to break the gel tends to increase and consequently the viscosity as well because over the reaction time the structure becomes more rigid opposing greater resistance to the flow.

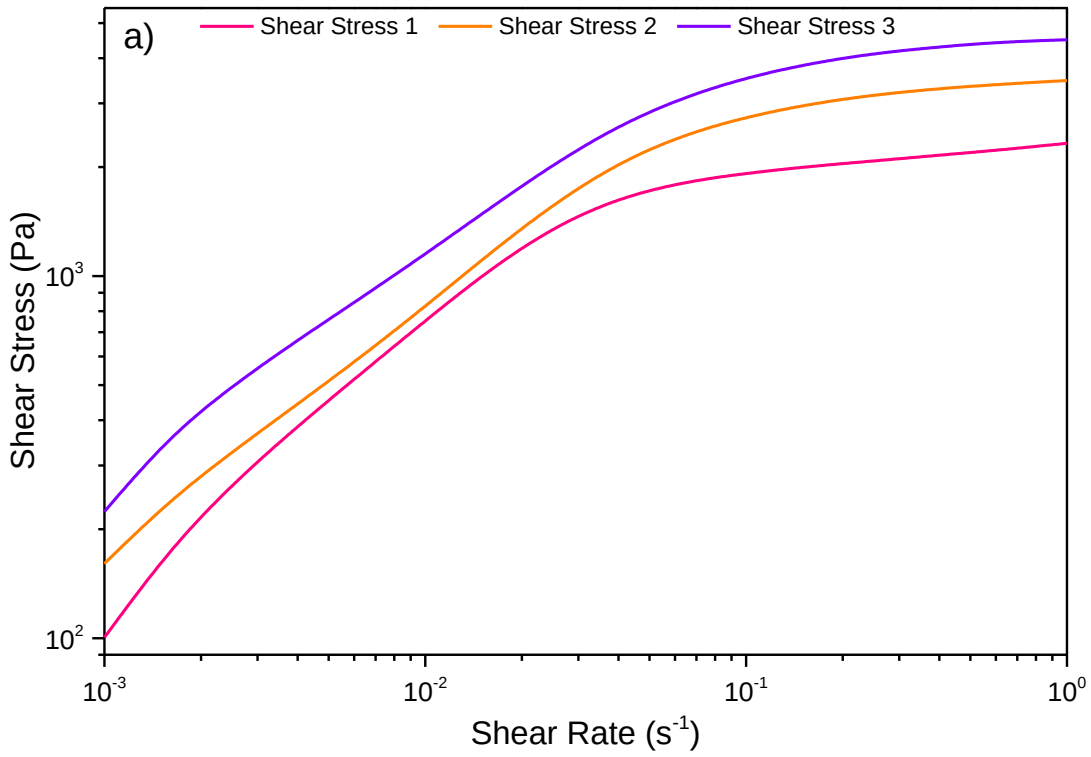

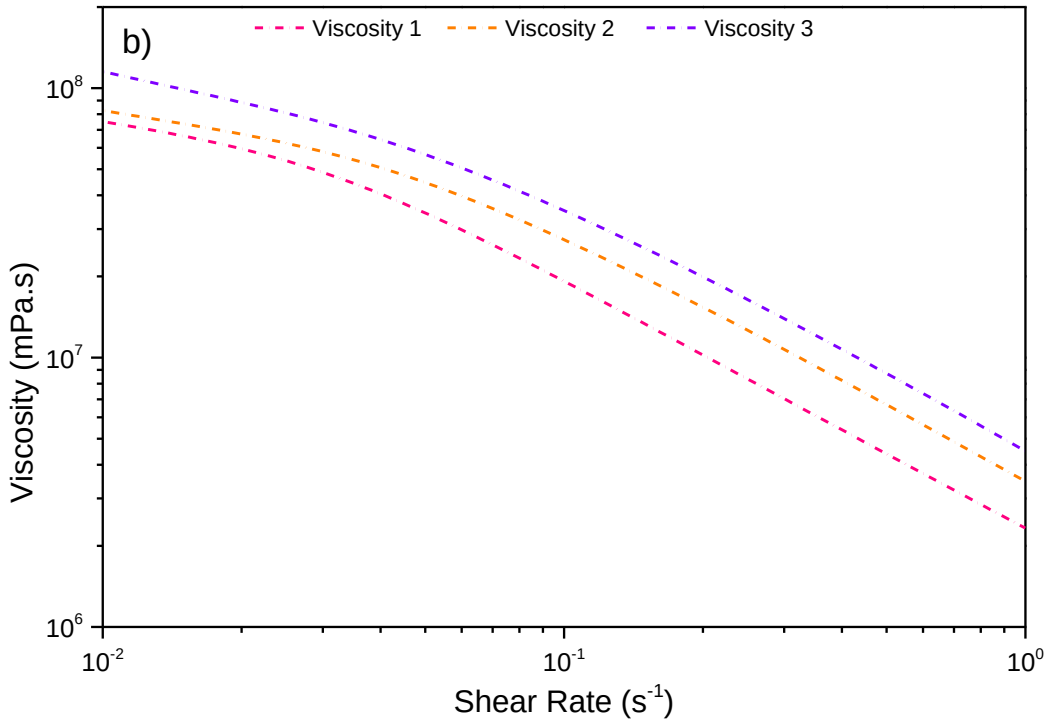

Figure 25. Steady rate sweep test performed on the 3D_Na_GP1 ink: a) flow curves and b) viscosity curves.

The breakage of the gel could be observed on the shear stress curve at the point where the slope of the curve changed. In the shear stress curve of the inks 3D_Na_GP1, 3D_K_GP1 and 3D_Na.K_GP the breakage occurs approximately at 3000, 2000 and 1500 Pa, respectively, with a very close shear rate for the three inks, between 0,02 and 0,1 s^{-1}. These values are much lower compared to the shear rates applied during printing, which are between 50 and 100 s^{-1}. The values obtained in this work for the geopolymer viscosity are slightly lower than those mentioned in the literature [52], this behavior is influenced by two factors: the geopolymer initial formulation of this work has a greater amount of water and the particles size of filler are slightly large (300 μm). The filler increases the initial viscosity, but, at the same time, worsens the gel property, since the added particles do not react with the geopolymer being formed.

The flow and viscosity curves for the three inks are shown in Figure 26, the shear stress and the viscosity were plotted versus the shear rate. All tests were performed after keeping the inks in the fridge for 30 min.

The 3D_Na.K_GP1 material is less viscous, possibly because the mixture of PEG and alkaline solution was not homogeneous in the ink preparation.

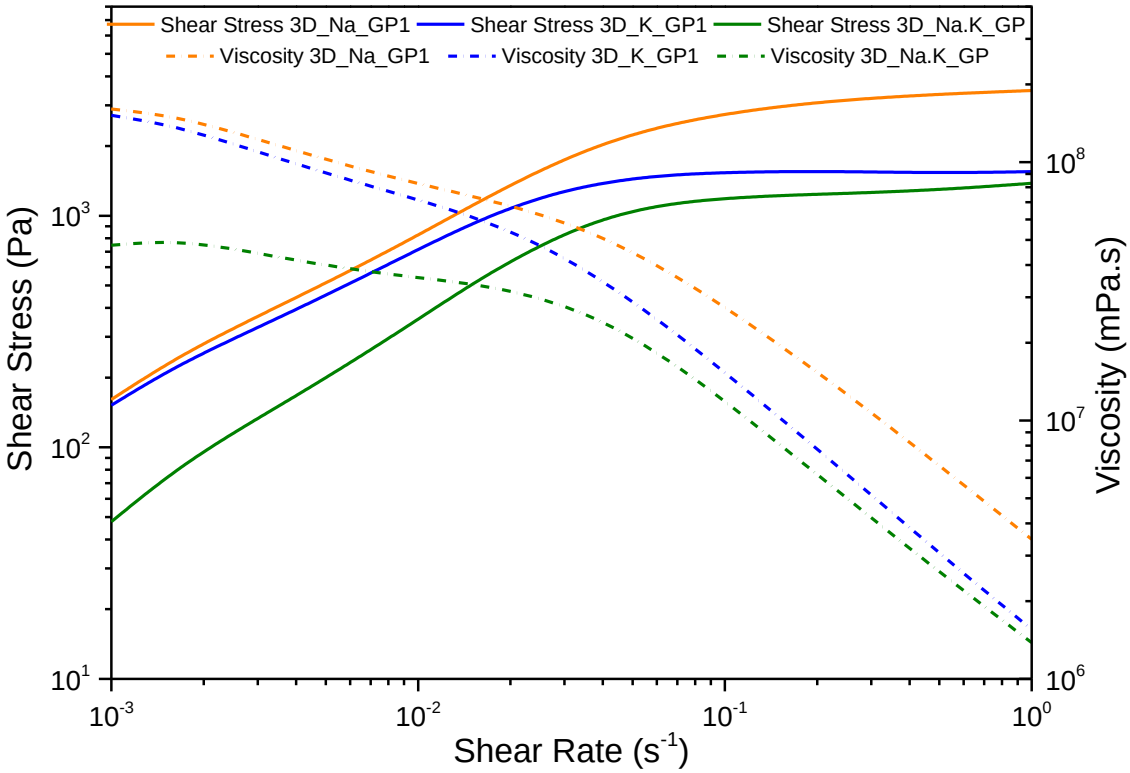

Figure 26. Steady rate sweep test performed on the three inks: flow curves and viscosity curves.

Fluids with pseudoplastic behavior generally require the application of a certain effort to start flow, this effort is defined as yield stress, below that value the material does not flow, but it has an elastic behavior and applying an effort exceeding the limit the material can pass from a solid-like state to a liquid-like one when its reticular structure breaks.

The plasticity phenomenon may be reversible or not, depending on the reconstruction of the material reticular structure. In the case of the geopolymer, the network that is formed constantly during the geopolymerization reaction is responsible for the elastic component, but the microstructural arrangement of the material is ruptured with stress above the yield stress, allowing the flow.

Figure 27 shows the graph of the storage modulus G' and loss modulus G" of the three inks after 30 min of rest in the fridge versus the shear strain.

The three materials had a similar behavior: initially, with low strain, the moduli decreased slowly, with increasing the shear strain both G' and G" decreased rapidly until the two curves intersection, and right after this crossing the values stabilized keeping the behavior.

In the literature [57] yield stress corresponds to 90% of the plateau modulus, in these tests this limit was determined by intersection of the G' and G" curve, since the curves do not have a clear transition point.

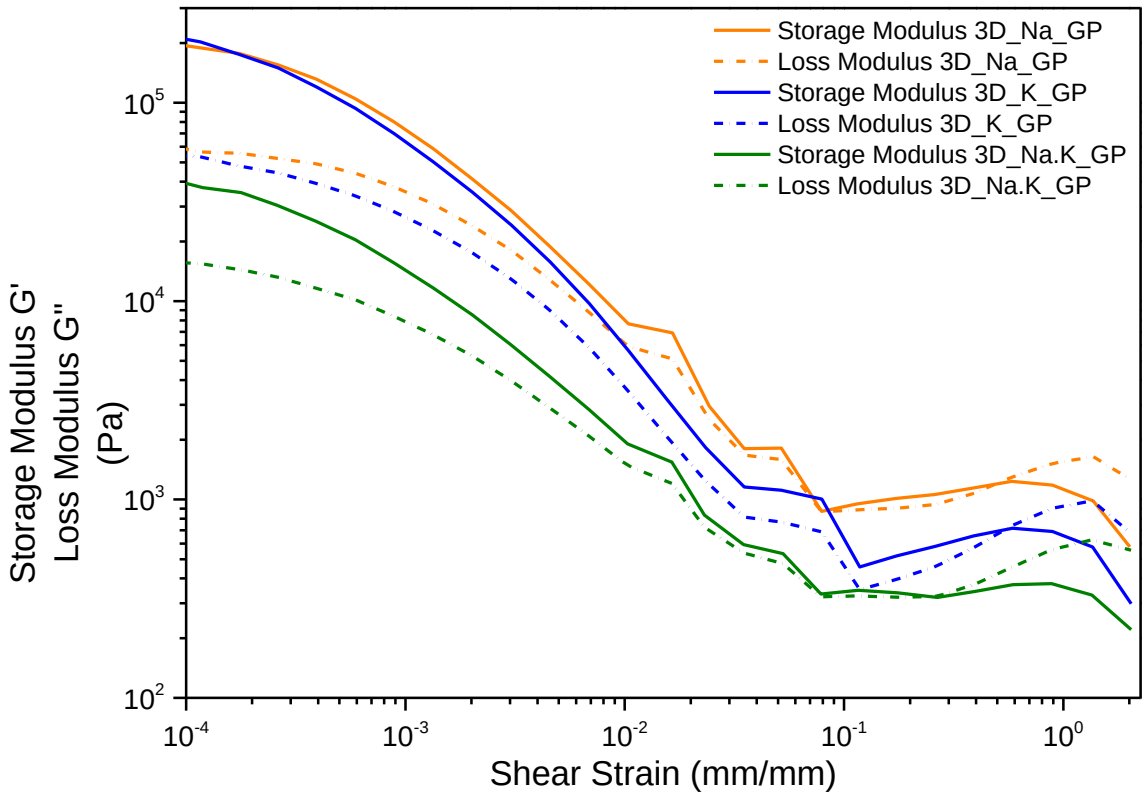

Figure 27. Dynamic strain sweep test performed on the three inks, G’ and G” modulus versus shear strain.

In the cross-section of G' with G" the analysis was slightly disturbed probably not by physical phenomena but because there was a series of mechanisms happening in that moment: the breaking of the gel of one part and the flow of the particles of another turned the system very sensitive and caused problems to the rheometer to keep the balance, however, it is visible that the crossing of the curves happened in this range. The values in which the rheometer did not maintain the equilibrium were eliminated, but the curves were not affected.

Data from the Storage Modulus of the 3D_Na_GP1, 3D_K_GP1 and 3D_Na.K_GP inks were used in Equation 3 to verify the condition for minimal deflection formulated by Smay et al. and the values are reported in Table 11, as well as the highest values achieved by G' from the dynamic strain sweep of the three inks.

According to the results obtained by calculations, the three inks could be used for DIW of geopolymeric lattices.

Table 11. Maximum G' values from the dynamic strain sweep test and the theorical G' calculated from the condition for minimal deflection.

Samples	3D_Na_GP1	3D_K_GP1	3D_Na.K_GP
G'_{max} (Pa)	210180	257790	45699
G'_{Smay} (Pa)	71.53	67.62	70.32

It is possible to observe, in Figure 28, the yield stress (crossover point) for the 3D_Na_GP1, 3D_K_GP1 and 3D_Na.K_GP inks was 100, 80 and 25 Pa, respectively, which proves that the sodium-based material forms a stronger gel than the others. 3D_Na.K_GP ink has a very low yield stress and there is a possibility that it may flow without applying pressure because it needs an effort that its own weight can provide.

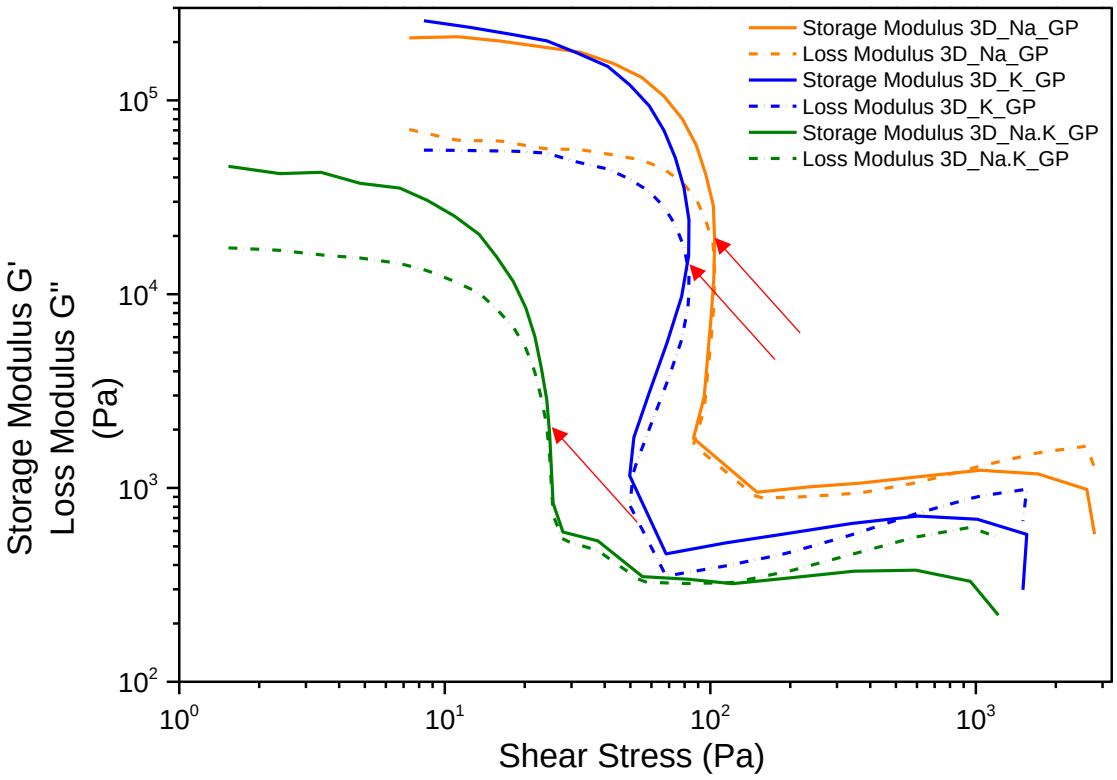

Figure 28. G' and G" moduli plotted versus shear stress.

The viscosity recovery analysis was done in two steps: at the beginning a shear rate corresponding to a stress higher than the yield stress was applied to break the

gel, simulating what actually happens during the printing process when the ink is extruded; this shear rate was applied for 1 min and then it was lowered to the minimum possible, in which the stress was not enough to break the gel, so it was possible to measure the viscosity recovery of the material versus the time (Figure 29).

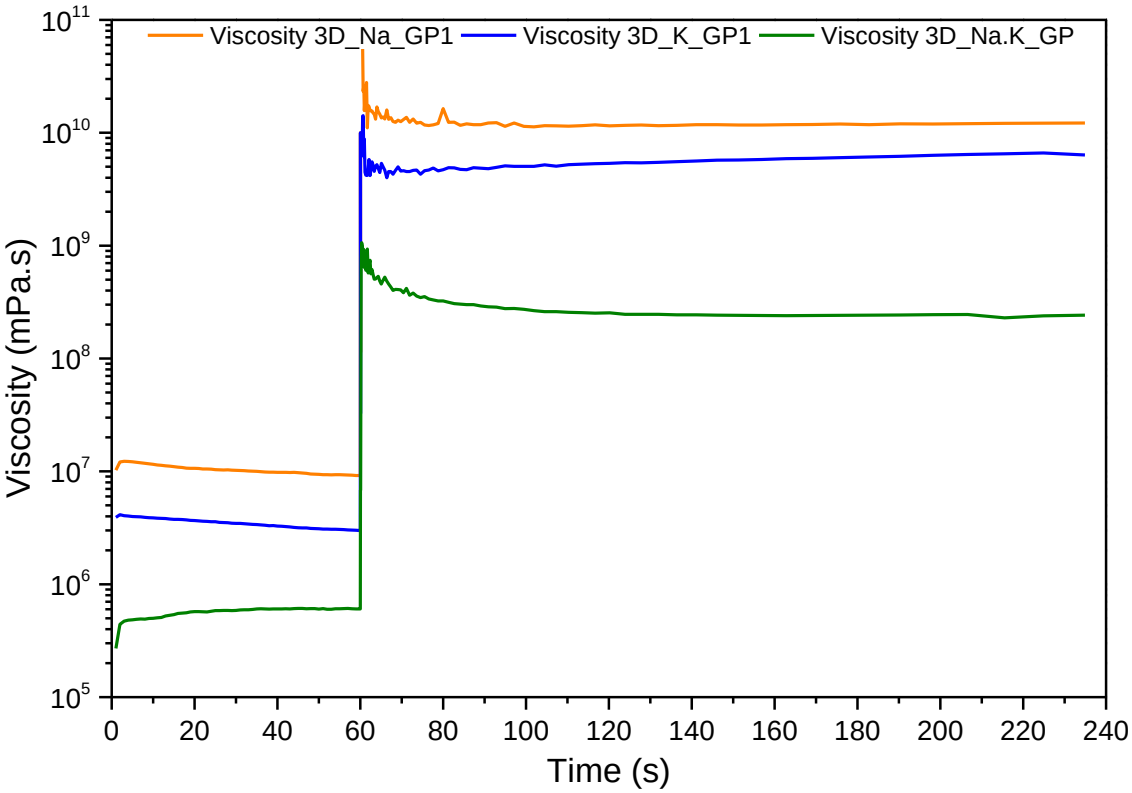

Figure 29. Viscosity recovery test performed on the three inks.

It was possible to observe that the three materials quickly reached plateau behavior. 3D_Na_GP1 and 3D_K_GP1 recovered the viscosity in a short time, around 10 s, and 3D_Na.K_GP took a little longer to reach the constant viscosity, approximately 20 s. The inks increased their viscosity by about three orders of magnitude in this time frame.

It was considered a viscosity value of 20 seconds (difference between the beginning of the second part of the viscosity recovery test, 60 s, and the time when the curves reached their plateau behavior, 80 s) to estimate the midspan deflection using Equations 4 and 5.

The calculated deflection for the 3D_Na_GP1, 3D_K_GP1 and 3D_Na.K_GP was 2.58, 4.68 and 18.22 µm, respectively, corresponding to 0.31%, 0.56% and 2.17%

of the filament diameter. These results confirmed that a structure printed with the three types of ink can retain its shape.

The rapid recovery of viscosity is the most important characteristic of an ideal ink, and from the results obtained it is possible to confirm that the inks have a suitable rheology for printing 3D structures by DIW. The rapid increase in viscosity, since the filament is deposited, reduces the deformation of the structure because it maintains the shape and supports the weight of the following layers.

The 3D_Na.K_GP ink, even if it recovers the viscosity rapidly, reaches a lower viscosity and yield stress values, which can be easily reached by the weight of the successive layers, consequently, its structure was more deformed as observed experimentally.

The initial increase of viscosity in the second step of the test is due to the presence of the filler, which needs time to slow down, so at the beginning it moves faster than the rheometer plate. It depends on the test and it does not describe the real behavior of the ink during extrusion.

Finally, the time sweep test was performed on the three inks (Figure 30). It was analyzed the progression of the geopolymerization reaction over the time.

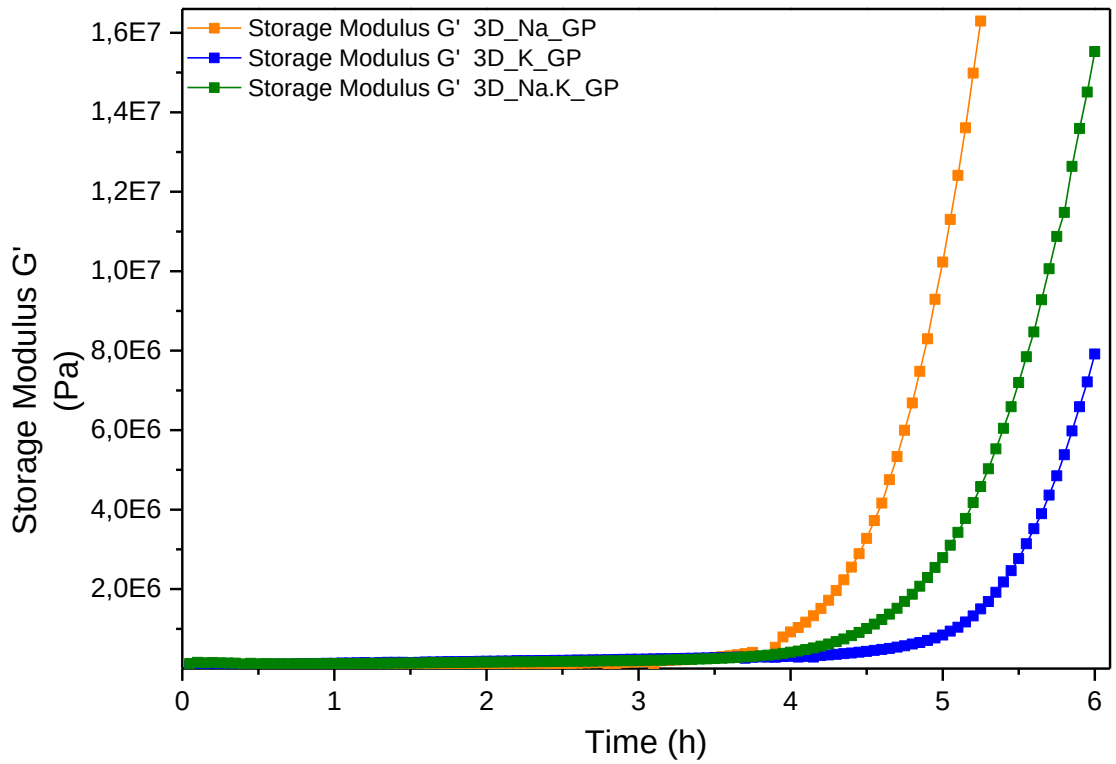

Figure 30. Time sweep test performed on the three inks.

According to the time sweep test, it was observed that the working time of the geopolymers, before starting the reaction, was respectively 4, 4.5 and 5 h for 3D_Na_GP1, 3D_Na.K_GP and 3D_K_GP1, and experimentally it was found that the inks could be printed for about 2 h; the total amount of ink was printed without hardening.

5.3. 3D GEOPOLYMER STRUCTURE

After the rheological investigation, the inks were used to manufacture lattice via DIW. The geometry chosen was a circular lattice with 24 mm diameter and 9.6 mm height with shifted layers and with 800 μm thick struts. The printing process is shown in Figure 31.

Figure 31. 3D printing process.

As seen with their rheology analysis, the inks have the requirements to be printed in 3D; the three structures are shown in Figure 32. For each type of ink ten samples were inspected and the values of average diameter, thickness and mass are reported in the Table 12. These values confirmed the good repeatability of the manufacturing procedure provided by the additive manufacturing approach.

Table 12. Dimension of three types of lattice.

Sample	Average diameter (mm)	Thickness (mm)	Mass (g)
3D_Na_GP1	24.3 ± 0.2	9.7 ± 0.2	4.0 ± 0.2
3D_K_GP1	24.4 ± 0.2	9.8 ± 0.2	3.7 ± 0.2
3D_Na.K_GP	22.1 ± 0.2	8.2 ± 0.2	3.8 ± 0.3

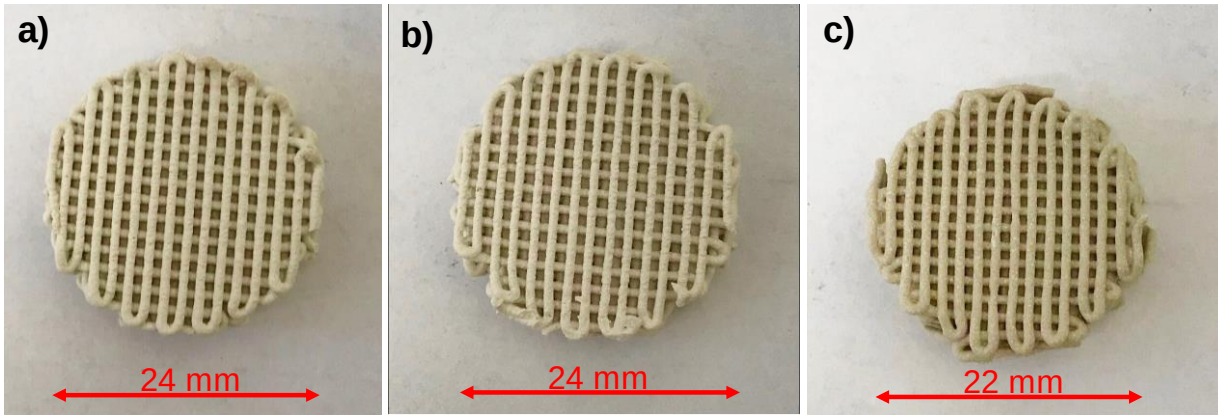

Figure 32. 3D-printed lattices using the material: a) 3D_Na_GP1; b) 3D_K_GP1; c) 3D_Na.KGP.

5.3.1. Physical, mechanical and morphological properties of the structures

The porosity of the design was obtained by Solidworks software, the open (OP) and total (TP) porosities were obtained through the measurement of the geometric density and the analysis by pycnometer of the apparent and real density, finally, the closed porosity was calculated by the difference between TP and OP, these results are reported in Table 13.

Since the designed porosity considers only the open channels within the structure, for the samples produced with the materials 3D_Na_GP1 and 3D_K_GP1, it was observed that the open porosity is slightly larger than the designed porosity, it is probably due to porosity of the filaments. On the other hand, for the structure produced with the ink 3D_Na.K_GP it was smaller because the layers collapsed in the medium, where it had less support.

Table 13. Physical properties for the structures: 3D_Na_GP1, 3D_K_GP1 and 3D_Na.K_GP.

Sample	3D_Na_GP1 (110°C)	3D_K_GP1 (110°C)	3D_Na.K_GP (110°C)
Designed porosity (vol%)	49.10	49.10	49.10
Open porosity (vol%)	55.40	63.75	42.59
Closed porosity (vol%)	1.03	0.17	0.48
Total porosity (vol%)	56.43	63.92	43.07

The mechanical test was done for the three types of structures: green and treated at 110 °C; twenty samples for each one (Table 14). The higher compressive strength of the treated samples is supposedly due to the finalization of the geopolymerization reaction. The removal of water is the main reason for the treatment, since it is a requirement for a better progress of the transesterification reaction, but there is also the advantage of improving the mechanical properties of the materials. As it was possible to see in the DSC graphs, with the heat treatment, the physical water is eliminated around 110 °C favoring the conclusion of the geopolimerization reaction.

Table 14. Mechanical compressive strength for structures: 3D_Na_GP1, 3D_K_GP1 and 3D_Na.K_GP.

Sample	Compressive Strength (Mpa)
3D_Na_GP1 (green)	2.74 ± 0.67
3D_Na_GP1 (110°C)	4.13 ± 1.21
3D_K_GP1 (green)	1.63 ± 0.47
3D_K_GP1 (110°C)	2.23 ± 0.59
3D_Na.K_GP (green)	6.23 ± 2.11
3D_Na.K_GP(110°C)	6.27 ± 1.03

As expected from a cellular ceramic material, such as a foam or a lattice, the porosity and the compressive strength are inversely proportional: as the porosity increases, the strength of the structure, this relation for the three materials is reported in Figure 33.

According to its rheology, the 3D_Na.K_GP ink was the less suitable to 3D printing, the filaments didn't quickly retain their shape and with the addition of successive layers the structure sank slightly, this provided lower porosity and consequently higher compressive strength than the structures produced with the 3D_Na_GP1 and 3D_K_GP1 inks.

The behavior for the three materials is very similar, depending on how porous the structure is, it can be noticed the difference of the compressive strength, however all values obtained are sufficient for the desired application, including these lattice-shaped geopolymers inside a reactor.

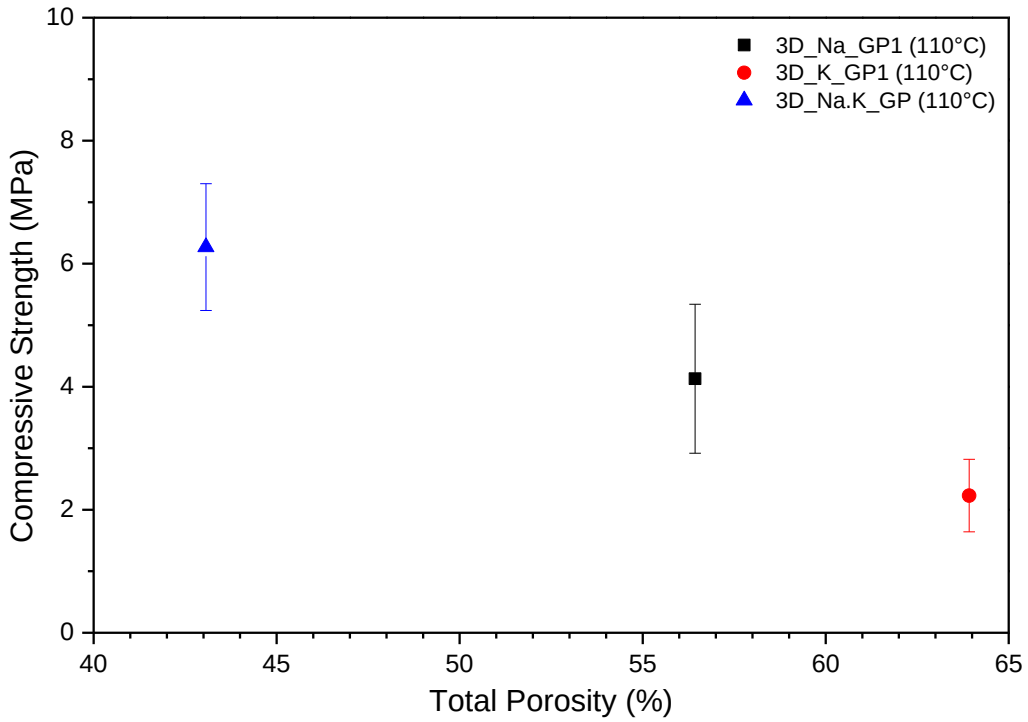

Figure 33. Compressive strength versus total porosity for the three types of lattices.

The results shown previously in relation to the porosity can be seen reflected in Figure 34, the pores were obtained in the mixing step of the geopolymer: considering the high viscosity of the material, when it is mixed it embodies air bubbles which remain in the filaments when they are printed. This image was obtained for the 3D_Na_GP1 structure, however, the behavior of the other inks is similar. Some pores of the structures have probably been closed due to the sanding of the extremities, but the porosity of the structure can also be proved by the BET analysis, which will be discussed later.

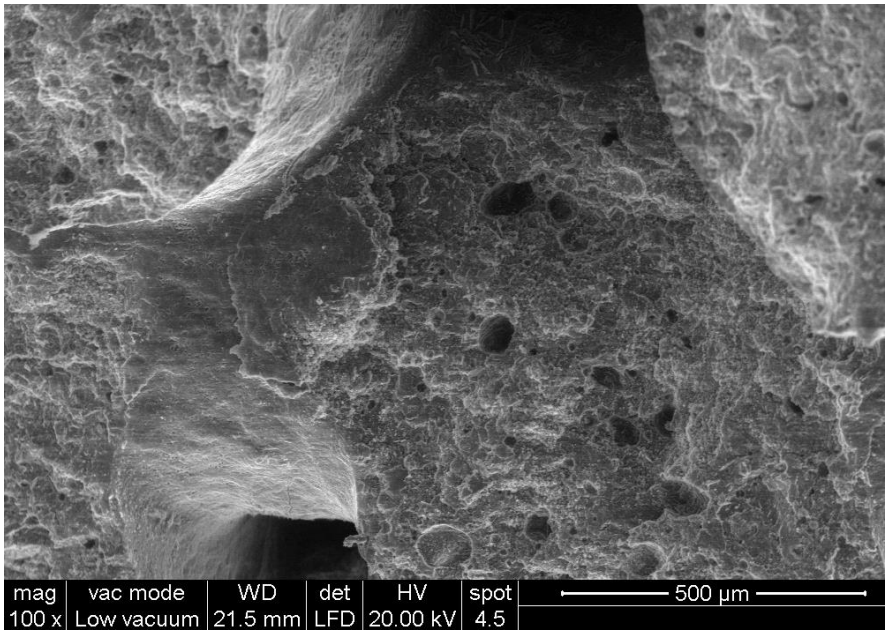

Figure 34. Scanning electron microscope image for the 3D_Na_GP1.

From the optical microscope pictures (Figure 35a;c;e) the filler (the lighter points) appears to be homogeneously distributed within the section of the filament. No interfaces were created between the particles because, probably, of an interaction between the forming geopolymer matrix and the filler, encompassing it in a cohesive way. From the scanning electron microscope image (SEM) (Figure 35b;d;f) it was not possible to distinguish the filler from the matrix because the composition of the materials are the same in relation to the species.

It was clear from the Figure 35f that even keeping the lattice shape, the filaments from the 3D_Na.K_GP structure did not retain their circular section, and it confirms its higher compressive strength and less porosity.

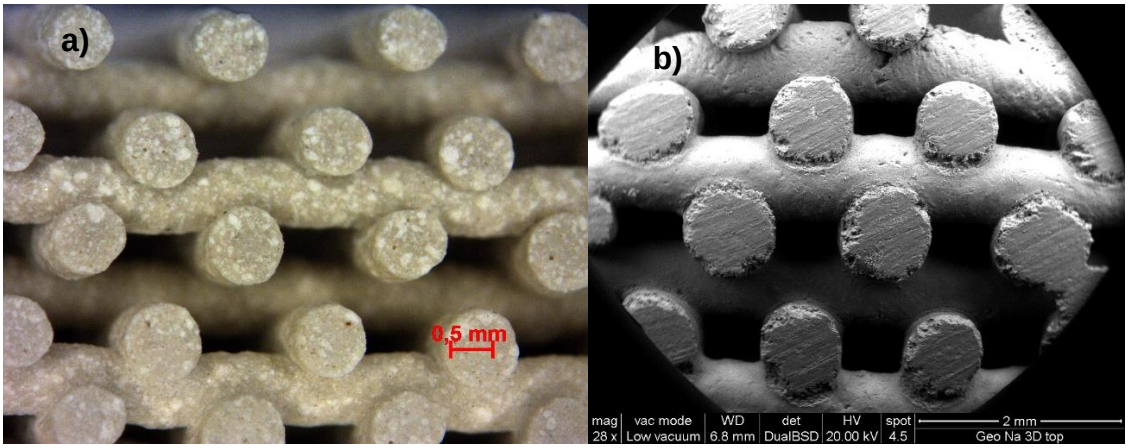

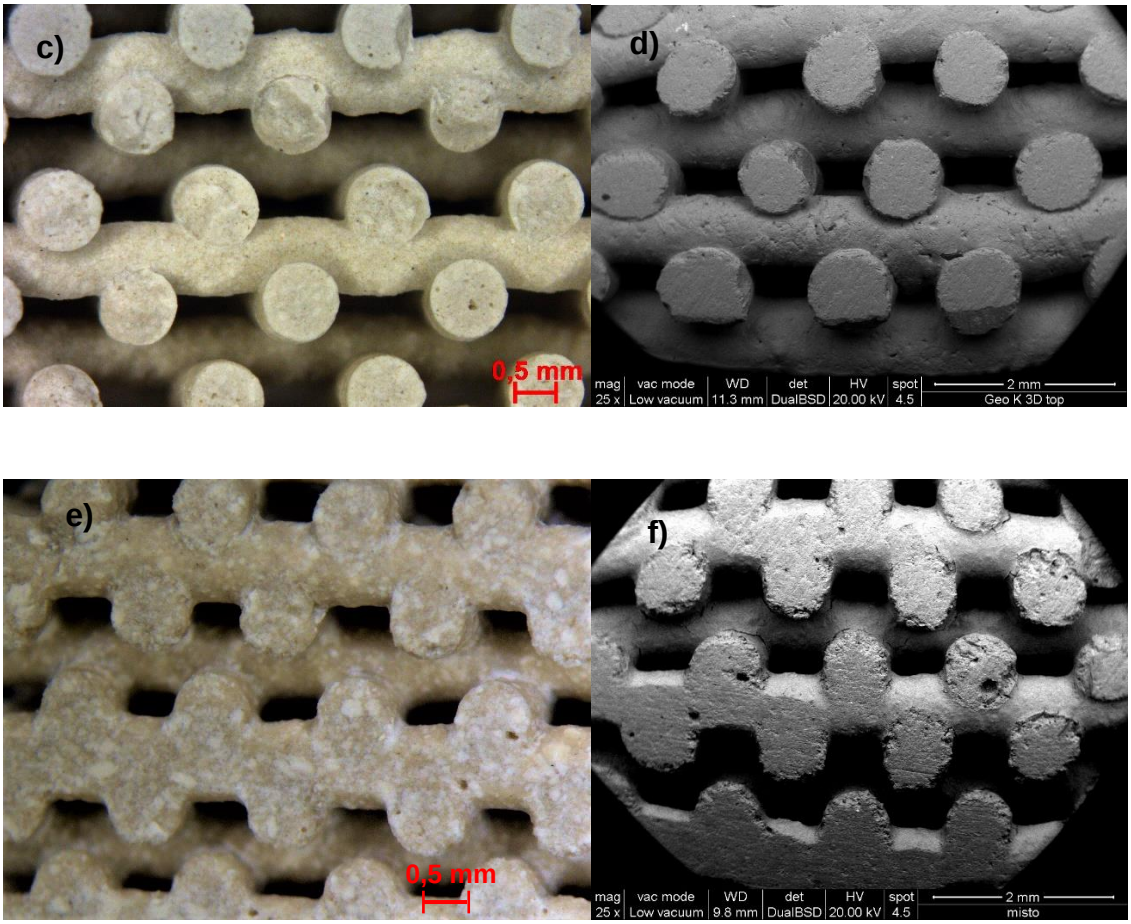

Figure 35. The side view of the samples from the optical microscope and Scanning electron microscope: 3D_Na_GP1; 3D_K_GP1; 3D_Na.K_GP.

5.3.2. Permeability analysis

The dynamic fluid data were acquired through permeability analyzes performed at UNAERP (Brazil) and were treated according to the least squares method using a parabolic model: $y = ax + bx^2$; the air velocity against pressure drop was plotted in the graph (Figure 36).

The parabolic relationship between the pressure drop parameter for compressible flow ($[P_i^2-P_o^2]/2P_oL$) and velocity of the air (v_s) was confirmed through the high-quality fitting of Forchheimer's equation; correlation coefficient (R^2) was very close to the unity for the triplicate samples (0,999 - 0,998). The air velocity ranged from 0 to 0,33 m/s for a pressure drop applied between 0 and 2 MPa/m.

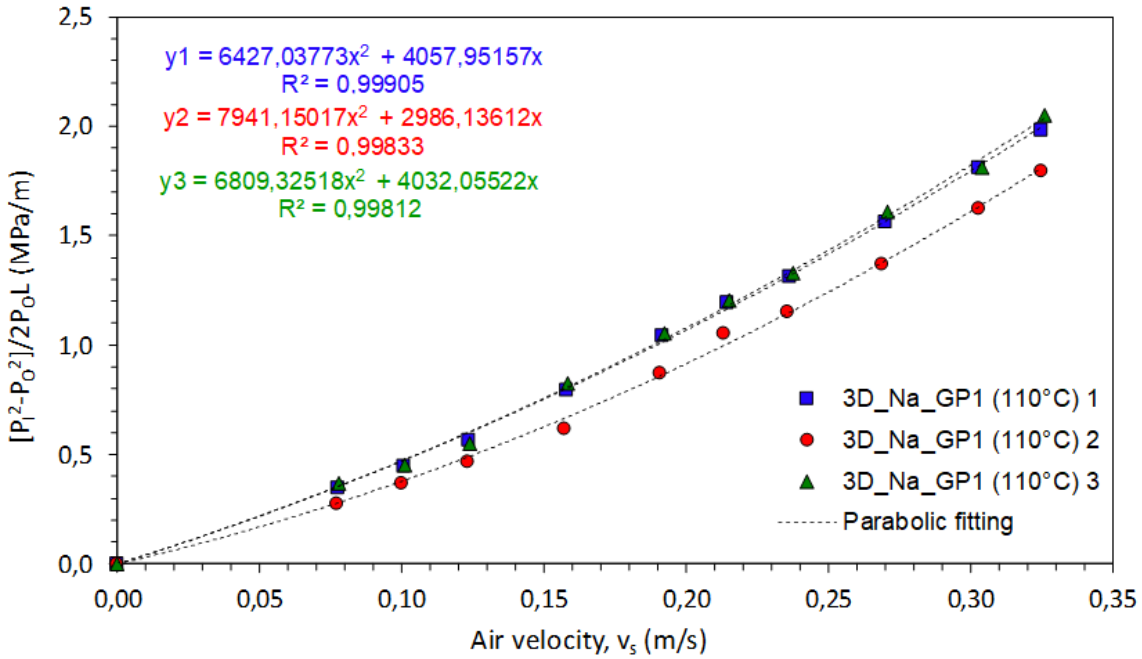

Figure 36. The air velocity versus pressure drop for the 3D_Na_GP1 samples.

The permeability parameters of Forchheimer's equation (Equation (8)) were calculated using the constants (a and b) obtained in the parabolic fitting by $k_1 = \mu/a$ and $k_2 = \rho/b$.

The values obtained for k_1 and k_2, as well as the average values and deviations for these constants are shown in Table 15 and the adapted version of a comprehensive map proposed by Innocentini et al. [58-61] that classifies different porous materials according to the ranges of their permeability coefficients k_1 and k_2 including the results for the lattice geopolymer made with the material 3D_Na_GP1 is shown in the Figure 37.

Table 15. Permeability constants obtained for the triplicate samples.

Sample	k_1 (m^2)	k_2 (m)
3D_Na_GP1 (110°C) - 1	4.62E-09	1.71E-4
3D_Na_GP1 (110°C) - 2	6.28E-09	1.38E-4
3D_Na_GP1 (110°C) - 3	4.65E-09	1.61E-4
average	5.19E-09	1.57E-4
deviation	9.50E-10	1.67E-5
CV (%)	18.31	10.68

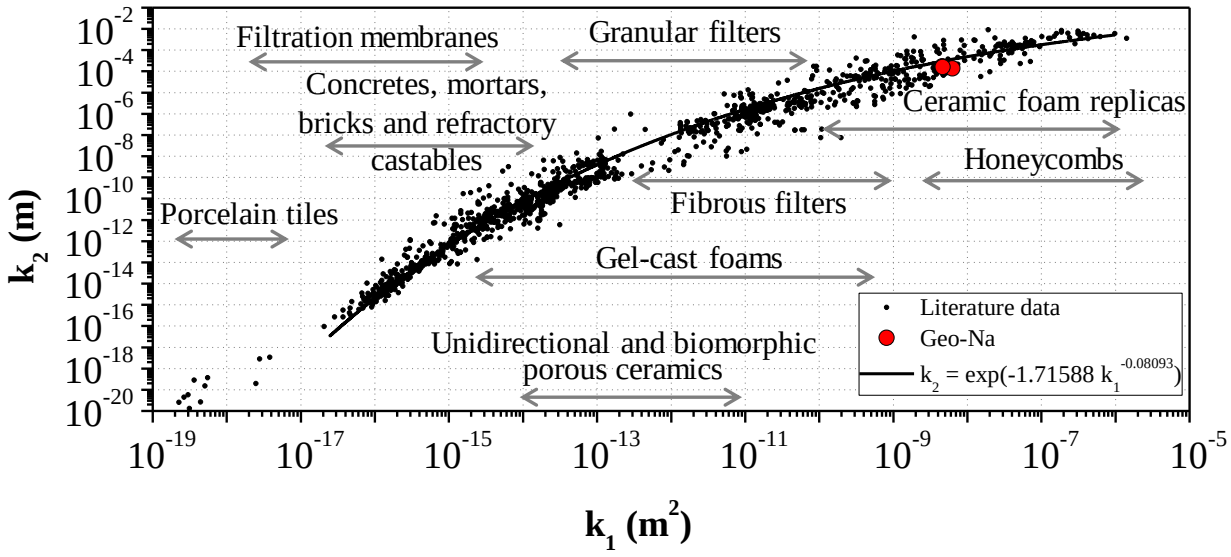

Figure 37. A comprehensive map of porous materials according to the ranges of their permeability coefficients (proposed by Innocentini et al.)

The permeability analysis was carried out to evaluate the easiness with which reactants pass through the 3D-printed lattices during the reaction, and with the values obtained for the constants it was verified that this lattice is in the same range of honeycombs, which are used typically as a filter, and have a good permeability.

5.4. BIODIESEL

5.4.1. Effect of water content in the geopolymer composition and influence of reaction conditions on the biodiesel conversion

The first investigation, concerning to biodiesel conversion, was made by comparing powdered geopolymers (Na_GP1 and Na_GP2) produced with the same molar ratio Na_2O/Al_2O_3 of 1.3, but varying the molar ratio H_2O/Al_2O_3 from 14.0 to 18.5.

The specific surface area, total pore volume and the average pore diameter for the Na_GP1 and Na_GP2 heat treated at four temperatures (110, 300, 500, 700 ºC) are shown in Table 16.

Table 16. BET analysis of Na_GP1 and Na_GP2.

Sample	Calcination temperature (°C)	Specific surface area (m^2/g)	Total pore volume (cm^3/g)	Average pore diameter (nm)
Na_GP1	110	32.62	0.30	34.42
	300	31.41	0.31	34.39
	500	27.43	0.28	34.46
	700	6.34	0.08	34.31
Na_GP2	110	15.68	0.14	3.93
	300	13.69	0.13	3.93
	500	11.87	0.14	24.22
	700	3.15	0.04	60.77

According to these results, the BET analysis indicated that, as the heat treatment temperature was increased from 110° to 700°C, the specific surface areas (SSA) of the Na_GP1 decreased from 32.62 to 6.34 m^2/g, while the values for Na_GP2 were practically half the Na_GP1 ones, since they decreased from 15.68 to 3.15 m^2/g.

As shown in Figure 38a, the total pore volume for the 110°, 300° and 500°C heat treated Na_GP1 remained around 0.3 cm^3/g, only when the material was heat treated at 700 °C the value was much lower (0.08 cm^3/g). The average pore diameter remained practically constant around 34.4 nm when increasing the treatment temperature.

The Na_GP2 had the same behavior regarding to the total pore volume (Figure 38b): the value remained around 0.14 cm^3/g at the first three temperatures and decreased to 0.04 cm^3/g in the 700 °C treated material. The average pore diameter for the treated material at the first two temperatures was 3.93 cm^3/g and for the material at 500 °C and 700 °C was 24.22 and 60.77 cm^3/g, respectively.

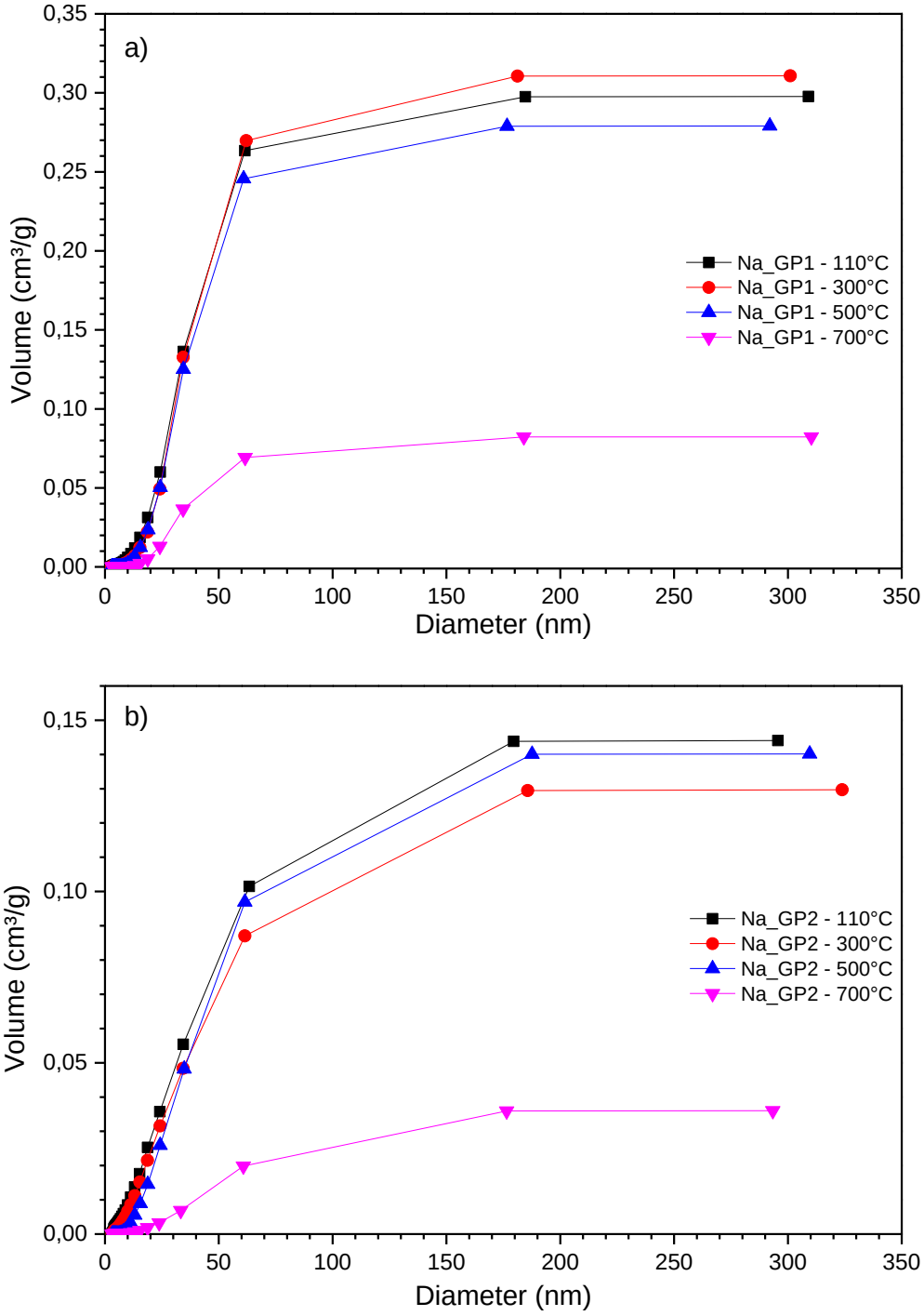

Figure 38. Total pore volume of the material: a) Na_GP1; b) Na_GP2.

In accordance to the International Union of Pure and Applied Chemistry (IUPAC) classification, the adsorbent pores were classified in three groups: pore with diameter less than 2 nm (micropore); pore with diameter between 2 and 50 nm (mesopore); and pore with diameter bigger than 50 nm (macropore).

The pore size distributions of the Na_GP1 and Na_GP2 are shown in the Figure 39a-b, respectively.

It can be observed that in both geopolymers no micropores are present, the mesopores predominate, varying from 10 to 50 nm, and also a part of the surface is occupied by macropores, ranging from 50 to 110 nm.

The mesopores give a higher contribution to the samples total pore volume; the macropores are fewer than the mesopores, however, they have a larger volume and they considerably increase the total volume. The low SSA of the 700 °C heat treated materials was in accordance with the low cumulative volume and with the pore distribution. The meso-porosity of the material is due to the geopolymerization reaction, the polycondensation of aluminosilicates, which produces water, and, in nanometric scale, its morphology, which is based on aggregation of spheroidal particles [15].

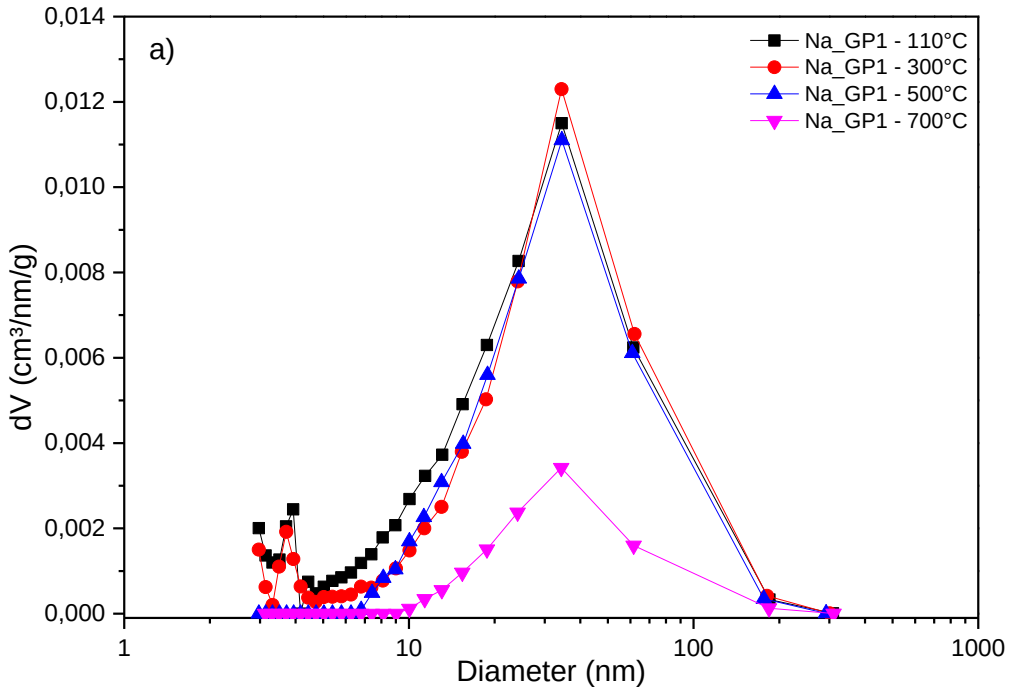

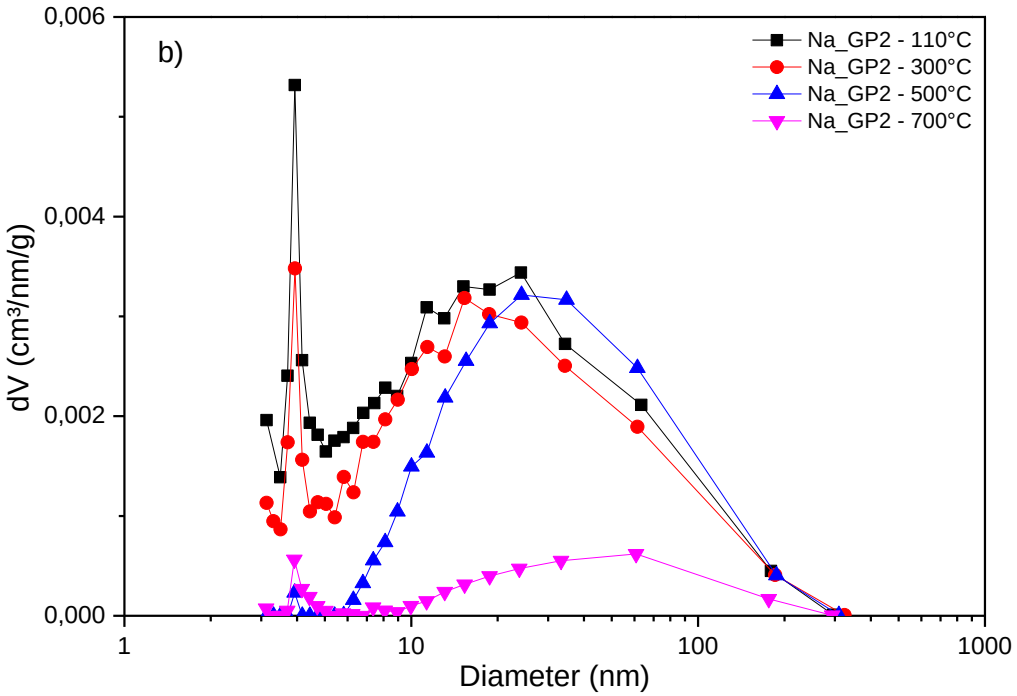

Figure 39. Pore distribution of the material: a) Na_GP1; b) Na_GP2.

The BET and BJH analysis were important for the geopolymer characterization because it could be related to the activity of the catalyst: the larger the surface area is, the higher the contact of the reagents with the catalyst is. The pore size distribution and the average pore diameter can affect the sedimentation and phases separation after the reaction.

Na_GP1 and Na_GP2 were used in the transesterification reaction as heterogeneous catalyst with the following reaction conditions: 3 wt.% of catalyst, 150% of methanol excess for 1 hour at 60 °C.

The catalytic activity of these materials was confirmed by gas chromatography analysis (GC) of the biodiesel phase of the samples, which underwent evaporation to remove excess methanol.

The Figure 40 shows the biodiesel conversion versus the heat treatment temperature for both materials.

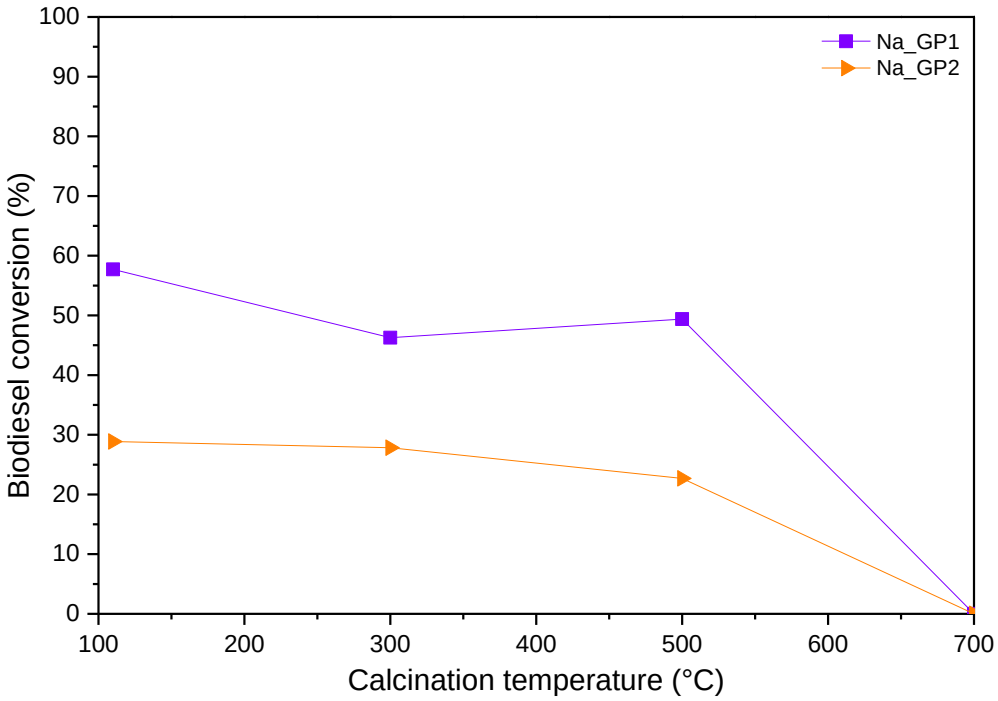

Figure 40. Evaluation of biodiesel conversion using Na_GP1 and Na_GP2 as catalyst in the transesterification reaction.

In both materials, increasing the heat treatment temperature the biodiesel conversion decreased, from approximately 60% to 0% for the Na_GP1 and from 30% to 0% for the Na_GP2.

Considering the low biodiesel yields, the reaction conditions were changed in relation to time and temperature, from 1 h and 60 °C to 2 h and 70 °C. The material used as catalyst for this evaluation was Na_GP1, which obtained better conversion when compared to Na_GP2. The conversion of the reaction versus the treatment temperature of the material for the two reaction conditions is shown in Figure 41.

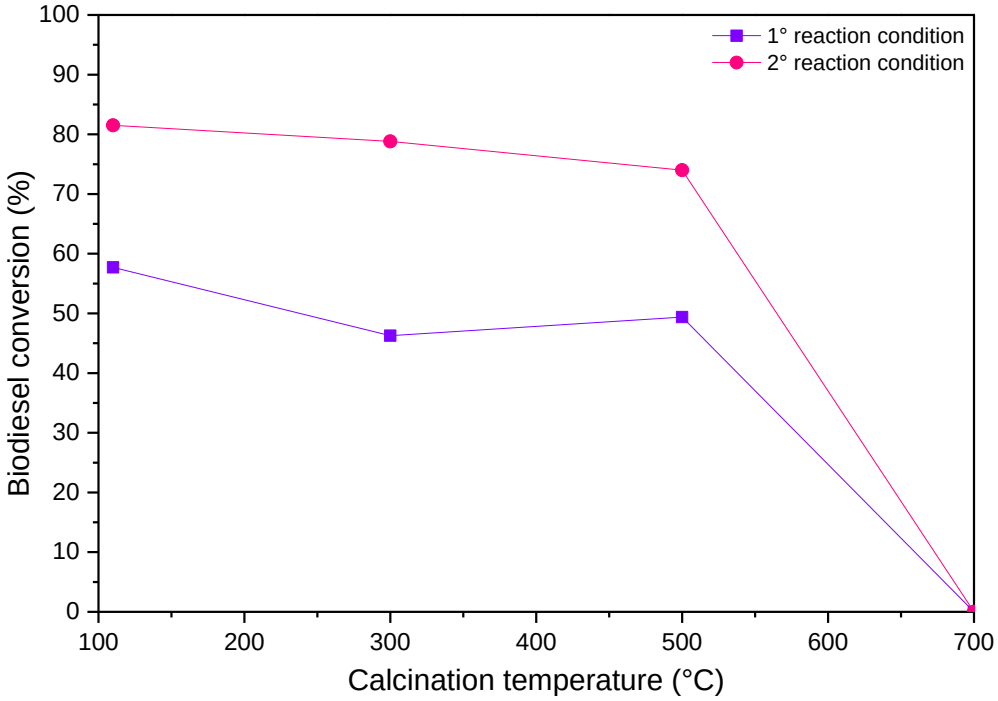

Figure 41. Evaluation of biodiesel conversion regarding the reaction conditions using Na_GP1.

The same behavior was observed in this evaluation, increasing the heat treatment temperature, the biodiesel conversion decreased. It is observed that the reaction operated with the second reaction condition had a higher biodiesel conversion in comparison to the reaction using the first reaction condition, ranging from ~82% to 0%.

The conversion of biodiesel can be visibly confirmed, because phase separation occurs after the end of the reaction. Figure 42a-d showed the phase separation for transesterification operated with the second reaction condition (2 h at 70 °C) using the Na_GP1 material. In this case, it was observed the success of the reaction with the formation of biodiesel (upper phase), the sub-product glycerol (intermediate phase) and the geopolymer powder in the bottom, for the material treated at 110, 300 and 500 °C (Figures 42a-c). The sample treated at 700 °C (Figure 42d) showed the presence of unreacted methanol in the upper phase, indicating that the reaction did not occur.

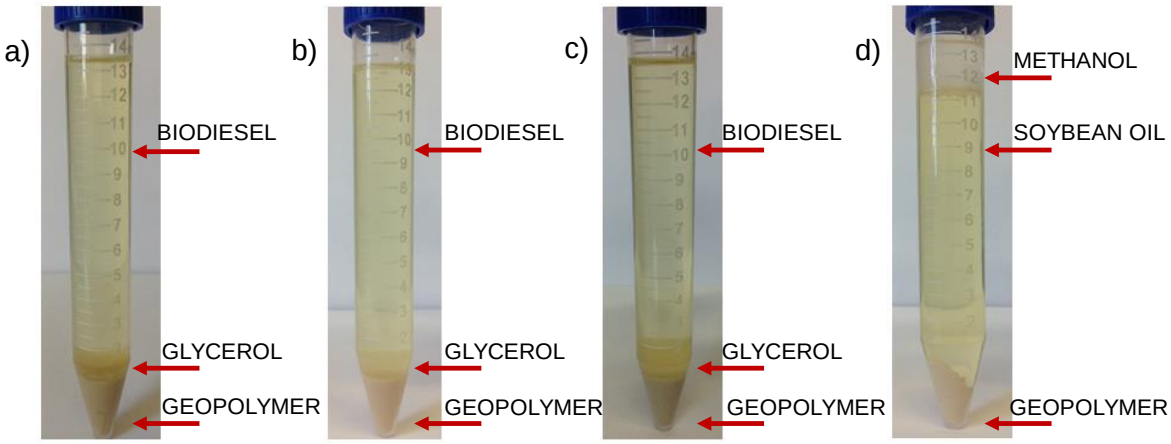

Figure 42. Transesterification reaction using the material Na_GP1 heat treated at: a) 110 °C; b) 300 °C; c) 500 °C; d) 700 °C.

Through the analysis of gas chromatography, it was possible to prove the success of the transesterification reaction and to quantify the biodiesel conversion. The graphs obtained in a typical gas chromatography analysis for the biodiesel samples are shown in Figure 43a-e.

Initially the analysis of completely esterified soybean oil (Figure 43a) was performed and it was considered as 100% conversion sample for comparison with the samples obtained by transesterification reactions using the geopolymers as catalysts.

In the chromatograms of the analyzed biodiesel samples it was possible to specify the types of esters formed (Figure 43b-e), since the retention time of each species is known. As the soybean oil used in all reactions of this work was always the same, the types of esters found were also the same. The first peak obtained at 16.15 min belongs to palmitic acid methyl ester (C16:0), then the internal standard peak was obtained at 17.17 min (species not present in the biodiesel sample added for curve normalization) and afterwards there were the peaks of linoleic acid methyl ester (C18:2) at 18.57 min, oleic acid methyl ester (C18:1) at 18.66 min and stearic acid methyl ester (C18:0) at 19.07 min.

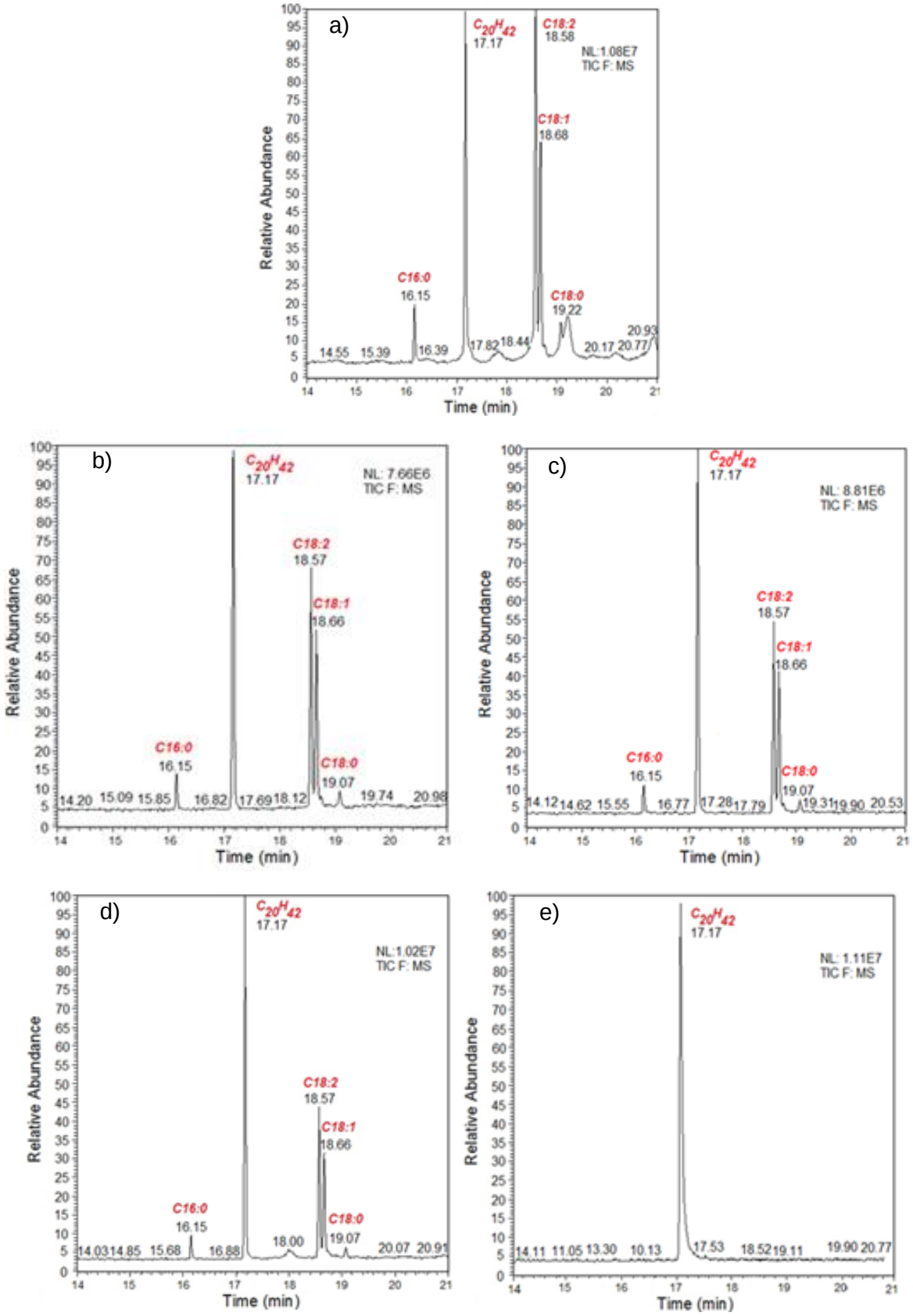

Figure 43. Gas chromatography analysis of: a) Completely esterified soybean oil; b) Na_GP1 at 110 °C; c) Na_GP1 at 300 °C; d) Na_GP1 at 500 °C; e) Na_GP1 at 700 °C.

5.4.2. Effect of alkali type and alkali content on the biodiesel conversion

Since, by operating with the second reaction condition (2 h at 70 °C), a higher biodiesel conversion was obtained for the treated material at the four temperatures, this condition was used to investigate the biodiesel yield using three different catalysts: Na_GP1, which, as previously proven, obtained higher conversion, K_GP1 and Na.K_GP.

The specific surface area, total pore volume and average pore diameter for the materials analyzed in this investigation are shown in Table 17.

Table 17. BET e BJH analysis for the materials: Na_GP1, K_GP1 e Na.K_GP.

Sample	Calcination temperature (°C)	Specific surface area (m^2/g)	Total pore volume (cm^3/g)	Average pore diameter (nm)
Na_GP1	110	32.62	0.30	34.42
	300	31.41	0.31	34.39
	500	27.43	0.28	34.46
	700	6.34	0.08	34.31
K_GP1	110	62.54	0.33	18.93
	300	42.18	0.29	18.71
	500	29.85	0.34	18.90
	700	28.64	0.31	18.93
Na.K_GP	110	8.35	0.12	62.38
	300	8.42	0.13	61.96
	500	4.74	0.10	63.09
	700	0	0	3.13

Regarding the characterization of the pores, the K_GP1 and the Na.K_GP have behavior similar to the Na _GP1 previously shown.

Increasing the treatment temperature of the material the SSA and the total pore volume of the K_GP1 decreased from 62.54 to 28.64 m^2/g and 0.33 to 0.31 cm^3/g, respectively (Figure 44a). For the Na.K_GP the low SSA was reflected in a low total pore volume (~12 cm^3/g) besides this sample heat-treated at 700 °C had its total pore volume equal to zero due to the absence of SSA (Figure 44b).

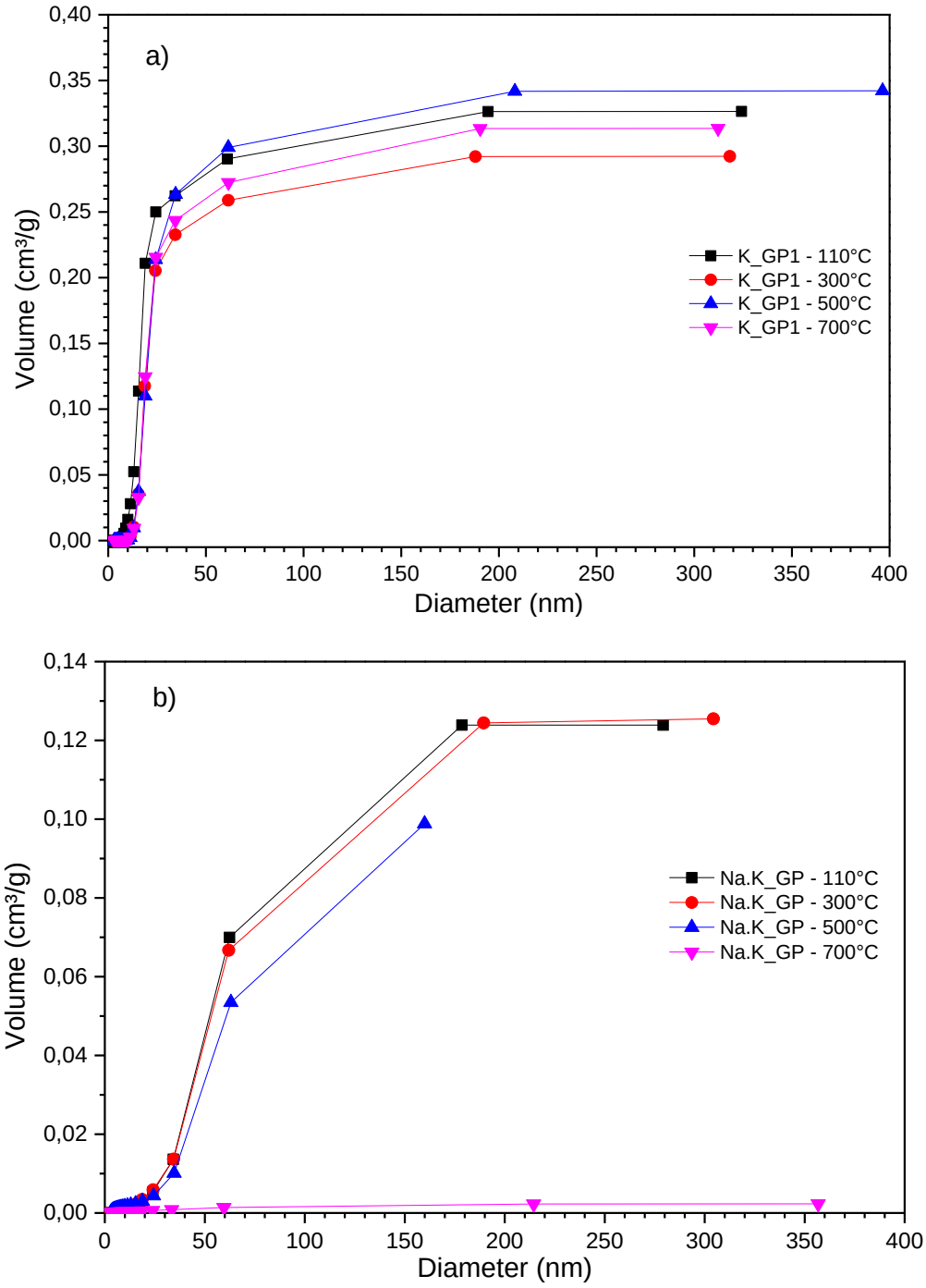

Figure 44. Total pore volume of the material: a) K_GP1; b) Na.K_GP.

K_GP1 had the lowest average pore diameter around 18 nm and its pore distribution was entirely in the range of mesopores (2-50 nm) (Figure 45a); Na.K_GP had a distribution strongly influenced by macropores (> 50 nm) with an average pore diameter of about 62 nm, the only exception was for the material treated at 700 °C, around 3 nm (Figure 45b).

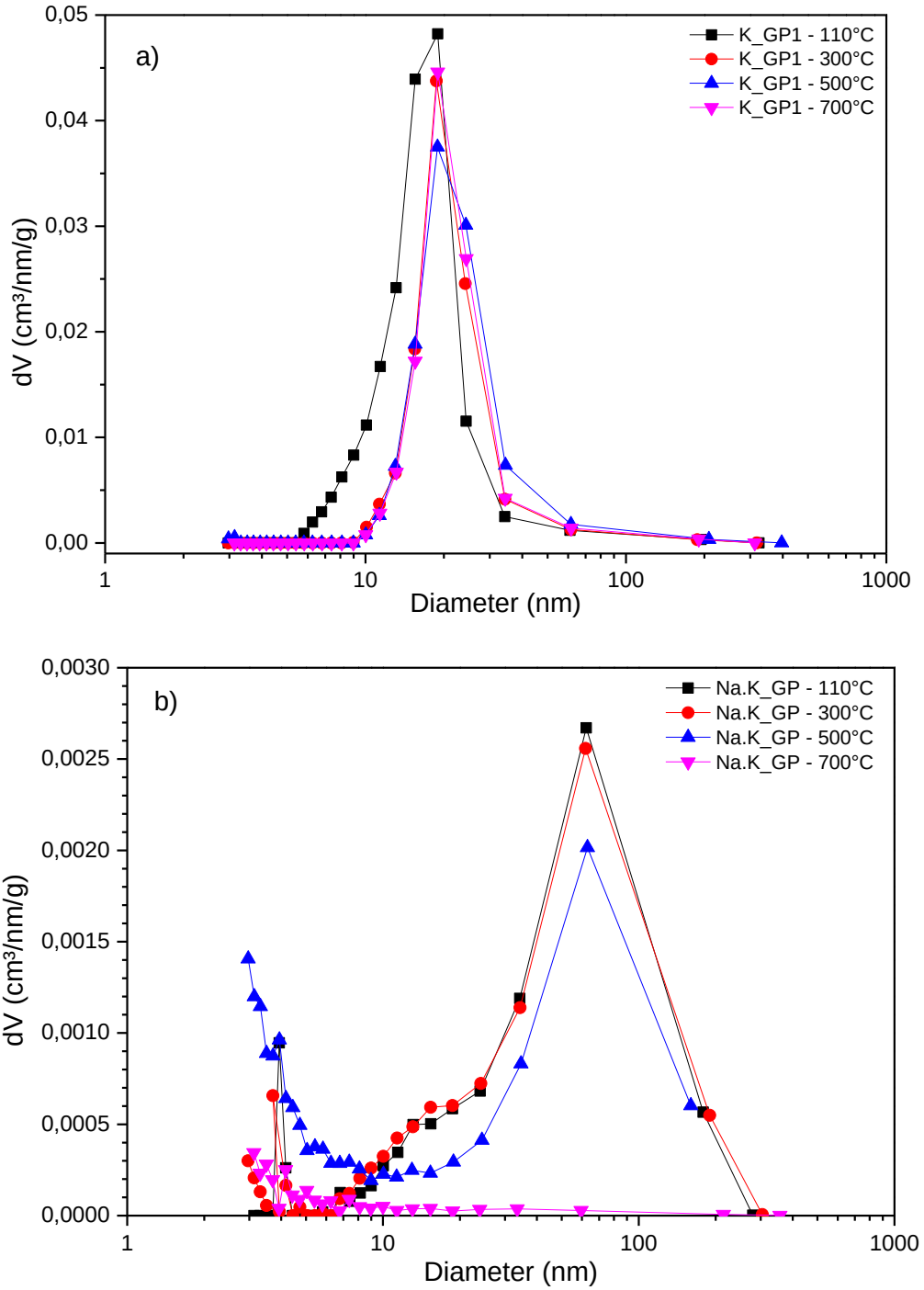

Figure 45. Pore distribution of the material: a) K_GP1; b) Na.K_GP.

After characterization of the materials, their catalytic activities were tested in the transesterification reaction with the previously determined reaction conditions. The Figure 46 shows the biodiesel yield versus the heat treatment temperature for the materials, and it was possible to observe the standard behavior for biodiesel conversion: increasing the sample treatment temperature the conversion decreased.

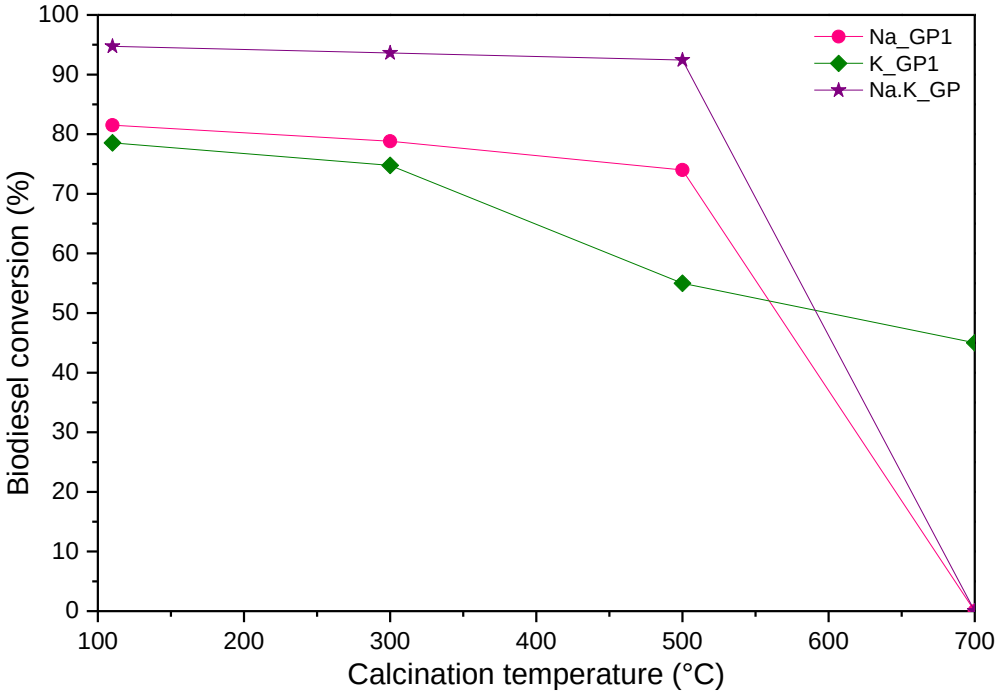

Figure 46. Evaluation of biodiesel conversion regarding the type of geopolymer.

Using the Na.K_GP as the catalyst, higher conversion values were obtained even though they had a lower specific surface area. There is probably some chemical interaction between Na and K in this material and, its use makes the pH of the solution more alkaline than the others. This investigation must be deepened in order to fully understand its behavior.

In order to choose the best material to be used as a heterogeneous catalyst, alkali leaching must be considered in addition to biodiesel conversion. This test was done in distilled water at 60 °C for 1 h using the three materials analyzed in this investigation.

According to the results shown in Table 18, in all three cases, increasing the treatment temperature, the leaching of alkali decreased due to the stabilization of the 3D network at high temperatures and the loss of ions from the structure becomes difficult.

Therefore, with the result of biodiesel yield and alkali leaching the material Na.K_GP heat-treated at 500 °C can be suggested as the best system to be used as a heterogeneous catalyst.

Table 18. Leaching of alkalis for Na_GP1, K_GP1 and Na.K_GP.

Calcination Temperature (°C)	Leaching of Na (%)	Leaching of K (%)	Leaching of Na and K (%)
110	18.8	20.0	74.0
300	16.7	22.3	30.0
500	11.7	26.0	8.3
700	2.9	6.1	7.4

In parallel to this investigation, the effect of the amount of alkali on the reaction conversion was analyzed. The K-based geopolymer was used for this analysis with the reaction condition of 2 h and 70 °C. Two other types of materials were produced, K_GP2 with molar ratio K_2O/Al_2O_3 of 1.35 and K_GP3 with molar ratio of 1.0, all samples were dried at 110 ° C before being used. The values found by the BET and BJH analysis for the three materials are shown in Table 19.

Table 19. BET e BJH analysis for the materials: K_GP1, K_GP2 e K_GP3.

Sample	Calcination temperature (°C)	Specific surface area (m^2/g)	Total pore volume (cm^3/g)	Average pore diameter (nm)
K_GP1	110	62.53	0.33	18.93
K_GP2	110	93.45	0.57	18.87
K_GP3	110	54.46	0.59	18.74

Increasing the amount of alkali in the material, the specific surface area increased and for the three materials the standard behavior of the pore distribution was maintained. There was no micropores present and most of the pores belonged to the mesopore range, between 7 and 70 nm (Figure 47a) and the total pore volume ranged from 0.33 to 0.59 cm^3/g (Figure 47b).

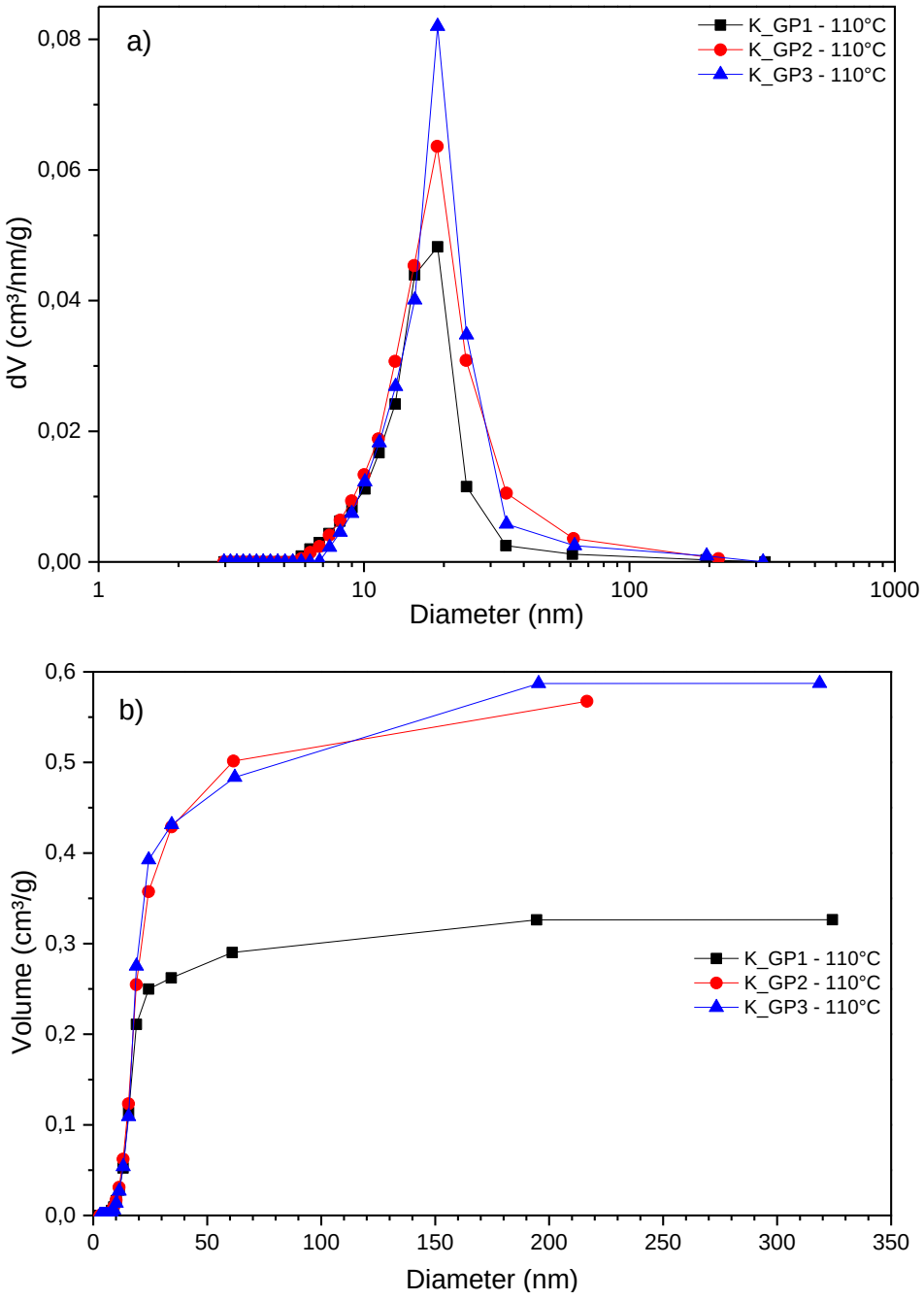

Figure 47. Characterization of the pores for the material K_GP1, K_GP2 and K_GP3, a) pore distribution; b) total pore volume.

For this investigation the three materials were tested in the transesterification reaction and the biodiesel conversion values are reported in Figure 48. It was observed that by increasing the amount of alkali in the geopolymer formulation, biodiesel yield increased due to the alkalinity of the solution.

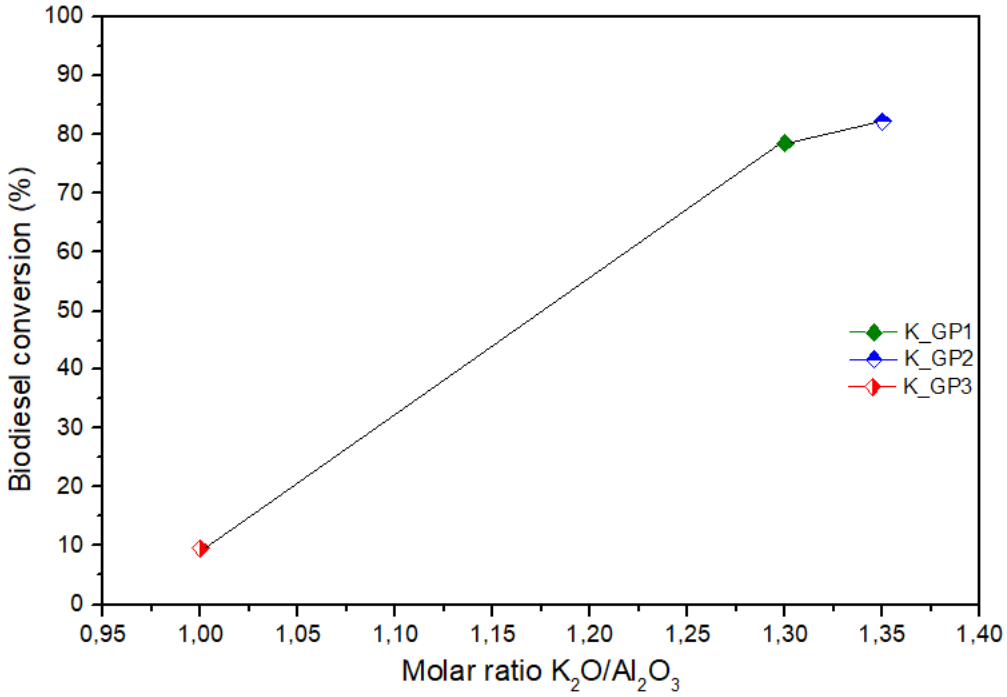

Figure 48. Evaluation of biodiesel conversion according to the amount of alkali in the geopolymer.

5.4.3. Effect of geopolymer morphology on the biodiesel conversion

(Partially published in: "Lattice-shaped geopolymer catalyst for biodiesel synthesis fabricated by additive manufacturing" Murilo D.M.Innocentini, Renata F.Botti, Paula M.Bassi, Cristina F.P.R.Paschoalato, Danilo L.Flumignan, Giorgia Franchin, Paolo Colombo; Ceramics International,Volume 45, Issue 1, January 2019, Pages 1443-1446) [62].

After confirming the catalytic activity of the geopolymer powder in the transesterification reaction, the 3D-printed structure of the 3D_Na_GP1 material was tested in the reaction.

The similarity of the SSA between the lattice and its finely ground powder (<125 μm), proves the reachability of the catalytic sites within the pores of the structure. These values, however, were lower than those found in the literature for powdered Ca-based geopolymer [63], and larger than the ones found for zeolite impregnated with KOH powder [64].

For this investigation, the reaction conditions were: 3 wt.% catalyst, 150% of methanol excess for 4 h at 70 °C; the catalytic activity of the structure was confirmed by gas chromatography analysis. Conversion values using both materials, as well as SSA and pore analysis, are reported in Table 20.

The fact that the conversion values measured for both samples are very similar indicates that, despite the lower SSA of the printed structure in relation to the powder, the distribution and the total pore volume had a very similar behavior, consequently the structure can be successfully employed as heterogeneous catalysis.

The range of pore distribution was between 20 and 300 nm and the total pore volume reached about 0.12 cm^3/g for both materials (Figure 49a-b).

Table 20. Biodiesel conversion and pore analysis for the 3D-printed structure.

Sample	Biodiesel conversion (%)	Specific surface area (m^2/g)	Total pore volume (cm^3/g)	Average pore diameter (nm)
Na_GP1 - 3D Structure	43.5	14.30	0.12	11.41
Na_GP1 - 3D Structure powder	51.8	14.87	0.12	11.41

Higher yields were found in the literature (>95%), but with different reaction conditions; for the test with powdered Ca-based geopolymer, it was used higher amount of catalyst (> 7.5 wt.%) and high excess methanol (5418%) [63]. For the reaction with powdered KOH-impregnated zeolite, it was used 6.4 wt.% of catalyst and ~283% excess methanol [64]. These authors also had to filter and wash the biodiesel to remove the catalyst and leached metals, which is undesirable considering the use of a heterogeneous catalyst.

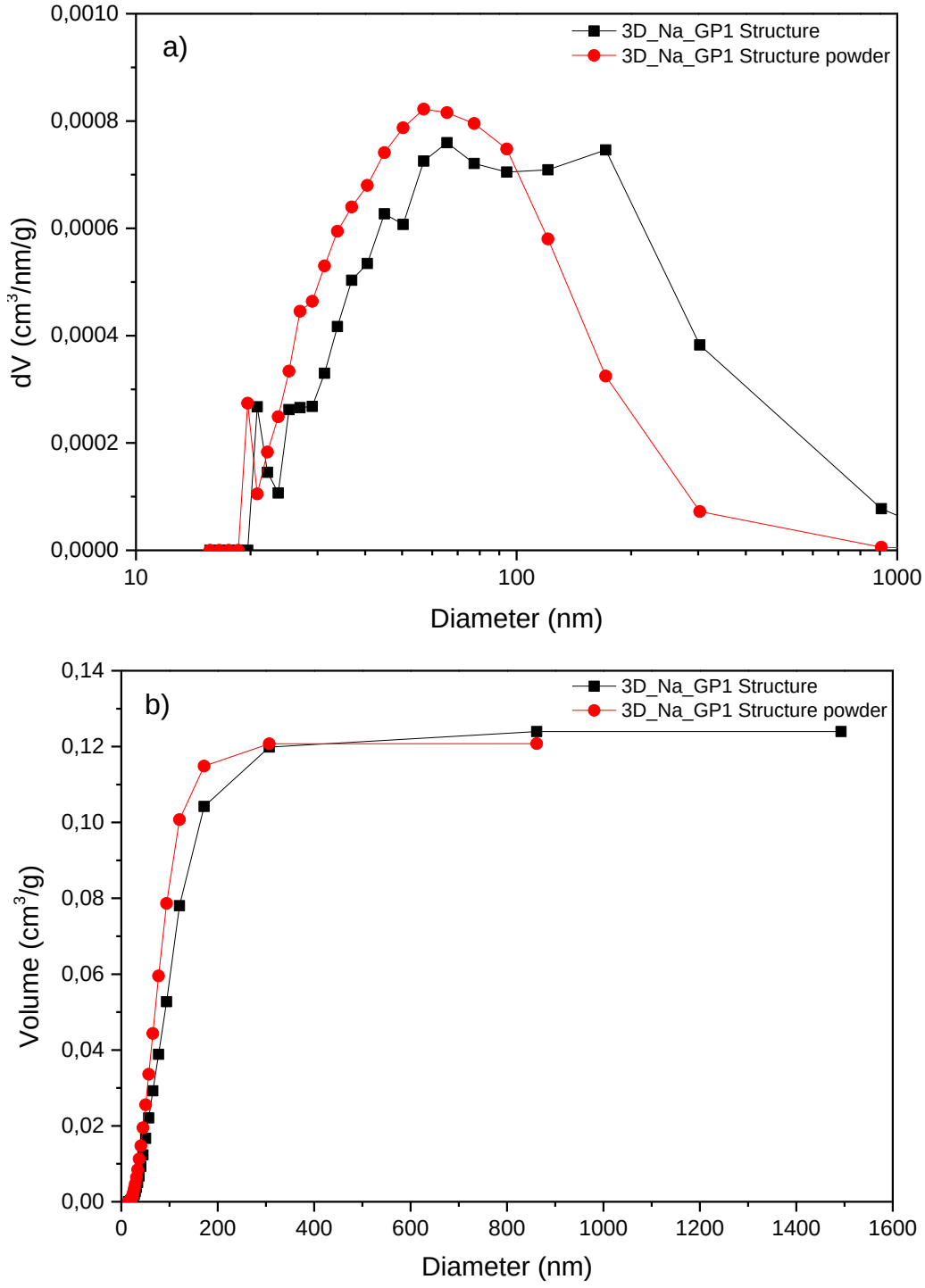

Figure 49. Pore distribution and total pore volume of: a) 3D_Na_GP1 structure; b) the powdered structure.

In a conventional homogeneous reaction, usually, it is used 1wt.% of oil as a catalyst (NaOH) which corresponds to 0.575 g of Na per 100 g of oil. In the reactions studied in this work, the catalyst was used in 3 wt.%, which is equivalent to 12 wt.% of Na, and represents 0.366 g Na per 100 g of oil.

Through the atomic absorption analysis, it was possible to quantify that 16.5 wt.% Na was leached from the material and this value represents only 0.06 g Na per 100 g oil, equivalent to 0.1% of NaOH in a homogeneous reaction, therefore considering that this quantity is very low for the transesterification reaction to occur, the geopolymer acted effectively as a heterogeneous catalyst.

6. CONCLUSIONS

The main objective of this work was to prove the efficiency of the use of geopolymers as a heterogeneous catalyst in the transesterification reaction using soybean oil as triglyceride by the methyl route.

The formulations for the preparation of the geopolymers were based on the range proposed by Davidovits [15] in previous studies. Na-based, K-based, and a geopolymer with the two alkalis were produced. The powdered materials were treated at four different temperatures (110, 300, 500 and 700 °C).

From the initial characterization by XRD analysis, it was shown that the material remained amorphous for all types and temperatures of treatment, without significant peaks for identification of the crystalline structure, besides the peaks belonging to the impurities coming from the raw material metakaolin, except for Na.K_GP, that at 700 °C the usual peaks of the kalsilite and nepheline crystalline phases were identified.

The temperature analysis of the materials was done through TGA/DSC and an endothermic peak for the three geopolymers was observed for physical water loss around 110 °C; above 720 °C exothermic peaks were identified for crystallization of the material. The thermogravimetric analysis showed that increasing temperature, the weight loss also increased, in a total of 11.5% for Na_GP1, 14.6% for K_GP1 and 11.1% for Na.K_GP, confirming that the K-based geopolymer had higher weight loss because it contained more water in its formulation.

According to the biodiesel yield using powdered geopolymers, by investigating the amount of water in the material formulation it was possible to observe that the geopolymer with higher molar ratio H_2O/Al_2O_3 had higher conversion, and was related to a higher SSA, since the water that was inside the structure, when eliminated, formed pores increasing the catalytic activity of the sample.

Testing two different reaction conditions, changing the temperature and the time from 60 °C and 1 h to 70 °C and 2 h, higher conversion was obtained for the reactions using Na_GP1 at the four treatment temperatures; this change favored the reaction in the direction of the products and was maintained as standard condition for the next reactions.

The analysis of the biodiesel conversion using the three types of materials with the same formulation, in terms of molar ratio, showed that Na.K_GP had higher

catalytic activity, supposedly can be related to pH reaction and to the release of alkalis. In the reaction where this material treated at 500 °C was used, resulted in high conversion and low leaching, probably because the leaching occurs differently from the materials only with Na or K, therefore, more chemical studies in this investigation should be done.

Rheology is an important aspect that was studied prior to the 3D printing process to understand ink behavior during printing. The three inks were suitable for 3D printing by DIW, however, 3D_Na.K_GP formed a weaker gel and with the weight of the successive layers of the lattice, the unsupported filaments tended to sink. This behavior was reflected in the properties of the structure, its porosity was smaller than the designed one and, consequently, increased its mechanical strength, because the structure had more support than the designed one. The other two lattices showed similar behavior in relation to rheology, and consequently their properties. Images of the optical microscope and SEM showed visibly these characteristics, besides showing good interaction of the matrix geopolymer with the added filler. The permeability of the sample 3D_Na_GP1 proved its use as a catalyst, being in the same range of honeycombs, normally with high permeability and used as filters.

In relation to the biodiesel yield using the geopolymeric lattice (3D_Na_GP1), the same reaction condition was first tested with the powder, but the reaction was incomplete, not separating the biodiesel phase, so the reaction time was increased to 4 h. The fact that the conversion values measured for the lattice (43%) and its finely grounded powder (51%) were very similar, indicates that, despite the lower SSA of the printed structure in relation to the powder, the structure can be successfully employed as heterogeneous catalysis.

In general, the best system, in terms of biodiesel conversion, was the Na.K_GP heat treated at 500 °C, nevertheless, an improvement in its rheology is necessary to, hopefully, be used as geopolymeric lattice in the biodiesel reaction and to obtain similar results as its powder version.

To verify the conversion efficiency of the other structures (3D_K_GP1, 3D_Na.K_GP) further studies are needed.

7. REFERENCES

[1] J. O. Maloney, Perry's Chemical Engineers' Handbook - 8th Edition.

[2] R. Fouquet, “Historical energy transitions: Speed, prices, and system transformation”, Energy Research & Social Science 22 (2016) 7-12.

[3] A. Gupta, “Climate Change and Kyoto Protocol: An Overview”, Handbook of Environmental and Sustainable Finance (2016), 3-23.

[4] Ş. E. C. Şenera, J. L. Sharpb, A. Anctilc, “Factors impacting diverging paths of renewable energy: A review”, Renewable and Sustainable Energy Reviews 81 (2018) 2335-2342.

[5] World Commission on Environment and Development, Our Common Future - Chapter 2, United Nation (1987)

[6] W. Xie, L. Zhao, “Production of biodiesel by transesterification of soybean oil”, Energy Conversion and Management 76 (2013) 55-62.

[7] S. Semwal, A. K. Arora, R. P. Badoni, D. K. Tuli, “Biodiesel production using heterogeneous catalysts”, Bioresource Technology 102 (2011) 2151-2161.

[8] A.P. Singh Chouhan, A.K. Sarma, “Modern heterogeneous catalysts for biodiesel production A comprehensive review”, Renewable and Sustainable Energy Reviews 15 (2011) 4378-4399.

[9] M. Feyzi, A. Hassankhani, H. R. Rafiee, “Preparation and characterization of Cs/Al/Fe3O4 nanocatalysts for biodiesel production”, Energy Conversion and Management 71 (2013) 62-68.

[10] W. Xie, H. Wang, H. Li, “Silica-Supported tin oxides as heterogeneous acid catalysts for transesterification of soybean oil with methanol”, Ind. Eng. Chem. Res., 51,1 (2012) 225-231.

[11] A. K. Endalew, Y. Kiros, R. Zanzi, “Inorganic heterogeneous catalysts for biodiesel production from vegetable oils”, Biomass and Bioenergy 35 (2011) 3787-3809.

[12] I.M. Atadashi, M.K. Aroua, A.R. Abdul Aziz, N.M.N. Sulaiman, “The effects of catalysts in biodiesel production: A review”, Journal of Industrial and Engineering Chemistry 19 (2013) 14-26.

[13] M. Zabeti, W. M. A. W. Daud, M. K. Aroua, “Activity of solid catalysts for biodiesel production: A review”, Fuel Processing Technology 90 (2009) 770-777.

[14] G. J. Suppes, M. A. Dasari, E. J. Doskocil, P. J. Mankidy, M. J. Goff, “Transesterification of soybean oil with zeolite and metal catalysts”, Applied Catalysis A: General 257 (2004) 213-223.
[15] J. Davidovits, Geopolymer Chemistry and Applications, Institut Géopolymere, 2011.
[16] C. Villa, E.T. Pecina, R. Torres, L. Gómez, “Geopolymer synthesis using alkaline activation of natural zeolite”, Construction and Building Materials 24 (2010) 2084-2090.
[17] P. Hlavácek, V. Smilauer, F. Skvára, L. Kopecky, R. Sulc, “Inorganic foams made from alkali-activated fly ash: Mechanical, chemicaland physical properties”, Journal of the European Ceramic Society 35 (2015) 703-709.
[18] M. Minelli, V. Medri, E. Papa, F. Miccio, E. Landi, F. Doghieri, “Geopolymers as solid adsorbent for CO2 capture”, Chemical Engineering Science 148 (2016) 267-274.
[19] C. Bai, P Colombo, “High-porosity geopolymer membrane supports by peroxide route with the addition of egg white as surfactant”, Ceramics International 43 (2017) 2267-2273.
[20] K. Zheng, L. Chen, M. Gbozee, “Thermal stability of geopolymers used as supporting materials for TiO2 film coating through sol-gel process: Feasibility and improvement”, Construction and Building Materials 125 (2016) 1114-1126.
[21] Yao Jun Zhang, Li Cai Liu, Yong Xu, Ya Chao Wang, De Long Xu, “A new alkali-activated steel slag-based cementitious material for photocatalytic degradation of organic pollutant from waste water”, Journal of Hazardous Materials 209-210 (2012) 146-150.
[22] S. Sharma, D. Medpelli, S. Chen, Dong-Kyun Seo “Calcium-modified hierarchically porous aluminosilicate geopolymer as a highly efficient regenerable catalyst for biodiesel production”, RSC Advances, 2015, 5, 65454.
[23] L. C. Meher, D. Vidya Sagar, S.N. Naik, “Technical aspects of biodiesel production by transesterification-a review”, Renewable and Sustainable Energy Reviews 10 (2006) 248-268.
[24] G. Knothe, J. V. Gerpen, J. Krahl, “The biodiesel Handbook”, 2005.
[25] F. E. Mahallawy, S. E. D. Haik, “Fundamentals and technology of combustion”, Ed. Elsevier, 2002.
[26] W. C. Lyons, “Standard Handbook of Petroleum & Natural Gas Engineering”, Ed. Gulf Publishing Company, Texas, V. 1, 1996.

[27] R. J. Brecha, “Emission scenarios in the face of fossil-fuel peaking”, Energy Policy 36 (2008) 3492-3504.
[28] L. Chiari, A. Zecca, “Constraints of fossil fuels depletion on global warming projections”, Energy Policy 39 (2011) 5026-5034.
[29] A. C. Marques, J. A. Fuinhas, D. A. Pereira, “Have fossil fuels been substituted by renewables? An empirical assessment for 10 European countries”, Energy Policy 116 (2018) 257-265.
[30] N. Gaurav, S. Sivasankari, G. S. Kiran, A. Ninawe, J. Selvin, “Utilization of bioresources for sustainable biofuels: A Review”, Renewable and Sustainable Energy Reviews 73 (2017) 205-214.
[31] F. Saladini, N. Patrizi, F. M. Pulselli, N. Marchettini, S. Bastianoni, “Guidelines for emergy evaluation of first, second and third generation biofuels”, Renewable and Sustainable Energy Reviews 66 (2016) 221-227.
[32] J. Walton, “The fuel possibilities of vegetable oils”, Gas Oil Power 33: 167-168 (1938); Chem. Abstr. 33: 8336 (1939).
[33] ANP- Agência Nacional de Petróleo, Gás Natural e Biocombustíveis (http://www.anp.gov.br/biocombustiveis/biodiesel) accessed 27/08/2018
[34] National Biodiesel Board (http://biodiesel.org/what-is-biodiesel/biodiesel-basics) accessed 27/08/2018
[35] Masjuki Hj. Hassan, Md. Abul Kalam “An overview of biofuel as a renewable energy source: development and challenges”, Procedia Engineering 56 (2013) 39-53.
[36] M. Mittelbach, “Diesel fuel derived from vegetable oils, VI: Specifications and quality control of biodiesel”, Bioresource Technology 56 (1996) 7-11.
[37] P. V. Rao, “Experimental Investigations on the Influence of Properties of Jatropha Biodiesel on Performance, Combustion, and Emission Characteristics of a DI-CI Engine”, World Academy of Science, Engineering and Technology 75 (2011) 855-868.
[38] B. S. Sánchez, G. Mendow, P. G. Levrand, C.A. Querini, “Optimization of biodiesel production process using sunflower oil and tetramethyl ammonium hydroxide as catalyst”, Fuel 113 (2013) 323-330.
[39] M. Zabeti, W. M. A. W. Daud, M. K. Aroua, “Activity of solid catalysts for biodiesel production: A review”, Fuel Processing Technology 90 (2009) 770-777.
[40] F. Ma, M. Hanna, “Biodiesel production – a review”, Bioresource Technology, 70 (1999) 1-15.

[41] U. Schuchardt, R. Sercheli, R. M. Vargas, “Transesterification of vegetable oils – a review”, J. Braz. Chem. Soc. 9[1] (1998) 199-210.
[42] M. Tariq, S. Ali, N. Khalid, “Activity of homogeneous and heterogeneous catalysts, spectroscopic and chromatographic characterization of biodiesel: A review”, Renewable and Sustainable Energy Reviews 16 (2012) 6303-6316.
[43] M. R. Avhad, J. M. Marchetti, “A review on recent advancement in catalytic materials for biodiesel production”, Renewable and Sustainable Energy Reviews 50 (2015) 696-718.
[44] A. Taguchi, F. Schüth, “Ordered mesoporous materials in catalysis”, Microporous and Mesoporous Materials 77 (2005) 1-45.
[45] A. Z. Abdullah, N. Razali, K. T. Lee, “Optimization of mesoporous K/SBA-15 catalyzed transesterification of palm oil using response surface methodology”, Fuel Processing Technology 90, 7-8, (2009), 958-964.
[46] J. L. Provis, J. S. J. van Deventer, Geopolymers structure, processing, properties and industrial applications (2009).
[47] D. Khale, R. Chaudhary, “Mechanism of geopolymerization and factors influencing its development: a review”, J Mater Sci (2007) 42:729-746
[48] P. Duxson, A. Fernández-Jiménez, J. L. Provis, G. C. Lukey, A. Palomo, J. S. J. van Deventer, “Geopolymer technology: the current state of the art”, Journal of Materials Science (2007) 42:2917-2933.
[49] ASTM Standard F2792, Standard Terminology for Additive Manufacturing Technologies. ASTM International, West Conshohocken, Pennsylvania, 2012.
[50] A. Zocca, P. Colombo, C. M. Gomes, J. Günster, “Additive Manufacturing of Ceramics: Issues, Potentialities, and Opportunities”, J. Am. Ceram. Soc., 98 [7] 1983-2001 (2015).
[51] J. a. Lewis, J.E. Smay, J. Stuecker, J. Cesarano, “Direct ink writing of three-dimensional ceramic structures”, J. Am. Ceram. Soc. 89 (2006) 3599-3609.
[52] G. Franchin, P. Scanferla, L. Zeffiro, H. Elsayed, A. Baliello, G. Giacomello, M. Pasetto, P. Colombo, “Direct ink writing of geopolymeric inks”, Journal of the European Ceramic Society 37 (2017) 2481-2489.
[53] J.E. Smay, J. Cesarano, J.A. Lewis, Colloidal inks for directed assembly of 3-Dperiodic structures, Langumuir 18 (2002) 5429-5437.

[54] T. Schlordt, F. Keppner, N. Travitzky, P. Greil, Robocasting of alumina latticetruss structures, J. Ceram. Sci. Technol. 3 (2012) 1-7.
[55] C. Bai, G. Franchin, H. Elsayed, A. Conte, P. Colombo, “High strength metakaolin-based geopolymer foams with variable macroporous structure”, Journal of the European Ceramic Society 36 (2016) 4243-4249.
[56] M. Romagnoli, C. Leonelli, E. Kamse, M. L. Gualtieri, “Rheology of geopolymer by DOE approach”, Construction and Building Materials 36 (2012) 251-258.
[57] A. Poulesquen, F. Frizon, D. Lambertin, “Rheological behavior of alkali-activated metakaolin during geopolymerization”, Journal of Non-Crystalline Solids 357 (2011) 3565-3571.
[58] M.D.M. Innocentini, P. Sepulveda, F. Ortega, Permeability, Chapter 4.2 in the book Cellular Ceramics: Structure, Manufacturing, Properties and Applications, Michael Scheffler (Editor), Paolo Colombo (Editor), ISBN: 3-527-31320-6 (2005).
[59] M.D.M. Innocentini, V.D. Rasteira, M. Potoczek, A. Chmielarz, E. Kocy’o. Physical, fluid dynamic and mechanical properties of alumina gel-cast foams manufactured using agarose or ovalbumin as gelling agents. Journal of Materials Research 32, 2810-2818 (2017).
[60] M.S. Cilla, M.D.M. Innocentini, M.R. Morelli, P. Colombo, “Geopolymer foams obtained by the saponification/peroxide/gelcasting combined route using different soap foam precursors”. Journal of the American Ceramic Society 100, 3440-3450 (2017).
[61] C. Vakifahmetoglu, D. Zeydanli, M.D.M. Innocentini, F.S. Ribeiro, P.R.O. Lasso, G.D. Soraru. “Gradient-Hierarchic-Aligned Porosity SiOC Ceramics”, Scientific Reports, v.7, p.41049 (2017)
[62] M.D.M. Innocentini, R.F. Botti, P.M. Bassi, C.F.P.R. Paschoalato, D.L.Flumignan, G. Franchin, P. Colombo, “Lattice-shaped geopolymer catalyst for biodiesel synthesis fabricated by additive manufacturing”, Ceramics International, Volume 45, Issue 1, January 2019, Pages 1443-1446)
[62] S. Sharma, D. Medpelli, S. Chen. D.-K. Seo, “Calcium-modified hierarchically porous aluminosilicate geopolymer as a highly efficient regenerable catalyst for biodiesel production”, RSC Advances 5 (2015) 65454-65461.
[63] N. Al-Jammal, Z. Al-Hamamre, M. Alnaief, “Manufacturing of zeolite based catalyst from zeolite tuft for biodiesel production from waste sunflower oil”, Renewable Energy 93 (2016) 449-459.

APPENDIX A

Initial page of the first patent (Chavanne-1937) that presents the transformation of vegetable oils into Biodiesel (alkyl esters) and its use as fuels.

Ministère des Affaires Économiques

Administration du Commerce Intérieur

SERVICE DE LA PROPRIÉTÉ INDUSTRIELLE ET COMMERCIALE

No. 422.877.

ROYAUME DE BELGIQUE

BREVET D'INVENTION

Le Ministre des Affaires Économiques

Vu la loi du 24 mai 1854;

Vu le procès-verbal dressé le 28 juillet 1937, à 12 h -,

au greffe du Gouvernement provincial du Brabant;

ARRÊTE :

Article 1. — *Il est délivré à* M^r Ch. G. Chavanne, 82, rue Berckmans, à Saint-Gilles - Bruxelles, repr. par M^e G. Vander Haeghen à Bruxelles

un brevet d'invention pour : Procédé de transformation d'huiles végétales en vue de leur utilisation comme carburants.

Article 2. — *Ce brevet lui est délivré sans examen préalable, à ses risques et périls, sans garantie soit de la réalité, de la nouveauté ou du mérite de l'invention, soit de l'exactitude de la description, et sans préjudice du droit des tiers.*

Au présent arrêté demeurera joint un des doubles de la spécification de l'invention (mémoire descriptif et éventuellement dessins) signés par l'intéressé et déposés à l'appui de sa demande de brevet.

Bruxelles, le 31 août 1937.

Au nom du Ministre et par délégation
~~Le Directeur général du Commerce Intérieur~~
Le Directeur, Chef de ~~Service~~ :

Tychon, com. 218, lot 1, 1936, 5000 ex.

APPENDIX B

Datasheet of Metakaolin CSC1200 - ARGICAL 1200 S.

Bal_Co
Via Radici in Piano, 525
41049 - Sassuolo (MO) - Italy
Phone n° 0536800558 - Fax n° 0536809014
www.balco.it

Sistema Qualità Certificato secondo la norma UNI EN ISO 9001:2008
Mod. 4.8 Rev. 3

SCHEDA TECNICA

CSC1200 - ARGICAL 1200 S METACAOLINO

Analisi chimica	Min	Tipica	Max
SiO_2		% 55.0	
Al_2O_3		% 39.0	
Fe_2O_3		% 1.8	
TiO_2		% 1.5	
Na_2O+K_2O		% 1.0	
CaO + MgO		% 0.6	
P.F.		% 1.0	
Granulometria			
< 2 µm		% 55	
Altre caratteristiche			
CARATTERISTICHE FISICHE TIPICHE:			
Indice pozzolanico		mgCa(OH)2 1400	
Bianchezza fotovolt filtro blu		% 74	
Superficie specifica (BET)		m²/g 19	
Assorbimento d'acqua (cono di Marsh)		g/Kg 1650	
Peso specifico		g/cm³ 2.2	
Densità apparente in mucchio		Kg/m³ 250	
Densità apparente compattata		Kg/m³ 400	
Grado di acidità		pH 6	
Informazioni generali			
Imballo "SA" in sacchi da 15 Kg			

Firma:

Revisione 1 del 21-09-2009
La presente annulla e sostituisce le precedenti

Pag.nr. 1